ABSTRACT

Straight, William Herbert. *Stratigraphic Distribution, Taphonomy, and Isotope Paleoecology of the Dinosaurian Fauna in the latest Campanian lower Horseshoe Canyon Formation, Alberta, Canada*, (Dale A. Russell and Reese E. Barrick, co-chairs of advisory committee).

Vertebrate fossils in the lower Horseshoe Canyon Formation are remains of dinosaurs, crocodilians, champsosaurs, turtles, and fish supported during the last ~2 m.y. of the Campanian by a coastal lake-strewn wetland occupying what is now south-central Alberta, Canada. Bones accumulated on the floodplain through attritional mortality and are preserved unweathered except for surface polish, scratches, and mottling characteristic of bioturbation during rapid burial in fine-grained sediment. Fossil-bearing sites cluster stratigraphically in laterally extensive horizons between thicker less fossil-rich intervals of similar fluvial strata. These horizons, formed by a long-term balance between bone supply, accommodation, and depositional rate, result from a newly recognized "floodplain fill" mode of preservation for vertebrate fossils and are analogous to marine condensed sections. Like condensed sections, these fossiliferous horizons lie adjacent to lithostratigraphic surfaces created by stillstands in base-level. Together, hiatal surfaces and fossiliferous horizons reveal repeating rhythms in the facies distribution and fluvial architecture. These rhythms, "packages" of strata bounded by hiatal surfaces, arose through two scales of variation in base-level: a grand-scale base-level cycle reflecting tectonic control during the construction of the clastic wedge, and a smaller "package"-scale cycle reflecting Milankovitch control over local climate and precipitation. Both the fluvial architecture and the accumulations of fossils are a consequence of this change in accommodation and sediment supply through time. Fossil evidence does not indicate a faunal change through time, but changes in climate through time resulted in a reduction in organic-rich mudrocks and coal, an increase in soil development, and changes in the dominant configuration for fossil preservation from sparse bonebeds to microsites. Climate change was also investigated through stable oxygen isotopes in tyrannosaur tooth enamel phosphate, which daily recorded the response of surface (drinking) water to changes in humidity and temperature. The enamel isotopic record shows a transition from highly variable, seasonal climate to relatively constant conditions, consistent with the interpretation of change in the stratigraphy and taphonomy. This combined application of architectural stratigraphy, vertebrate taphonomy, and stable isotope paleoecology represents a new approach for paleontologists interested in evaluating changes through geologic time in paleoenvironment and animal communities in a fluvial succession.

Stratigraphic Distribution, Taphonomy, and Isotope Paleoecology of the Dinosaurian Fauna in the Latest Campanian Lower Horseshoe Canyon Formation, Alberta, Canada

By

William H. Straight

A dissertation submitted to the graduate faculty of

North Carolina State University

in partial fulfillment of

the requirements for the degree of

Doctor of Philosophy

Department of Marine, Earth, and Atmospheric Sciences

Raleigh

2003

APPROVED BY:

Chairman, Advisory Committee

Co-Chair, Advisory Committee

Member, Advisory Committee

Member, Advisory Committee

Member, Advisory Committee

PERSONAL BIOGRAPHY

William Herbert Straight was born November 10th, 1967 to Dr. James W. and Roberta C. Straight at Sandia Military Base in Albuquerque, NM. He graduated from the high school in Los Alamos, NM, in 1986, then majored in geology at New Mexico Institute of Mining and Technology in Socorro, NM. His program there included an apprenticeship as a fossil preparator in the paleontology lab of the New Mexico Bureau of Mines under mentor Dr. Donald Wolberg and three years as a geochemist in a co-operative research program at Los Alamos National Laboratory under Dr. David Janecky, participating in a variety of projects including a geochemical tracer experiment in the hydrothermal spring systems of Yellowstone National Park . Will graduated with a Bachelors of Science in Geology from New Mexico Tech *Magna Cum Laude* in 1993. Will then began work under Dr. Thomas Lehman at Texas Tech University in Lubbock, TX. Will wrote a thesis on the stratigraphy and vertebrate paleontology around the Cretaceous-Tertiary boundary section in Big Bend National Park, TX, and graduated from TTU with an M.S. degree in 1996. Will then moved to Raleigh, NC, one of the first two graduate students in a new program at NCSU under Drs. Dale Russell, Reese Barrick, and Elisabeth Wheeler. His dissertation project began with an introduction to Dr. David Eberth of the Royal Tyrrell Museum of Palaeontology in Drumheller, Alberta, and he spent the summers of 1997 and 1998 doing fieldwork in the Red Deer River Valley of Alberta. Will's present work represents a synthesis of data collected during those surveys of the fossils and rocks of the lower Horseshoe Canyon Formation, applying techniques in sequence stratigraphy, taphonomy, and stable isotope paleoecology to reveal patterns of depositional and climate change that occurred in southern Alberta during latest Campanian time. Will presently resides in Raleigh, NC, and works as an isotope geochemist at the Duke Environmental Stable Isotope Laboratory at Duke University in Durham, NC.

TABLE OF CONTENTS

LIST OF TABLES

Chapter 1

Chapter 2

Chapter 3

LIST OF FIGURES

Chapter 1

Chapter 2

Chapter 3

Chapter 4

CHAPTER ONE

Testing the Utility of Vertebrate Remains in Recognizing Patterns in Fluvial Deposits: An Example from the lower Horseshoe Canyon Formation, Alberta

WILLIAM H. STRAIGHT

Marine, Earth, and Atmospheric Sciences Department,

Box 8208, North Carolina State University, Raleigh, NC 27695

DAVID A. EBERTH

Royal Tyrrell Museum of Palaeontology, Box 7500,

Drumheller, AB T0J 0Y0, Canada

Published

Straight, W.H., and Eberth, D.A., 2002. *Testing the utility of vertebrate remains in recognizing patterns in fluvial deposits: An example from the lower Horseshoe Canyon Formation, Alberta*. Palaios v. 17, no. 5, p. 472-490.

Depositional cycles in fluvial successions are described here as chronostratigraphic packages of strata founded on a laterally extensive, scour-based, amalgamated channel-sand body, overlain by mudrocks, isolated channel fills, avulsion and splay complexes, and paleosols. Ten packages are described from the lower Horseshoe Canyon Formation (Campanian-Maastrichtian), one of a succession of clastic wedges filling the Alberta foreland basin in south-central Alberta. The structure of these packages is consistent with the fall-rise-fall cycle of base-level described in other studies, but the package-bounding scours and internal surfaces are discontinuous and difficult to trace in the mudrock-dominated strata. Terrestrial vertebrate fossils are preserved in relatively fossiliferous, facies-independent horizons 1 to 3 m thick that statistically correlate with the stratigraphic position of package scours and surfaces. Fossiliferous horizons formed as a result of attritional accumulation under an optimum, relatively low, regional deposition rate. Not only do these horizons aid in locating package surfaces, but they also provide insight to the interaction of the package-scale, base-level oscillation with the larger-scale fluctuation in accommodation associated with the formation of the clastic wedge. As such, fossiliferous horizons in the Horseshoe Canyon Formation make better boundary markers than do paleosols, splays, coal seams, or even the surfaces associated with package structure. Therefore, the vertebrate fossil record may supply a means of stratigraphically evaluating sections in other locations in which typical sedimentological and architectural cues for surfaces are absent.

INTRODUCTION

Facies and structural elements in fluvial successions regularly are described in terms of a subtle, repeating pattern of fining-upward packages. The typical package structure includes basal, laterally extensive scour-bottomed sandstone sheets or amalgamated sandstone bodies, overlain by sheets of mudrock encasing lenses of sand, in turn overlain by coal, laminated mudrocks, or paleosols. Whereas older studies of fluvial deposits report these patterns as details of facies architecture, recent research interprets fining-upward packages as indicators of cyclic base-level change (Table 1; for a complete review, see Blum and Törnqvist, 2000). Distinctive contacts recurring in successive packages, especially the erosional scour present under most sandstones, have been interpreted as important surfaces in both allostratigraphic (Bhattacharya, 1989; Cant,

1998) and sequence stratigraphic (Shanley and McCabe, 1991; Aitken and Flint, 1995; Kamola and Van Wagoner, 1995) frameworks. In each case, these results are based on sedimentologic evidence alone. In fluvial strata, cross-cutting relationships, lateral facies transitions, pinch-outs, reworking, bioturbation, and stacking of similar facies can obscure or destroy such boundaries. Any additional information potentially useful for tracing stratigraphically important contacts or surfaces should be exploited. In marine stratigraphy, invertebrate fossil evidence has been used to locate surfaces (Kidwell, 1986, 1988a,b, 1989; Banerjee and Kidwell, 1991; Brett, 1995, 1998; Holland, 1995; Tew and Mancini, 1995). Many fluvial successions with repeating packages also include fossil remains, particularly those of large terrestrial animals such as dinosaurs and mammals. Taphonomy is the focus of many studies in which stratigraphic packages are described (Wood, 1985; Behrensmeyer, 1987; Wood et al., 1988; Davies-Vollum and Wing, 1998). A recent inquiry into vertebrate fossils in the Two Medicine Formation (Rogers and Kidwell, 2000) found no correlation between third-order sequence boundaries and fossil distribution. To date, terrestrial fossil occurrences essentially have been neglected as potential indicators of higher-order (fourth- or fifth-order) stratigraphic surfaces and patterns of stratigraphic cyclicity in fluvial successions.

The present work focuses on exposures of the lower Horseshoe Canyon Formation (HCF) of south-central Alberta, a succession of latest Campanian to earliest Maastrichtian fluvial strata. The first goal of this study is to describe repeating cycles of facies and structures in the lower HCF from sedimentologic information. The second goal is to describe the distribution of vertebrate fossils in the lower HCF. The distribution of fossils is tested for correspondence both with the stratigraphic data and with the cycles in fluvial deposition, with particular attention to the potential usefulness of fossils as markers for important stratigraphic surfaces. The interpreted depositional history from the stratigraphic and fossil record then is compared to other documented stratigraphies.

HORSESHOE CANYON FORMATION

The Horseshoe Canyon Formation (HCF) consists of estuarine and fluvial sandstones, mudrocks, and coal, part of a succession of clastic wedges shed into the Cretaceous Interior Seaway from a thrust belt to the west (Cant and Stockmal, 1989; Jerzykiewicz and Norris, 1993; Hamblin, 1998a; Fig. 1). The HCF lies over

the marginal-marine Bearpaw Formation and is underlain by the Whitemud, Battle, and Scollard formations, collectively forming the Edmonton Group (Allan, 1922; Allan and Sanderson, 1945; Ower, 1960; Shepheard and Hills, 1970; Irish, 1970; Nurkowski, 1980; Hamblin, 1998a). The informally named Drumheller Marine Tongue (DMT) records a minor transgressive episode (Langston, 1959b; Russell and Chamney, 1967), recently correlated to the Campanian/Maastrichtian boundary (Lerbekmo, pers. comm., 2000), that divides the HCF into upper and lower successions of subequal thickness (Nurkowski and Rahmani, 1984). Up to 165 m of the lower HCF and the overlying 30 m of the DMT represent approximately 2 myr of relatively continuous deposition, and constitute a cycle of aggradation and progradation of a clastic wedge, ending with the final incursion and retreat of the Bearpaw Sea into south-central Alberta (Catuneanu and Sweet, 1999). Exposures of this interval were studied in a 35-km transect along the Red Deer River Valley around Drumheller, Alberta (Fig. 2).

The upper Bearpaw and basal Horseshoe Canyon formations previously have been described in terms of repeating shoaling- and fining-upward packages, partitioned by discontinuities interpreted as incisions and flooding surfaces (Waheed, 1983; Rahmani, 1988; Ainsworth, 1994; Ainsworth and Walker, 1994; Eberth, 1995). Extension of these surfaces into the updip fluvial succession has not been attempted because the surfaces are obscured by the absence of marine ichnofossils and by lateral lithofacies variation. Coal seams used as informal stratigraphic markers in the HCF (Gibson, 1977; Nurkowski and Rahmani, 1984; McCabe et al., 1989; Hamblin, 1998a,b) have been numbered as Coal Seam 0 above the Bearpaw/HCF contact to Coal Seam 10 within the DMT. However, coal seams are more numerous in the HCF than this scheme suggests, in many places pinching out or splitting (Figs. 3 and 4). Multiple coal seams, occurring in intervals averaging 10 m in thickness and separated by relatively organic-poor intervals of 30 m or more, are more reliable as gross stratigraphic markers than are individual discontinuous seams (Straight and Eberth, 1998).

The Red Deer River dissects the lower HCF to expose dip sections on steep valley walls and strike sections in the tributary coulees, allowing the examination of stratigraphy and facies distribution in three dimensions. Shallow dip (<2° to the north-northwest) and limited distortion allow study of each surface and package laterally over tens of kilometers. Prior stratigraphic work in the transitional deposits at the base of the Horseshoe Canyon/Bearpaw Formation contact (Rahmani, 1988, 1989; Ainsworth, 1991, 1994; Eberth, 1995,

1996) offers the opportunity to correlate fluvial chronostratigraphic markers with a framework of marine-margin chronostratigraphic surfaces. Finally, vertebrate fossils in the HCF are plentiful, rapidly exposed by erosion, and have not been subjected to prolonged organized collecting, permitting a relatively unbiased measurement of fossil abundance, density, facies relationship, and taphonomy.

STRATIGRAPHIC METHODS

Nine stratigraphic sections were measured using conventional field techniques on the eastern Red Deer River Valley wall between Hoodoos Provincial Park (17 km southeast of Drumheller) and Starland Municipal Park (22 km north-northwest of Drumheller). Data for these measured sections are available as part of the online repository (Appendix). In addition, 35 photographic mosaics cover over 50 km of outcrop. A composite mosaic (Figs. 3 and 4) was assembled from these data to show the architecture of the exposures of the lower HCF and DMT.

FACIES ASSOCIATIONS

Coarse sediments constitute slightly less than half the sediments throughout the HCF and range from very fine to medium mature litharenitic sandstone, usually white, tan, or yellow. Siltstone is typically gray or green-gray, whereas claystone although uncommon in the HCF is generally black, brown, or tan. Mudrocks contain variable proportions of swelling clays, disseminated plant fragments, and amber. Roots, preserved as black carbonaceous films and as red-brown iron oxide casts, are common in some mudrocks. Sub-bituminous coal and lignite form laterally extensive seams averaging 45 cm in thickness and commonly incorporate compressed, partly silicified wood fragments. Siderite nodules, many surrounding bone or silicified wood, form clusters or stringers and range in size from paper-thin sheets to nodules 60 cm in diameter. These sediments are organized into 17 facies in the HCF (Table 2; Fig. 5) and are arranged into facies associations based on common juxtapositions seen in the field: (1) plane-bedded to crossbedded sandstone bodies, (2) terrace-forming sheet sandstone bodies, (3) mud-draped crossbedded sandstone bodies, (4) sandstone-mudstone couplet sheets, (5) organic-rich mudrocks, and (6) organic-poor mudrocks.

Plane-Bedded to Crossbedded Sandstone Bodies

Medium-grained litharenitic sandstone deposits appear as a sheet or complex stack of sheets and lenses throughout the lower HCF. Individual lenses are from 1 to 3 m thick, in many cases with tapering wing-like lateral extensions of the flat upper margin extending the cross-section to >100 m in width. Each unit generally fines upward and lies on a sharp, erosional boundary across which grain size abruptly increases. Isolated sandstone bodies incised into underlying mudstone facies are typically strongly convex-up.

Individual beds in this assemblage average 1 m in thickness, and are distinguished by their shape and internal structure (Fig. 5A). The sharp basal contact is overlain by trough-crossbeds (St) and a sparse assortment of gravel-sized fragments of reworked nodules, fossilized wood, and bone (Gl). Thicker sandstone bodies also may feature planar crossbeds (Sp), and sheet-like bodies display low-angle inclined surfaces (Sl), usually covered with a thin veneer of mud and/or coalified plant fragments. Ripple-lamination in small sandstone channel fills (Sr) occurs at some upper, abrupt gradational contacts of sandstone bodies with overlying mudrocks. Bedding surfaces usually are obscure, most often revealed in the presence of erosion-resistant nodules, stringers, or thin sheets of siderite and patchy calcite cement.

This association, also described from the HCF by others (Pagani, 1985; Rahmani, 1988, 1989), represents a fluvial channel in a low-sinuosity fluvial system. The fining-upward bedding and the inclined surfaces imply the presence of laterally migrating point bars, but these are not numerous in the HCF sandstone bodies. Channel amalgamation, crosscutting bedding surfaces, basal trough crossbedding, and fossiliferous lags at the base of the association suggest channel incision occurred during relatively high-energy flow. The waning-flow progression of bedforms, the abrupt decline in grain size below the upper contact, and the muddy intercalations at the upper contact are interpreted to signal abrupt abandonment of channels followed by prolonged infilling by fine clastic material.

Terrace-Forming Sandstone Bodies

Broad, radially thinning sheets of medium sandstone make excellent visual markers around Drumheller, forming benches traceable up to 4 km along the exposure. The resistant nature of these benches, exposed in three dimensions by the dissection of the strata by coulees and the valley wall flanking the Red

Deer River, demonstrates that each of these units has a laterally extensive, flat-based lenticular shape, up to 2 m thick at its thickest and distally splitting into two or more sandstone sheets intercalated with mudrocks.

The thickest portions of each sheet (Fig. 5B) feature two or more 0.5-m-thick tabular units of trough crossbeds (St) or planar crossbeds (Sp), with bedding surfaces marked in places by gravel-sized fragments of wood, bone, reworked nodules, and rounded mudstone clasts (Gl). Laterally, each sheet pinches and the crossbedded facies grades into thin tabular beds of low-angle plane beds (Sl) intercalated with less common ripple-laminated channel lenses with erosional concave-up bases in places strewn with gravel-sized fragments of wood and bone (Sr). Distally these facies are displaced by beds <10 cm thick of ripple-laminated very fine sandstone or siltstone (Sf).

This association is interpreted as a crevasse-splay or avulsion complex, with the thickest area of the sheet representing filled channels closest to the crevasse. The lateral variation in lithology and internal architecture in splays and avulsions have been described by studies of ancient and modern examples (Ghosh, 1987; Smith et al., 1989; Törnqvist, 1993). The relatively coarse material, crossbedding, and small channels of the thicker portions of these terrace-forming sandstones suggest rapidly modified anastomosing flow. The absence of evidence indicating bioturbation or pedogenesis indicates that this facies was deposited and buried quickly, in keeping with the rapid aggradation associated with modern avulsions (Smith et al., 1989; Nanson and Knighton, 1996).

Mud-Draped Crossbedded Sandstone Bodies

Broad belts of litharenitic sandstone >100 m wide and up to 15 m deep fill concave-up erosional incisions into the laminated mudstone of the upper Bearpaw Formation. Erosional bases of smaller lens-shaped bodies, each >10 m wide and 1-4 m thick, stack atop one another and internally subdivide the belt. Each of these lens-shaped sandstone bodies is partitioned internally by low-angle planar bedding surfaces, which pinch out against or are truncated by the small-scale scours. Sediments of this association grade upward and downdip into mudrocks.

Sandstone dominates the association, with individual beds fining upward (Fig. 5C). Bedding surfaces are present but obscure, particularly in the basal half of the fill. Basal beds feature large-scale trough-

crossbeds (St) and tilted blocks up to 4 m long of laminated strata (Gb) with an apron of coarse debris, including chunks of the block, reworked nodules, rip-up clasts, and *Teredolites*-bored logs on one side. Similar but more sparse lags (Gl) reveal a few internal bedding surfaces. Tabular sheets of planar crossbeds (Sp) overlie the trough-crossbedded facies in places. The upper half of each belt features thin inclined beds of fine sandstone draped with brown mudstone and/or plant hash (Sl), a facies representing about half the fill of each body. The transition to overlying mudrocks is gradational but relatively abrupt. Siderite cements *Ophiomorpha* burrow-fills and other ichnofossils near some upper contacts, and calcite-cemented sandstone reveals bedding surfaces.

This association has been described in previous work as representing a tidally influenced upper and middle estuarine channel (Rahmani and Hills, 1982; Rahmani, 1988, 1989; Bhattacharya, 1989; Ainsworth, 1991, 1994; Eberth, 1995, 1996). The fining-upward trend, the abundant trough crossbedding, bank-collapse blocks with attendant wedges of debris attenuated downstream, and crosscutting erosional scours at several scales indicate incised channel deposition (Rahmani, 1989). The mud drapes vary cyclically in thickness and are doubled in places, characteristic of tidally influenced slack-water deposition (Rahmani, 1989; Ainsworth, 1994). The alternating sandstone-mudstone bedding also is known as inclined heterolithic stratification (IHS) and is characteristic of migrating sandstone bars in an estuarine channel (Wood et al., 1988; Facies E of Rahmani, 1989; Eberth, 1995).

Sandstone-Mudstone Couplet Sheets

This facies association consists of >1-m-thick sheets with sharp, relatively flat, non-erosive contacts. Between Coal Seams 0 and 1, this facies grades laterally over several kilometers into a crossbedded sandstone body with mud drapes (facies association described above) at the base of the HCF. It also forms most of the Drumheller Marine Tongue interval surrounding Coal Seam 10.

Paired flat or gently undulating laminae of very fine sandstone and pale green or gray silty mudstone (Se) form stacks of couplets characteristic of this association (Fig. 5D). Sandstone laminae are generally the thicker of the pair, are ripple-laminated, and rest on an irregular but sharp base. Thick mudstone laminae feature amber, freshwater bivalve fragments, bone fragments, and teeth. In a few places, the flat bedding is

interrupted by irregular clusters of jumbled, broken *Ostrea* and *Crassostrea* in calcite-cemented siltstone (So). Below Coal Seam 1, this facies is bioturbated extensively (*Diplocraterion*, *Ophiomorpha*, *Macaronichnus*) and overlies a plane-crossbedded sandstone with coal clasts, sulfur minerals, and glauconite (Sb).

This association represents a filled lagoon in an estuary. The sandstone-mudstone couplets record washover events or storms interrupting otherwise calm deposition in a back-barrier lagoon. Just above Coal Seam 1 near Willow Creek, this facies also preserves undulating bedding and reworked coalified fragments that suggest storm-driven oscillatory flow in the estuary. The types of bioturbation seen there and presence of glauconite also imply shallow marine conditions. In strata of the Drumheller Marine Tongue, this facies does not include undulatory bedding, reworking, or bioturbation, and couplets are generally thinner and feature a greater component of mud, reflecting a less active back-barrier lagoon. The presence of both brackish and freshwater invertebrate and terrestrial vertebrate fossils in DMT mudrocks suggest that these facies may record the limit of marine influence in the lagoon (Haglund, 2001) or that storm runoff periodically flushed fragmentary terrestrial vertebrate remains into a lagoon.

Organic-Rich Mudrocks

Carbonaceous mudrocks occur within many of the sandy associations, but four intervals of the lower HCF are dominated by these facies, each a virtually uninterrupted, flat, thickly bedded sheet 10-15 m thick. These intervals include several coal seams (informally termed a “swarm” by Straight and Eberth, 1998), are separated from similar swarms by up to 30 m of sandy facies, and are generally lighter in color and contain less coal than the next oldest swarm. Photomosaic images document few crosscutting relationships in this association, although coal seams do split in places.

Seams of blocky bituminous coal (C) include lignite, partly silicified wood fragments, stumps, amber, bentonite, and, below Coal Seam 2.0, sulfur minerals (Fig. 5E). In swarms, several 0.1-m-thick coal seams are interbedded with blocky pale gray and laminated fissile black shaly mudstone (Fa). Plant fragments, black root traces, slickensides, and amber increase in abundance proportionally with darkening color, whereas bone is rare. Coal seams in many places lie on a thin, cemented pink mudstone (Ff) featuring slickensides, amber, root traces, and wood fragments; coals at the top of each swarm also underlie this facies. In a few exposures, coal

seams appear to arch over 20-m-wide lenses of thinly bedded silty mudstone and sandstone couplets (Sn); the same facies appears as laterally extensive sheets between carbonaceous seams in strata just below the DMT. A massive dark brown claystone with a granular parting (Fe) frequently overlies the coal seams in the middle and upper portion of each swarm. Isolated lenses of sandstone <1 m thick are encased in mudrocks between some of the coal seams.

This association is interpreted as sediments deposited in a saturated floodplain backswamp. The sulfur minerals, stumps, and woodgrounds of the coals lowest in section (Seams 0, 1, and 2 of Gibson, 1977) represent wetlands under marine influence. Thinner blocky coals represent freshwater abandoned-channel swamps. Thin coals containing amber and wood fragments may have been deposited on swampy, rapidly accreting, low-gradient floodplains (Nanson and Knighton, 1996), preserved by the thinly bedded mud/sand couplets representing floodplain levees. Slickensides in the pale mudstone facies indicate seasonal drying of swampland, preventing peat accumulation (Retallack, 1990; Aslan and Autin, 1998, 1999). The slickensides, cementation, and rooting in the cemented horizons above and below the coal seams indicate periods of pedogenesis. The brown granular facies may represent freshwater marsh deposits (Retallack, 1990) or those of distal splays or avulsions (Törnqvist, 1993).

Organic-Poor Mudrocks

Although the mudrock content of lower HCF strata remains relatively constant (mean 55%) through the section, thin intervals dominated by this association occur more frequently toward the top, at the expense of more organic-rich mudrocks, which dominate or exclusively comprise fine-grained intervals toward the base of the section. The fine-grained facies of the organic-poor association also are found as minor components of intervals dominated by the more coarse-grained associations described above. In the field, organic-poor mudrock facies appear to grade laterally over >100 m into one another, but photomosaic images show that unit relationships and shapes are highly variable. Contacts between units of this association range from simple horizontal stratification to irregular and intensely crosscut; units vary in form from laterally tapering, flat sheets to broad, shallow mud-filled scours with irregularly truncated upper margins. Numerous small channel fills and larger stacked channel complexes incise into or even through this convoluted bedding scheme.

Orange, red-brown, or tan silty mudstone with thick sandy laminae (Fo) include oxide-cast root traces, siderite nodules, and slickensides (Fig. 5F). Similar blocky green-gray mudstone with distorted enclaves of siltstone (Fg) includes bright green traces of hydrophilic clay, mica flakes, root traces, and tiny bone fragments. Gray carbonaceous mudstone with sparse coaly particles (Fa) appears as 0.1-m-thick discontinuous seams. Silicified wood, sparse amber, and oxide-casts of roots and leaves occur in couplets of green-gray or tan very fine sandstone and silty mudstone (Sn). Clusters and strings of siderite nodules are not limited to bedding planes, in places crossing distinct contacts. In some places, polygonal networks of vein-like siderite concretions appear in patches on exposed bedding planes.

This association is interpreted as a seasonally dry, inland floodplain with slow deposition relative to facies of the organic-rich association. The sandier facies represent broad, low-angle levees and splay lobes, pedogenically developed and churned into underlying sediments by rooting, reworking, repeated wetting and desiccation, and possibly dinosaur trampling. Mudstone-filled channels may represent abandoned channels (Rahmani, 1988), and the alternating horizontally bedded sandstone and mudstone represent intercalating levee and thin distal splay deposits as described by Ghosh (1987). Blocky peds, nearly homogenous grain size, clay illuviation, and oxide casts of roots in the fine-grained facies imply advanced pedogenesis relative to other paleosols in the HCF.

PALEONTOLOGICAL AND STATISTICAL METHODS

Eight areas in the lower HCF (Fig. 2) were chosen for surveys of exposed fossil remains. Each area covers at least 250,000 m^2 and was selected for minimal slumping, minimal vegetative cover, and low slope with few slope breaks to provide good overall exposure without over-emphasizing the tops of resistant units. Surveys were conducted in areas with limited recent collecting. For each site (herein a square meter containing one or more fossil remains) encountered during the survey, position was recorded geographically by GPS and stratigraphically in relation to at least two stratigraphic markers including coal seams and terraces. For each of the 527 sites recorded in the lower HCF, position, facies, and proximity to adjacent sites were tabulated for statistical studies (Appendix).

Three statistical analyses were applied to facies and fossil distribution data from this study to determine if the stratigraphic distribution of fossil sites is dependent upon the stratigraphic arrangement of facies, facies association, and/or lithostratigraphic surfaces. The first analysis is a comparison between facies data from measured sections and facies data from the fossil surveys, treating the entire lower HCF as a single unit. In order to test the stratigraphic dispersion of fossil sites for dependence upon (1) facies distribution and (2) lithostratigraphic surface distribution (described below), however, facies and fossil data were binned into 4-meter-thick intervals. Incremental binning of the data was applied to avoid the *a priori* assumption of stratigraphic patterns in one or both data sets. Interval thickness was chosen to minimize ties in rank among stratigraphic position data while retaining the non-random distribution of facies and fossil sites evident in the sections and fossil stratigraphy (Fig. 6). Three non-parametric statistical tests were used for the analyses: the Spearman Rank correlation and Chi-squared Two-sample tests for their ability to handle the ordinal fossil count, and the Kolmogorov-Smirnov test for its additional comparison of sample dispersion. Each group of independent data was also compared to at least ten synthetic, randomly-generated fossil distributions to determine if the real fossil site data correlated better than a random stratigraphic dispersion of fossils.

Most of the fossils were left undisturbed during the survey, although a few specimens were collected for geochemical and mineralogical analysis. For each of 19 powdered bone samples from the lower HCF, a diffraction pattern from 5 to 65 2θ was collected on a Rigaku D/Max-B X-ray diffractor to test for diagenetic alteration of fossil remains (Appendix).

DISTRIBUTION OF VERTEBRATE REMAINS

In the lower 90 m of the study section, fossil sites are clustered within 1-to-4-m-thick fossiliferous horizons (Fig. 6), with the intervening strata virtually devoid of fossils. In the upper half of the section, similar fossiliferous horizons are thinner, and the intervening strata contain some sites. Strata of the DMT are impoverished in fossil remains, with a few thin horizons bearing the majority of sites. Within each fossiliferous horizon, sites occur in up to four types of spatial arrangements. Solitary fossils separated by at least 20 m from any other remains account for 50% of lower HCF sites. Several sites at the same stratigraphic level in the same geographic area are termed bonebeds and appear in two forms in the lower HCF. Sparse

bonebeds have 1-2 fossils per site, with sites separated by up to 5 m, but this low fossil density often covers more than 100 m^2. Sparse bonebeds account for 37% of the sites documented in the lower HCF. A packed bonebed can cover up to 20 m^2, with each site holding several bones lying in contact, immediately adjacent to one or more sites. Packed bonebeds occur in four horizons within the surveyed areas, but together cover almost 40 m^2, accounting for 7% of the documented sites. The remaining 6% come from microsites, accumulations of tiny fragmentary remains of small freshwater vertebrates and weathered teeth of dinosaurs and mammals (Brinkman, 1990). An individual microsite may cover 10 m^2 but can also occur as a patchwork of smaller sites in similar facies along a stratigraphic horizon. The dominance of solitary and sparse-bonebed sites indicates attritional accumulation as the mode in the lower HCF.

Fossils in the lower HCF are preserved as pale blue, purple, tan, brown, or glassy black bones and bone fragments up to 150 cm in longest dimension. Results of X-ray diffraction (Appendix) indicate that fossils throughout the lower HCF are preserved as carbonate hydroxyapatite, consistent with fossilization in fluvial sediments and with minimal diagenetic change (Lucas and Prévôt, 1991; Person et al., 1995), even where specimens preserved in coal appear corroded. Facies data from the fossil surveys correlate closely with bulk facies distribution from the lower HCF stratigraphic sections (Table 3). Mudrock facies and coal contain 66% of lower HCF sites, and facies characteristic of floodplain environments (mudrocks, coal, and splay sediments) contain 85% of the sites (Table 4). Most of the bone in channel facies occur alone, usually on bedding surfaces with reworked mud, reworked siderite clasts, and wood fragments. However, within each fossiliferous horizon, sites occur in a broad mix of facies, associated with lateral facies change. Non-fossiliferous intervals incorporate the same or greater thickness of facies in which fossils elsewhere in the section are preserved in abundance. Thus, the stratigraphic arrangement of facies and fossils is not consistent.

To test the hypothesis that the stratigraphic arrangement of fossils is independent of facies arrangement, facies data from the measured sections and fossil sites were subdivided into 4-m-thick intervals and compared statistically (Table 5). The stratigraphic distribution of fossil sites was compared to the percentage of each facies at the 0.05 level of significance for each test. All Spearman rank correlation tests rejected the hypothesis (no relationship), except for facies Fo, which was significantly related at the 0.01 level; the other statistical tests of distribution were rejected. Statistical tests on ten synthetic fossil distribution

models also rejected relationships for each facies most of the time, although the Spearman Rank correlation test detected a relationship once for each of five of the facies (Table 5). Similar tests comparing the distribution of facies associations to that of fossil sites also generally rejected a relationship. In essence, fossil sites are distributed randomly through the facies of the lower HCF. Therefore, the stratigraphic pattern in fossil distribution (Fig. 6) is related to some characteristic of ecology, burial, or preservation other than lithology.

STACKING PATTERNS IN FACIES ASSOCIATIONS

A typical stacking pattern in the arrangement of facies associations of the lower HCF is herein termed a *package*, a fining-upward, laterally continuous interval of strata bounded by erosional surfaces. The package pattern repeats ten times through the lower HCF section, although some packages are incomplete. These ten packages are designated informally here as "A" at the base of the lower HCF to "J" in the DMT (Fig. 6). Based on measured sections, field observations, and outcrop photographs of the ten packages in the lower HCF, a typical 30-m-thick package consists of eight intervals defined by their facies association (Fig. 7).

Interval a (Facies Association 1)

The irregular scour under a broad sandstone sheet is the basal contact for the typical package. Overlying the scour is a sandstone channel fill capped by lateral accretion surfaces that alternate upward with thin beds of mudstone. Locally, channels filled with fine sandstone incise the top of this sheet and in places are stacked several deep.

Interval b (Facies Association 5)

A relatively thick interval of organic-rich mudrocks includes as many as four coal seams, progressively thinner and more woody upward in section. Sandy channel fills encased in the mudrocks are up to a meter thick and are commonly are lens-shaped, although some are sheet-like and up to 100 meters wide.

Interval c (Facies Associations 5 and 2)

An interval of gray mudrocks encases small channel lenses and less common crevasse-splay sheets with narrow stacked channel fills on top. The channels are 0.5 m thick and up to 25 m wide, whereas the splays extend over 100 m laterally with sharp flat bases that locally incise underlying strata. Coal seams are thin and shaly, but root casts and siderite concretions are more abundant upsection.

Interval d (Facies Associations 6 and 2)

Pale gray or tan mudrocks intercalate with coaly carbonaceous shale and thin tabular splays and finer-grained, more irregular silty levee couplets. Individual beds are usually less than 10 cm thick, laterally discontinuous over 10 m, heavily rooted, and contain common siderite concretions.

Interval e (Facies Association 2)

Point-bar sandstone beds 2 m thick extend laterally over 100 m, incised in places by small sandy channel fills. A sparse veneer of plant fragments, leaves, and reworked siderite concretions marks the presence of lateral accretion surfaces, which otherwise usually are distorted or not preserved.

Interval f (Facies Association 6)

One or two thin carbonaceous mudstone beds intercalate with shallow crosscutting lenses of clay-rich, mottled green or tan siltstone and mudstone with common root casts.

Interval g (Facies Associations 1 and 2)

Stacked splays and small channel fills intercalate with sheets of sandy levee couplets. Bedding surfaces are hard to detect in most places, but where seen are nearly flat, slightly inclined, or contorted. The scour at the base of the overlying package irregularly incises these sediments.

Variations

In the field, many packages differ from the archetype (Fig. 7) in some details. The basal interval of the lowermost package (A, Fig. 6) differs in that an estuary fill complex (Facies Association 3) overlies the

basal scour and a washover fan and tidal flat deposit (Association 4) overlies the internal surface at Willow Creek. An extremely large channel complex overlies the same internal surface just southeast of Aerial, AB (Fig. 3). The four uppermost packages in the study (packages G, H, I, and J, the top 70 meters of the section, Fig. 6) are part of the Drumheller Marine Tongue and feature washovers and tidal flats (Association 4) instead of channels and organic-rich mudrocks. In terms of thickness, the packages of the lower HCF fall into three groups: (1) packages A-D are each ~31 m thick, matching the typical package; (2) packages E-G successively decrease in thickness; and (3) packages H-J are each ~12 m thick (Fig. 6). The organic-rich lower intervals are compressed and splays and stacks of levee couplets are common in the thinner packages.

Two surfaces stand out in the package archetype (Fig. 7). The basal scour is laterally discontinuous, detectable under adjacent channel fills but untraceable in mudrocks between them. Because the channel fills vary slightly in thickness, the stratigraphic position of the scour varies by up to 4 m. A second surface under interval “e” divides the archetype into unequal parts and is marked by a sharp irregular contact across which grain size abruptly increases. This internal surface is distinct from the basal scour by more localized erosion and by less vertical variation in position. In the field, these surfaces occasionally are detectable using changes in facies color and grain size. Stratigraphically below the internal surface, carbonaceous root casts are very common. Unusually large siderite nodules and nodule clusters occur up to 2 m beneath each type of surface (Fig. 6), and more prominently under the basal scour. Basal scours tend to be easier to locate in measured sections and in the field than the internal surfaces, but evidence for the internal surfaces in packages G-J is equivocal, indicating that those surfaces may not always be preserved.

FOSSIL OCCURRENCE IN PACKAGES

Packages of the lower HCF fall into three categories regarding the position of fossiliferous horizons. Packages A-D each feature a 2-to-3-m-thick horizon just under the internal surface (Fig. 6), with less productive horizons underneath. The first three packages also include thick sheets of essentially non-fossiliferous strata, whereas three minor fossiliferous horizons occur in package D in addition to the primary one associated with the internal surface. Packages E-H each feature a 1-to-2-m-thick horizon just above the

basal scour (Fig. 6), with less productive auxiliary horizons immediately above. Packages I and J are essentially non-fossiliferous.

When the stratigraphic position of package surfaces (basal scours and internal surfaces) is compared to the stratigraphic position of fossiliferous horizons, the correspondence is visually striking (Fig. 6). The most productive fossiliferous horizon associated with the internal surface occurs in package C, with an almost symmetrical decline in fossil yield at internal surfaces up- (packages D and E) and down-section (packages B and A). Similarly, the most productive horizon associated with the basal scour occurs in package F, with symmetrically declining yield up- (packages G and H) and down-section (packages F and E). To test the visual correlation between horizons and surfaces, the same statistical methods applied to the facies data were used to compare the stratigraphic position of surfaces with the position of fossiliferous horizons. Horizon position was determined by marking each 4-m-thick interval with 10 or more sites (the mean number of sites for a 4-m-thick interval of the lower HCF). All three tests show significant relationship between surfaces and fossil horizons at the 0.01 level of significance (Table 6). Of twenty tests of synthetic, random horizon distributions, none detected a relationship at the 0.01 level of significance, although three were significantly related in the Kolmogorov-Smirnov test at the 0.05 level. Therefore, fossiliferous horizons are stratigraphically non-random and correlate with package surfaces, indicating that the timing and circumstances of their formation are related. The lithostratigraphic characteristics and the fossil record independently subdivide the packages of the lower HCF into the same three groups (A-D, E-G, and H-J), suggesting that the relationship is depositional and connected to larger-scale controls.

INTERPRETATION OF PACKAGE DEPOSITION

The repeating packages in the lower Horseshoe Canyon Formation are interpreted as a depositional response to a fall-rise-fall cycle in base level. During late base-level fall, low-sinuosity meandering rivers locally incised and reworked older floodplain deposits. The crosscutting scours made by the laterally migrating channels formed the irregular erosional basal surface (interval a; Fig. 7) that continued to expand until after base level began to rise again (e.g., Ghosh, 1987; Aitken and Flint, 1995; Cant, 1998; Robinson and McCabe, 1998).

During early base-level rise, accommodation increased, filling channels with coarse bedload, building laterally migrating point bars, and turning interfluves into marshes (see also Shanley and McCabe, 1994). As accommodation increased rapidly, levees grew and avulsion replaced migration as the common type of channel switching, creating stacked, amalgamated channel sandstone bodies (interval a; Fig. 7). Levees also partitioned the floodplain, temporarily starving the poorly drained interfluves of sediment supply, permitting available accommodation to fill with thick peat. At the climax of the rate of base-level rise, accommodation reached a maximum, and river competence and gradient each reached a minimum. Avulsions and splays periodically deposited sheets of mud in interfluves (interval b), and the channel system split into a system of anastomosing distributaries (Törnqvist, 1993, describes a similar transition in the Rhine-Meuse delta during late Holocene base-level rise). The geometries of channel fills in the lower HCF packages suggest that drainage planform alternated between a Type 1b or 1c (anastomosing river system depositing mostly organic-rich mud by avulsion) and Type 3 (mixed-load laterally active anabranching rivers) *sensu* Nanson and Knighton (1996) during the deposition of each package. Owing to increasing accommodation, these narrow streams were abandoned and filled rapidly (see Smith et al., 1989; Nadon, 1994), preserved as encased channel fills. As aggradation exceeded accommodation, better-drained forest soils formed on broad levees at the expense of interfluve bogs (interval c). From waning base-level rise to highstand, accommodation decreased, and abandoned channels, avulsions, and splays left thinner, more closely packed sandy deposits between thinly bedded floodplain mudrocks (interval d; Törnqvist, 1993). Two-thirds of the typical package accumulated between the highest rate of base-level rise and immediately after highstand, following the model of Posamentier and Vail (1988).

During highstand, the anastomosing channels coalesced into fewer channels (Smith et al., 1989) and built levees of silty sand, forming the internal surface of the typical package (interval e). Avulsion ceased, and vegetated soils that developed on levees restricted lateral migration. The upward broadening and thinning of channel sandstone bodies and the upward increase in paleosol maturity in the package archetype resulted from diminishing accommodation space on the floodplain following highstand, in accordance with Wright and Marriott's (1993) model. During early base-level fall, the distributaries coalesced through channel abandonment, forming ribbon-like depressions filled with organic-rich silt and mud (interval f). A few

channels gradually assumed the majority of the discharge, and rare floods or crevassing events resulted in stacks of extensive thin splays (preserved and modern examples described by Lehman, 1982; Smith and Perez-Arlucea, 1994) rather than new channels (interval g). The abandonment of the floodplain during late base-level fall resulted in long periods of pedogenesis (see Behrensmeyer, 1987; Bown and Kraus, 1993; Willis and Behrensmeyer, 1994; Behrensmeyer et al., 1995 for examples from the Siwaliks and from the Willwood Formation) between local deposition of sheets of muddy sediments from levees and distal splays (see Ghosh, 1987). Carbon dioxide from the decay of buried organic material and iron leached during soil formation mixed at the top of the water table and precipitated nodular siderite. During middle and late base-level fall, the river system reverted to a single-channel drainage that reworked uppermost floodplain sediments by lateral migration, creating the scour at the base of the next package, thereby completing the depositional cycle.

The variation of form among the ten packages in the lower HCF is interpreted as a response to the base-level rise and fall associated with the construction of the clastic wedge, occurring over a period of approximately 2 myr (Catuneanu and Sweet, 1999). The combination of this grand-scale cycle of base-level change (Fig. 8A) with ten smaller oscillations (Fig. 8B) describes a complex variation in accommodation availability through time (Fig. 8C). During later grand base-level rise and stillstand, accommodation space was produced continuously through each package-scale cycle, resulting in several full-thickness, thickly-bedded packages with more accumulation below the internal surface than above (packages A-D, Fig. 6). Coals, organic-rich mudrocks, and encased channel fills common in these packages are consistent with rapid aggradation. After grand highstand, the smaller cycle base-level fall allowed periods of zero and negative net accommodation, producing progressively thinner packages with greater erosional truncation at the tops (packages E-G). Reduced accommodation during the formation of these packages resulted in thin bedding, pedogenesis of mudrocks, and stacking of splays and levees, all characteristics of progradation and bypass. Grand base-level fall resulted in complete bypass or erosion during times of zero accommodation in each smaller-scale cycle, resulting in very little or no deposition and possibly creating a significant unconformity in the fluvial strata. During grand-cycle lowstand, the small-scale variation again controlled deposition, resulting in thin packages containing levees, paleosols, and possibly marine influence, and recording only small net accommodation increases (packages H-J).

Under this interpretation, the two surfaces in each package mark important changes in the rate of creation of accommodation space. The scour at the base of each package represents a surface of floodplain abandonment and incision during base-level lowstand. These surfaces incise paleosols and underlie point bar accumulations, both suggesting low accommodation availability. The internal surface in each package records base-level highstand. As no inundation occurs, this is not a true flooding surface, which does not form in floodplain deposits. Instead it marks the change from aggradation to progradation and bypass, a reduction in the rate of formation of accommodation space. This reduction creates the division of the typical package; the post-highstand deposits are thinner than pre-highstand in thick packages, and absent in thin packages.

INTERPRETATION OF FOSSIL HORIZON DEVELOPMENT

Structure, thickness, content, and stratigraphic position of fossiliferous horizons in the lower HCF packages were controlled by regional deposition rate, modified by the related interplay of the grand- and package-scale cycles in accommodation. Burial of fossils occurred during periods in which the mean regional depositional rate achieved a specific low, optimum rate for bone burial. Above this rate, individual bones were buried and preserved but highly dispersed in large volumes of sediment; below this rate, bones decomposed at the surface prior to burial or were exhumed and destroyed during periods of reworking. The density of fossil sites declines in the intervals immediately above and below fossiliferous horizons; if the site density in the fossiliferous horizon records an optimum burial rate, these less fossiliferous intervals suggest a burial rate diverging from the optimum through time.

During periods in which the grand-scale cycle of base level change boosted accommodation space when package-scale base-level rose (packages A-D, Fig. 6), potential fossils were swamped by sediment except during package highstand and fall, when mean deposition rates were least. At grand-cycle maximum, mean depositional rate was close to the optimum throughout package deposition, resulting in a scatter of sites through the package (package D) while still emphasizing depositional rate minima associated with package surfaces. Early grand-cycle fall reduced accommodation space during package-scale base-level rise and eliminated it after package-scale highstand, creating successively thinner packages without internal surfaces (packages E-G), in which the optimum depositional rate was recorded only after each package scour formed.

During grand-cycle fall, accommodation space was seldom available, allowing long-term pedogenesis and possibly erosion of previously deposited fossiliferous strata. During grand-cycle recovery, accommodation space was available only during package-scale base-level rise, forming thin packages with sparse fossiliferous horizons above each basal scour (packages H-J).

A model of lower HCF deposition based on the simple curves describing accommodation availability through time (Fig. 8A-C) can be extended to test depositional rate as a control for fossil preservation. Assuming that at each time increment the available accommodation was filled, a relative proxy for depositional rate can be calculated (Fig. 8D, E). Changing the model's vertical axis from time (Fig. 8E) to preserved accommodation displays accumulated thickness in a simulation of the HCF rock record (Fig. 8F, G). The model predicts the division of the hypothetical succession into ten intervals, each bounded by lowstand markers and each split unevenly by highstand markers. If the lowstand and highstand markers in the hypothetical succession correspond to the basal scour and internal surfaces, respectively, of HCF packages, then the ten hypothetical packages in the model also have a similar three-fold hierarchy of form as the lower HCF (4 large packages of nearly equal thickness; 3 packages of successively diminishing thickness; and 3 thin packages without highstand markers; Fig. 8F). Although the model provides no prediction for actual counts of fossil sites per increment of deposition, a relative measure of the potential for bone burial can be calculated by comparing the depositional rate in each increment to an optimum bone burial rate (Fig. 8G). In increments in which the depositional rate is similar to the optimum burial rate, the likelihood of burying bone is high, whereas for increments with a dissimilar depositional rate the likelihood is low or zero. The resulting distribution and shape of peaks in fossil burial potential in the model (Fig. 8G) resemble the stratigraphic position and shape of fossiliferous horizons in the lower HCF (dense isolated horizons on highstands in lower packages; thinner and weaker horizons on stillstands in middle packages; and a non-fossiliferous gap at the top). Changing any one of the parameters (cycle amplitudes and offsets, optimum burial rate, subsidence rate, etc.) in this mathematical model creates a very different distribution of fossiliferous and nonfossiliferous intervals, suggesting that terrestrial vertebrate distribution may allow for a semi-quantitative discrimination of various local controls on accommodation. Similar, more comprehensive numerical models have predicted complex patterns of fossil distribution in marine sequences as a succession of fossiliferous horizons and nonfossiliferous intervals

(Holland, 1995, 2000; Holland and Patzkowsky, 1999). The model used herein is included as part of the data repository (Appendix).

DISCUSSION: FLUVIAL PACKAGES

The typical lower HCF package described here is similar to models developed from other fluvial successions. Portions of the Kaiparowits Plateau and the Book Cliffs of Utah each have been used to design an architectural model for cyclic fluvial deposition (Shanley and McCabe, 1991, 1993, 1995; Kamola and Van Wagoner, 1995; Olsen et al., 1995). Studies of stacked paleosols in alluvial successions have produced similar results (Behrensmeyer, 1987; Bown and Kraus, 1987, 1993; Behrensmeyer et al., 1995; Currie, 1997). Theoretical interpretations of fluvial sedimentation describe repeating cycles in facies and architecture (Goodwin and Anderson, 1985; Posamentier and Vail, 1988; Galloway, 1989; Jordan and Flemings, 1991; Wright and Marriott, 1993; Martinsen et al., 1999). Both types of interpretations attribute the facies distribution and structure to variations of accommodation controlled, in turn, by three component forces: tectonic uplift and subsidence, eustasy, and climate. Of these three, subsidence appears to have played a crucial role in the relatively continuous production of accommodation space, possibly as the mechanism behind the grand-scale variation in base-level (Shanley and McCabe, 1998). The package-scale rhythms in fluvial strata occur on time-scales consistent with Milankovitch cycles and may represent direct climatic control on precipitation (Martinius, 2000) or some indirect control, such as fluctuations of sea-ice volume during the Cretaceous (Stoll and Schrag, 1996; Miller et al., 1999). Given the number of different regions, depositional environments, and time intervals in which the same general rhythm forms in fully fluvial strata, package structure appears to be independent of the individual factors controlling accommodation and base level.

A critical element in the description of accommodation-controlled repeating structure in sedimentary successions is the presence of easily detectable reference surfaces, but these lithologic boundaries are difficult to recognize in fluvial rocks. In coastal margin and marine settings, unconformities at the juxtaposition of marine and fluvial facies mark flooding and withdrawal surfaces, but these boundaries disappear inland with the absence of marine facies. For example, an extensively bioturbated surface beneath Coal Seam 1 in the basal HCF exposures near Willow Creek is associated with a drop in mean sea level (Ainsworth, 1991, 1994;

Straight and Eberth, 1998) but is not traceable more than 3.2 km updip. Ideally, transgressive flooding surfaces, represented in shelf deposits as the condensed section, should correlate inland to the entire portion of the typical package beneath the internal surface rather than the surface itself. Although the basal scours under sandstone bodies create easily visible surfaces representing the base-level lowstand, these are laterally discontinuous in the lower HCF (Fig. 3) and untraceable in thick intervals of mudrocks. Best and Ashworth (1997) cautioned against the interpretation of scours as bounding surfaces where scour relief is less than five times the bankfull depth and interbasin continuity of surfaces cannot be ascertained, both of which are true in the lower HCF. Further, the scour is not truly isochronous, formed by lateral migration and/or channel avulsion over a period of relatively low accommodation (Wright and Marriott, 1993; Olsen et al., 1995).

In the absence of clear lithological surfaces, the tops and bottoms of marker intervals might be used as reference points, but these similarly are unreliable in the lower HCF. The sandstone units and coal seams make poor markers because they are laterally discontinuous, removed by later erosion in places, and highly variable in thickness, internal construction, and content. Laterally continuous splays form terraces that resist erosion and may represent a short enough time interval to make useful markers, but all four such terraces in the 210 m of the lower HCF cluster between Coal Seams 7 and 8b, a range of about 30 m vertically. Paleosols of the lower HCF are often little more than zones of preserved rooting, and are too rare and too poorly developed to serve adequately as markers. Intense leaching zones are absent in the lower HCF. In this case, lithologic surfaces alone are not adequate to subdivide the lower HCF. Thus, package structure is described here first on the basis of repeating stacking patterns in facies associations, rather than starting with the identification of important surfaces.

In contrast to other markers, fossiliferous horizons in the lower HCF are laterally extensive, relatively continuous, and independent of facies. They can be identified easily in the field, even in intervals dominated by mudrocks or paleosols. They correlate stratigraphically to the position of the important internal surfaces and basal scours of the packages in the lower HCF. Horizon density and composition appear to provide information on variations in accommodation within packages as well as variation between packages. Hence, the terrestrial fossil record provides a powerful tool to aid in the recognition, description, and interpretation of package structure in the lower HCF, and possibly in other time-equivalent strata.

The terrestrial fossil record at other sites may reflect package structure similar to that of the lower HCF. The stratigraphic distribution of dinosaur remains in the upper 60 m of the Hell Creek Formation from Montana (Sheehan et al., 2000) is described in terms of individual animals rather than sites, but particular intervals stand out as relatively more fossiliferous horizons than the formation average. The variation in fossil yield may indicate the presence of important surfaces associated with depositional cycles. Vertebrate remains were preserved in migrating point bars in highly sinuous meandering river systems of the Dinosaur Park Formation (Wood et al., 1988; Eberth, 1990; Brinkman et al., 1998), as reworked lags in the channels of the Straight Cliffs of Utah (Shanley and McCabe, 1991, 1993, 1995; Shanley et al., 1992), in channel lags, abandoned channel fill, splays, and paleosols in the Siwalik Dhok Pathan and Nagri Formations of Pakistan (Badgley, 1986; Behrensmeyer, 1987, 1988; Willis and Behrensmeyer, 1994), and in well-developed cross-cutting soil horizons of the Eocene Willwood Formation (Bown and Kraus, 1993). All these facies are associated with low, stable or falling accommodation. Such conditions are consistent with the formation of fossiliferous horizons during stillstands, as in the lower HCF.

Although the terrestrial vertebrate fossil record of the Campanian Two Medicine Formation is similar to that the lower HCF, there appears to be only poor correlation between stratigraphic position of two third-order sequence boundaries and the distribution of vertebrate remains (Rogers and Kidwell, 2000). The difference in correlation may have arisen because the surfaces revealed by horizons in the lower HCF are probably of fourth or higher order because they represent internal partitions of a single clastic wedge. If a third-order surface is present in the lower HCF, it would be at the base of the Drumheller Marine Tongue, the scour between packages G and H. Fossil remains are comparatively rare in package G and package H is almost nonfossiliferous, consistent with the results of Rogers and Kidwell (2000). The relatively shorter duration of fourth- or higher-order depositional hiatuses may make them more compatible with taphonomic processes than the duration of third-order breaks.

DISCUSSION: HORIZON FORMATION

In the present interpretation, sedimentation rate is the dominant control on the distribution of fossil sites in the lower HCF. Vertebrate remains are effectively large (grain-size) clasts; hence, their accumulation

and burial depend at least in part on accommodation availability and sediment supply. Bonebeds and fossiliferous horizons accumulated in conjunction with surfaces associated with low but nonzero accommodation and therefore under a low regional sedimentation rate. However, other potential controls of site distribution and preservation—ecological distribution of animals, environment, and post-depositional diagenetic pathway—must be examined as potentially important factors in the accumulation of lower HCF fossiliferous horizons.

Diagenesis after burial selectively favors or destroys accumulations based on groundwater and sediment chemistry. Fossiliferous horizons might be formed by selective, post-burial destruction of bone by some combination of pedogenic processes, groundwater dissolution, and microbial activity. However, most fossils in the lower HCF are buried in clay-rich mudrocks, generally more resistant to groundwater flow than sandy channel facies. Lower HCF strata are also entirely lacking bone casts or pseudomorphs. Mineralization from groundwater in sandy facies formed siderite nodules around bones instead of dissolving them. The abundance of siderite in lower HCF argues for high groundwater pH (Bao et al., 1998), well above levels at which bone mineral is insoluble (Lucas and Prévôt, 1991). Even where remains were deposited in peat, wherein groundwater pH approached bone solubility, HCF fossils are composed of carbonate hydroxyapatite, typical of fossilization in fluvial deposits with little alteration except recrystallization (Lucas and Prévôt, 1991; Person et al., 1995). Although diagenesis may act as a regulator of fossil preservation in some fluvial successions, it is a minor participant in the lower HCF.

Environment controls the effects of climate, precipitation, surface exposure, and topography on the spatial distribution of remains. Hence, where environmental control is dominant, the distribution of fossil sites would likely be a patchy, facies-dependent distribution, consistent with a mosaic of local microenvironments, rather than a facies-independent, even spread of remains. Given the lack of correlation between facies and sites in the lower HCF, specific microenvironments do not appear to have contributed to bone preservation. Although facies associations representing the suite of interfluve environments incorporate the majority of sites in the lower HCF, there are intervals of equal thickness and of the same associations that are essentially nonfossiliferous. Thus, environment appears to be a secondary control of fossil distribution in the lower HCF.

The ecological distribution of animals and plants controls the diversity and abundance of remains supplied to the taphonomic filter. Fossiliferous horizons might result if faunal populations on the clastic wedge were strongly variable. However, horizons formed by this control should have no particular connection to depositional surfaces unless the variations in population density were indirectly controlled by another factor that also contributed to burial, such as sedimentation rate or environment. For example, a highly populated ecotone that paralleled a coastline and moved with it during base-level changes might have buried remains only during the formation of highstand surfaces. In order to form the fossiliferous horizons preserved in the lower HCF, the terrain flanking the ecotone would have been nearly uninhabited, inconsistent with modern tetrapod population distribution. To produce the fossil record of the lower HCF, a second high-population ecotone would have had to parallel the first to manufacture horizons associated with lowstand deposits. Although unlikely, this scenario cannot be ruled out by the sedimentologic and taphonomic data presented here.

SUMMARY

A growing mass of research into terrestrial strata reveals repeating rhythms in fluvial deposits. A similar pattern was found in the tidally influenced coastal margin and fluvial sediments of the lower Horseshoe Canyon Formation, exposed in the Red Deer River Valley around Drumheller, Alberta, Canada. In this 210-m-thick clastic succession, each repetition of the package occurs as an upward-fining chronostratigraphic sheet of strata, with a basal scour-bottomed sandstone body or amalgamated channel sandstone, overlain by mudrocks encasing narrow sand-filled channels, then splays, levees, and/or paleosols. The vertical and lateral juxtaposition of facies in each of the ten packages was moderated by a fall-rise-fall cycle in base-level, consistent with interpretations of package-like rhythms of other studies. Two important stratigraphic surfaces in the typical package, the basal scour and an internal surface, correspond to the base-level highstand and lowstand, respectively. These surfaces are laterally discontinuous, hard to locate in the field, and not always preserved, limiting their usefulness in assembling a sequence-stratigraphic framework in this fluvial succession.

Terrestrial vertebrate fossil occurrence in the lower HCF, based on field surveys of surface fossil yield, is facies-independent but linked to cyclic stacking patterns in fluvial facies. Relatively high-density accumulations of fossil sites (horizons) correspond to most of the stratigraphic surfaces preserved in the ten packages in the lower HCF. Fossiliferous horizons were formed by low sedimentation rate and low accommodation associated with stillstands. Variations in the fossil density of successive horizons through the lower HCF arise from the interaction of the package-scale base-level cycle with the grand-scale cycle associated with the formation of the clastic wedge. The lowest four packages, A through D, are each ~31 m thick and feature a fossiliferous horizon on the internal (highstand) surface. Packages E through G are successively thinner and feature fossiliferous horizons on each basal scour and numerous solitary sites throughout. Packages H, I, and J are associated with the transgressive Drumheller Marine Tongue and are nearly nonfossiliferous.

Terrestrial vertebrate fossils have received little attention as information from which to construct stratigraphic frameworks in fluvial successions, but in the lower Horseshoe Canyon Formation they not only recapitulate nearly invisible stratigraphic surfaces but also provide insight into the interplay of two scales of base-level variation. Earlier studies indicate that fossil distribution in other fluvial successions may preserve information for the construction of architectural frameworks. The fossil distributions within other fluvial successions need to be tested to assess the power and scope of the terrestrial fossil record as a tool for revealing stratigraphic frameworks.

ACKNOWLEDGEMENTS

The senior author wishes to thank Jonathan Perry and Patty Ralrick for extreme dedication during the field surveys. Thanks to the families of Victor Garson, David Hardy, Tyler and Randy James, Clint Moar, Brian Neill, Arnold Pascoe, Lloyd Riggs, Robert Tolman, Harry Wade, and Clint Watson for access to exposures on family property in the Drumheller area; please request permission before visiting any site on private property. Special thanks to Becky Kowalchuk, Donna Sloan, and the rest of the staff and students at the Royal Tyrrell Museum. The assistance, criticisms, and patience of Reese Barrick, Elana Leithold, Dale Russell, Alan Coulson, and two anonymous reviewers are appreciated. This project was partially funded by the Heaton

Student Support Grant through the Royal Tyrrell Museum of Palaeontology and by donations to the Sedimentary Geology Program by numerous hydrocarbon companies in Western Canada.

LITERATURE CITED

Ainsworth, R.B., 1991, Sedimentology and high resolution sequence stratigraphy of the Bearpaw-Horseshoe Canyon Transition (Upper Cretaceous), Drumheller, Alberta, Canada: Unpublished Master's Thesis, McMaster University, Hamilton, Ontario. 213 p.

Ainsworth, R.B., 1994, Marginal marine sedimentology and high resolution sequence analysis; Bearpaw-Horseshoe Canyon transition, Drumheller, Alberta, Canada: Bulletin of Canadian Petroleum Geology, v. 42, p. 26-54.

Ainsworth, R.B., and Walker, R.G., 1994, Control of estuarine valley-fill deposition by fluctuations of relative sea-level, Cretaceous Bearpaw-Horseshoe Canyon Transition, Drumheller, Alberta, Canada: *in* Dalrymple, R.W., and Zaitlin, B.A., eds., Incised-valley systems: Origin and sedimentary sequences: Society of Economic Paleontologists and Mineralogists, Special Publication No. 51, p. 159-174.

Aitken, J.F., and Flint, S.S., 1994, High-frequency sequences and the nature of incised-valley fills in fluvial systems of the Breathitt Group (Pennsylvanian), Appalachian Foreland Basin, Eastern Kentucky: *in* Dalrymple, R.W., and Zaitlin, B.A., eds., Incised-valley systems: Origin and sedimentary sequences: Society of Economic Paleontologists and Mineralogists, Special Publication No. 51, p. 353-368.

Aitken, J.F., and Flint, S.S., 1995, The application of high-resolution sequence stratigraphy to fluvial systems: A case study from the Upper Carboniferous Breathitt Group, eastern Kentucky, USA: Sedimentology, v. 42, p. 3-30.

Allan, J.A., 1922, Geology of the Drumheller coal field, Alberta: Research Council of Alberta, Report 4, 78 p.

Allan, J.A., and Sanderson, J.O.G., 1945, Geology of the Red Deer and Rosebud sheets, Alberta: Research Council of Alberta, Report 13, 115 p.

Aslan, A., and Autin, W.J., 1998, Holocene flood-plain soil formation in the southern lower Mississippi Valley: Implications for interpreting alluvial paleosols: Geological Society of America Bulletin, v. 110, p. 433-449.

Aslan, A., and Autin, W.J., 1999, Evolution of the Holocene Mississippian River floodplain, Ferriday, Louisiana: Insights on the origin of find-grained floodplain: Journal of Sedimentary Research, v. 69, p. 800-815.

Badgley, C., 1986, Taphonomy of mammalian fossil remains from Siwalik rocks of Pakistan: Paleobiology, v. 12, p. 119-142.

Banerjee, I., and Kidwell, S.M., 1991, Significance of molluscan shell beds in sequence stratigraphy: An example from the lower Cretaceous Manville Group of Canada: Sedimentology, v. 38, p. 913-934.

Bao, H., Koch, P. L., and Hepple, R. P., 1998, Hematite and calcite coatings on fossil vertebrates: Journal of Sedimentary Research, v.68, p. 727-738.

Behrensmeyer, A.K., 1987, Miocene fluvial facies and vertebrate taphonomy in northern Pakistan: *in* Ethridge, F.G., Flores, R.M., and Harvey, M.D., eds., Recent developments in fluvial sedimentology: Society of Economic Paleontologists and Mineralogists, Special Publication No. 39, p. 169-176.

Behrensmeyer, A.K., 1988, Vertebrate preservation in fluvial channels: Palaeogeography, Palaeoclimatology, Palaeoecology, v. 63, p. 183-199.

Behrensmeyer, A.K., Willis, B.J., and Quade, J., 1995, Floodplains and paleosols of Pakistan Neogene and Wyoming Paleogene deposits: A comparative study: Palaeogeography, Palaeoclimatology, Palaeoecology, v. 115, p. 37-90.

Best, J.L., and Ashworth, P.J., 1997, Scour in large braided rivers and the recognition of sequence stratigraphic boundaries: Nature, v. 387, p. 275-277.

Bhattacharya, J., 1989, Estuarine channel fills in the Upper Cretaceous Dunvegan Formation: core examples: *in* Reinson, G.E., ed., Modern and ancient examples of clastic tidal deposits: A core and peel workshop, Canadian Society of Petroleum Geologists' Short Course Guide: Second International Research Symposium on Clastic Tidal Deposits, Calgary, Alberta, p. 37-49.

Blum, M.D., and Törnqvist, T.E., 2000, Fluvial response to climate and sea-level change: A review and look forward: Sedimentology, v.47, p. 2-48.

Bown, T.M., and Kraus, M.J., 1987, Integration of channel and floodplain suites, I. Developmental sequence and lateral relations of alluvial paleosols: Journal of Sedimentary Petrology, v. 57, p. 587-601.

Bown, T.M., and Kraus, M.J., 1993, Time-stratigraphic reconstruction of paleopedologic, sedimentologic, and biotic events (Willwood Formation, Lower Eocene, northwest Wyoming, U.S.A.): PALAIOS, v. 8, p. 68-80.

Brett, C.E., 1995, Sequence stratigraphy, biostratigraphy, and taphonomy in shallow marine environments: PALAIOS, v. 10, p. 597-616.

Brett, C.E., 1998, Sequence stratigraphy, paleoecology, and evolution: Biotic clues and responses to sea-level fluctuations: PALAIOS, v. 13, p. 241-262.

Breyer, J.A., 1997, Sequence stratigraphy of Gulf Coast lignite, Wilcox Group (Paleogene), south Texas: Journal of Sedimentary Research v. B67, p. 1018-1029.

Brinkman, D.B., 1990, Paleoecology of the Judith River Formation (Campanian) of Dinosaur Provincial Park, Alberta, Canada: Evidence from vertebrate microfossil localities: Palaeogeography, Palaeoclimatology, Palaeoecology, v. 78, p. 37-54.

Brinkman, D.B., Ryan, M., and Eberth, D.A., 1998, The paleogeographic and stratigraphic distribution of Ceratopsids (Ornithischia) in the Upper Judith River Group of Western Canada: PALAIOS, v. 13, p. 160-169.

Cant, D.J., 1998, Sequence stratigraphy, subsidence rates, and alluvial facies, Mannville group, Alberta foreland basin: *in* Shanley, K.W., and McCabe, P.J., eds., Relative role of eustasy, climate, and tectonism in continental rocks: Society of Economic Paleontologists and Mineralogists, Special Publication No. 59, p. 49-64.

Cant, D.J., and Stockmal, G.S., 1989, The Alberta foreland basin: Relationship between stratigraphy and Cordilleran terrane-accretion events: Canadian Journal of Earth Sciences, v. 26, p. 1964-1975.

Catuneanu, O., and Sweet, A.R., 1999, Maastrichtian-Paleocene foreland-basin stratigraphies, western Canada: A reciprocal sequence architecture: Canadian Journal of Earth Science, v. 36, p. 685-703.

Currie, B.S., 1997, Sequence stratigraphy of non-marine Jurassic-Cretaceous rocks, central Cordilleran foreland-basin system: Geological Society of America Bulletin, v.109, p.1206-1222.

Davies-Vollum, K.S., and Wing, S.L., 1998, Sedimentological, taphonomic, and climatic aspects of Eocene swamp deposits (Willwood Formation, Bighorn Basin, Wyoming): PALAIOS, v. 13, p. 28-40.

Eberth, D.A., 1990, Stratigraphy and sedimentology of vertebrate microfossil sites in the uppermost Judith River Formation (Campanian), Dinosaur Provincial Park, Alberta, Canada: Palaeogeography, Palaeoclimatology, Palaeoecology, v. 78, p. 1-35.

Eberth, D.A., 1995, Bearpaw/Horseshoe Canyon Formation transition (Maastrichtian) in the East Coulee/ Willow Creek area: Field Trip Guidebook, Canadian Society of Petroleum Geologists One Day Field Trip, 43 p.

Eberth, D.A., 1996, Origin and significance of mud-filled incised valleys (Upper Cretaceous) in southern Alberta, Canada: Sedimentology, v. 43, p. 459-477.

Galloway, W.E., 1989, Genetic stratigraphic sequences in basin analysis I: Architecture and genesis of flooding-surface bounded depositional units: American Association of Petroleum Geologists Bulletin, v. 73, p. 125-142.

Ghosh, S.K., 1987, Cyclicity and facies characters of alluvial sediment in the Upper Paleozoic Monongahela-Dunkard Groups, Central West Virginia: *in* Ethridge, F.G., Flores, R.M., and Harvey, M.D., eds., Recent developments in fluvial sedimentology: Society of Economic Paleontologists and Mineralogists, Special Publication No. 39, p. 159-168.

Gibson, D.W., 1977, Upper Cretaceous and Tertiary coal-bearing strata in the Drumheller-Ardley region, Red Deer River Valley, Alberta: Geological Survey of Canada Paper 76-35, 41 p.

Goodwin, P.W., and Anderson, E.J., 1985, Punctuated aggradational cycles: A general hypothesis of episodic stratigraphic accumulation: Journal of Geology, v. 93, p. 515-533.

Haglund, W.M., 2001, Faunal distribution within the Drumheller Marine Tongue: *in* Allen, H., ed., Alberta Palaeontological Society Fifth Annual Symposium Abstracts, Mount Royal College, Calgary, Alberta, University of Calgary Press, p. 25.

Hamblin, A.P., 1998a, Detailed outcrop measured sections of the St. Mary River/Horseshoe Canyon Formations, Little Bow River and Travers Reservoir, near Carmangay, southern Alberta: Geological Survey of Canada Open File Report 3574, 9 p.

Hamblin, A.P., 1998b, Edmonton Group / St. Mary River Formation: Summary of literature and concepts: Geological Survey of Canada Open File Report 3578, 36 p.

Holbrook, J.M., and White, D.C., 1998, Evidence for subtle uplift from lithofacies distribution and sequence architecture: Examples from lower Cretaceous strata of northeastern New Mexico: *in* Shanley, K.W., and McCabe, P.J., eds., Relative role of eustasy, climate, and tectonism in continental rocks: Society of Economic Paleontologists and Mineralogists, Special Publication No. 59, p. 124-132.

Holland, S.M., 1995, The stratigraphic distribution of fossils: Paleobiology, v. 21, p. 92-109.

Holland, S.M., 2000, The quality of the fossil record: A sequence stratigraphic perspective: Paleobiology, v. 26, p. 148-168.

Holland, S.M., and Patzkowsky, M.E., 1999, Models for simulating the fossil record: Geology, v. 27, p. 491-494.

Irish, E.J.W., 1970, The Edmonton Group of south-central Alberta: Bulletin of Canadian Petroleum Geology, v. 18, p. 125-155.

Jerzykiewicz, T., and Norris, D.K., 1993, Evolution of the Laramide Foredeep and the adjacent thrust belt in southern Alberta: Geological Survey of Canada Open File Report 2663, 98 p.

Jordan, T.E., and Flemings, P.B., 1991, Large-scale stratigraphic architecture, eustatic variation, and unsteady tectonism: A theoretical evaluation: Journal of Geophysical Research, v. 96B, p. 6681-6699.

Kamola, D.L., and Van Wagoner, J.C., 1995, Stratigraphy and facies architecture of parasequences with examples from the Spring Canyon Member, Blackhawk Formation, Utah: *in* Van Wagoner, J.C., and Bertram, G.T., eds., Sequence stratigraphy of foreland basin deposits: Outcrop and subsurface examples from the Cretaceous of North America: American Association of Petroleum Geologists, Memoir 64, p. 27-55.

Kidwell, S.M., 1986, Models for fossil concentrations: Paleobiologic implications: Paleobiology, v. 12, p. 6-24.

Kidwell, S.M., 1988a, Taphonomic comparison of passive and active continental margins: Neogene shell beds of the Atlantic coastal plain and northern Gulf of California: Palaeogeography, Palaeoclimatology, Palaeoecology, v. 63, p. 201-223.

Kidwell, S.M., 1988b, Reciprocal sedimentation and noncorrelative hiatuses in marine-paralic siliciclastics: Miocene outcrop evidence: Geology, v. 16, p. 609-612.

Kidwell, S.M., 1989, Stratigraphic condensation of marine transgressive records: Origin of major shell deposits in the Miocene of Maryland: Journal of Geology, v. 97, p. 1-24.

Langston, W. Jr., 1959, Alberta and fossil vertebrates: Alberta Society of Petroleum Geologists 9th Annual Field Conference Guidebook—Moose Mountain-Drumheller, p. 8-12.

Legarreta, L., and Uliana, M.A., 1998, Anatomy of hinterland depositional sequences: Upper Cretaceous fluvial strata, Neuquen Basin, west-central Argentina: *in* Shanley, K.W., and McCabe, P.J., eds., Relative role of eustasy, climate, and tectonism in continental rocks: Society of Economic Paleontologists and Mineralogists, Special Publication No. 59, p. 83-92.

Lehman, T.M., 1982, A Ceratopsian Bone Bed from the Aguja Formation (Upper Cretaceous) Big Bend National Park, Texas: Unpublished Master's thesis, University of Texas at Austin, 210 p.

Lucas, J., and Prévôt, L.E., 1991, Phosphates and fossil preservation: *in* Allison, P.A. and Briggs, D. E. G., eds., Taphonomy: Releasing the Data Locked in the Fossil Record, Plenum Press, New York, p. 389-409.

Martinius, A.W., 2000, Labyrinthine facies architecture of the Tortola fluvial system and controls on deposition (Late Oligocene-Early Miocene, Loranca Basin, Spain): Journal of Sedimentary Research, v. B70, p. 850-867.

Martinsen, O.J., Ryseth, A., Helland-Hansen, W., Flesche, H., Torkildsen, G., and Idil, S., 1999, Stratigraphic base-level and fluvial architecture: Ericson Sandstone (Campanian), Rock Springs Uplift, SW Wyoming, USA: Sedimentology, v. 46, p. 235-259.

McCabe, P.J., Strobl, R.S., Macdonald, D.E., Nurkowski, J.R., and Bosman, A., 1989, An evaluation of the coal resources of the Horseshoe Canyon Formation and laterally equivalent strata, to a depth of 400m, in the Alberta plains area: Alberta Research Council Open File Report No. 1989-07 A, 75 p.

Miall, A.D., 1978, Facies types and vertical profile models in braided river deposits: a summary: *in* Miall, A.D., ed., Fluvial Sedimentology: Canadian Society of Petroleum Geologists, Memoir 5, p. 597-604.

Miall, A.D., 1992, Alluvial deposits: *in* Walker, R.G., and James, N.P., eds., Facies Models: Response to Sea Level Change: Geological Association of Canada, p. 119-142.

Miller, G.M., Barrera, E., Olsson, R.K., Sugarman, P.J., and Savin, S.M., 1999, Does ice drive early Maastrichtian eustasy?: Geology, v. 27, p. 783-786.

Nadon, G.C., 1994, The genesis and recognition of anastomosed fluvial deposits: Data from the St. Mary River Formation, southwestern Alberta, Canada: Journal of Sedimentary Research, v. B64, p. 451-463.

Nanson, G.C., and Knighton, A.D., 1996, Anabranching rivers: Their causes, character, and classification: Earth Surface Process and Landforms, v. 21, p. 217-239.

Nichols, G.J., and Hirst, J.P., 1998, Alluvial fans and fluvial distributary systems, Oligo-Miocene, northern Spain: Contrasting processes and products: Journal of Sedimentary Research, v. A68, p. 879-889.

Nurkowski, J.R., 1980, Geology and coal resources of the upper part of the Horseshoe Canyon Formation, Red Deer area, Alberta: Alberta Research Council Open File Report No. 1980-10, 47 p.

Nurkowski, J.R., and Rahmani, R.A., 1984, Cretaceous fluvio-lacustrine coal-bearing sequence, Red Deer area, Alberta, Canada: *in* Rahmani, R.A., and Flores, R.M., eds., Sedimentology of coal and coal-bearing sequences: International Association of Sedimentologists Special Publication No. 7, p. 163-176.

Olsen, T., Steel, R., Hogseth, K., Skar, T., and Roe, S.L., 1995, Sequential architecture in a fluvial succession: Sequence stratigraphy in the Upper Cretaceous Mesa Verde Group, Price Canyon, Utah: Journal of Sedimentary Research, v. B65, p. 265-280.

Ower, J.R., 1960, The Edmonton Formation: Journal of the Alberta Society of Petroleum Geologists, v. 8, p. 309-323.

Pagani, S.E., 1985, A sand-filled meandering channel, upper Horseshoe Canyon Formation (Upper Cretaceous), Drumheller, Alberta: Unpublished Bachelor's Thesis, McMaster University, Hamilton, Ontario, Canada, 92 p.

Person, A., Bocherens, H., Saliege, J.F., Paris, F., Zeitoun, V., and Gerard, M., 1995, Early diagenetic evolution of bone phosphate: An X-ray diffractometry analysis: Journal of Archaeological Science, v. 22, p. 211-221.

Posamentier, H.W., and Vail, P.R., 1988, Eustatic controls on clastic deposition, II. Sequence and systems tract models: *in* Wilgus, C.K., Hastings, B.S., Kendall, C.G.S., Posamentier, H.W., Ross, C.A., and Van Wagoner, J.C., eds., Sea-level changes: An integrated approach: Society of Economic Paleontologists and Mineralogists, Special Publication No. 42, p. 125-154.

Rahmani, R.A., 1988, Estuarine tidal channel and nearshore sedimentation of a Late Cretaceous epicontinental sea, Drumheller, Alberta, Canada: *in* de Boer, P.L., van Gelder, A., and Nio, S.D. eds., Tidal-Influenced Sedimentary Environments and Facies: D. Reidel Publishing Company, Dordrecht, p. 433-471.

Rahmani, R.A., 1989, Cretaceous tidal estuarine and deltaic deposits, Drumheller, Alberta: Canadian Society of Petroleum Geologists' field guide, Second International Research Symposium on Clastic Tidal Deposits, Calgary, Alberta, 55 p.

Rahmani, R.A., and Hills, L.V., 1982, Facies relationships and paleoenvironments of a Late Cretaceous tide-dominated delta, Drumheller, Alberta: Canadian Society of Petroleum Geologists Field Guide, Trip 6, AAPG Annual Convention, Calgary, 43 p.

Retallack, G.J., 1990, Soils of the Past: An Introduction to Paleopedology: Harper Collins Academic Press, London, 520 p.

Robinson, J.W., and McCabe, P.J., 1998, Evolution of a braided river system: the Salt Wash Member of the Morrison Formation (Jurassic) in southern Utah: *in* Shanley, K.W., and McCabe, P.J., eds., Relative role of eustasy, climate, and tectonism in continental rocks: Society of Economic Paleontologists and Mineralogists, Special Publication No. 59, p. 93-107.

Rogers, R.R., and Kidwell, S.M., 2000, Association and taphonomy of terrestrial vertebrate fossils with terrestrial discontinuity surfaces in Judith River Formation, Montana: Journal of Geology, v. 108, p. 131-154.

Russell, D.A., and Chamney, T.P., 1967, Notes on the biostratigraphy of dinosaurian and microfossil faunas in the Edmonton Formation (Cretaceous), Alberta: National Museum of Canada, Natural History Paper 35, 22 p.

Shanley, K.W., and McCabe, P.J., 1991, Predicting facies architecture through sequence stratigraphy—An example from the Kaiparowits Plateau, Utah: Geology, v. 19, p. 742-745.

Shanley, K.W., and McCabe, P.J., 1993, Alluvial architecture in a sequence stratigraphic framework: a case history from the Upper Cretaceous of southern Utah, USA: *in* Flint, S., and Bryant, I.D., eds., Quantitative Description and Modeling of Clastic Hydrocarbon Reservoirs and Outcrop Analogues: International Association of Sedimentologists, Special Publication No. 15, p. 21-56.

Shanley, K.W., and McCabe, P.J., 1994, Perspectives on the sequence stratigraphy of continental strata: American Association of Petroleum Geologists Bulletin, v. 78, No. 4, p. 544-568.

Shanley, K.W., and McCabe, P. J., 1995, Sequence stratigraphy of Turonian-Santonian strata, Kaiparowits Plateau, southern Utah, USA: Implications for regional correlation and foreland basin evolution: *in* van Wagoner, J.C., and Bertram, G.T., eds., Remote Sensing: Outcrop and subsurface examples from the Cretaceous of North America: American Association of Petroleum Geologists Memoir 64, p. 103-136.

Shanley, K.W., and McCabe, P.J., 1998, Relative role of eustasy, climate, and tectonism in continental rocks: an introduction: *in* Shanley, K.W., and McCabe, P.J., eds., Relative role of eustasy, climate, and tectonism in continental rocks: Society of Economic Paleontologists and Mineralogists, Special Publication No. 59, p. iii-iv.

Shanley, K.W., McCabe, P.J., and Hettinger, R.D., 1992, Tidal influence in Cretaceous fluvial strata from Utah: A key sequence stratigraphic interpretation: Sedimentology, v. 39, p. 905-930.

Sheehan, P.M., Fastovsky, D.E., Barreto, C., and Hoffmann, R.G., 2000, Dinosaur abundance was not declining in a "3 m gap" at the top of the Hell Creek Formation, Montana and North Dakota: Geology, v. 28, p. 523-526.

Shepheard, W.W., and Hills, L.V., 1970, Depositional environments of the Bearpaw-Horseshoe Canyon (Upper Cretaceous) transition zone, Drumheller “Badlands,” Alberta: Bulletin of Canadian Petroleum Geology, v. 18, p. 166-215.

Smith, N.D., and Perez-Arlucea, M., 1994, Fine-grained splay deposition in the avulsion belt of the lower Saskatchewan River, Canada: Journal of Sedimentary Research, v. B64, p. 159-168.

Smith, N.D., Cross, T.A., Dufficy, J.P., and Clough, S.R., 1989, Anatomy of an avulsion: Sedimentology, v. 36, p. 1-23.

Stoll, H.M., and Schrag, D.P., 1996, Evidence for glacial control of rapid sea level changes in the Early Cretaceous: Science, v. 272, p. 1771-1774.

Straight, W.H., and Eberth, D.A., 1998, Sequences, stratigraphy, and depositional environments of the Horseshoe Canyon Formation in the Drumheller region: Geo-Triad Convention Post-meeting Field Trip 6, guidebook, 56 p.

Tew, B.H., and Mancini, E.A., 1995, An integrated stratigraphic method for paleogeographic reconstruction: Examples from the Jackson and Vicksburg Groups of the eastern Gulf Coast plain: PALAIOS, v. 10, p. 133-153.

Törnqvist, T.E., 1993, Holocene alternation of meandering and anastomosing fluvial systems in the Rhine-Meuse Delta (Central Netherlands) controlled by sea-level rise and subsoil erodability: Journal of Sedimentary Petrology, v. 63, p. 683-693.

Van Wagoner, J.C., 1995, Sequence stratigraphy and marine to nonmarine facies architecture of foreland basin strata, Book Cliffs, Utah, USA: *in* Van Wagoner, J.C., and Bertram, G.T., eds., Sequence stratigraphy of foreland basin deposits: outcrop and subsurface examples from the Cretaceous of North America, American Association of Petroleum Geologists, Memoir 64, p. 137-223.

Waheed, A., 1983, Sedimentology of the coal-bearing Bearpaw-Horseshoe Canyon Formation (Upper Cretaceous), Drumheller Area, Alberta, Canada: Unpublished Master's Thesis, University of Toronto, 161 p.

Willis, B.J., and Behrensmeyer, A.K., 1994, Architecture of Miocene overbank deposits in Northern Pakistan: Journal of Sedimentary Research, v. 64, p. 60-67.

Wood, J.M., 1985, High-sinuosity, fluvially-dominated palaeochannel sedimentation on an Upper Cretaceous coastal plain: the Judith River Formation, "Cathedral" area, Dinosaur Provincial Park, Alberta: Unpublished Master's Thesis, University of Calgary, Alberta, 215 p.

Wood, J.M., Thomas, R.G., Visser, J., 1988, Fluvial processes and vertebrate taphonomy: the upper Cretaceous Judith River Formation, south-central Dinosaur Provincial Park, Alberta, Canada: Palaeogeography, Palaeoclimatology, Palaeoecology, v. 66, p. 127-143.

Wright, V.P., and Marriott, S.B., 1993, The sequence stratigraphy of fluvial depositional systems: The role of floodplain sediment storage: Sedimentary Geology, v. 86, p. 203-210.

APPENDIX

The nine measured sections comprising the lithostratigraphic component of the project are available at SEPM's Data Repository site: http://www.ngdc.noaa.gov/mgg/sepm/archive/straight2002_01. A series of stratigraphic columns are provided in .jpg format; the symbol key and diagram legend are included with the short Wolf Coulee section (WolfKey.jpg).

The repository also includes three Microsoft Office 2000 Excel spreadsheets. The first, *Sites*, lists the GPS and elevation position for each site, as well as the taxa, site type, facies, and package. The second, *XRDdata*, features the results from X-ray diffraction; four representative diffraction patterns are included in .jpg format. The third spreadsheet, *Model*, is the numerical model of fossil distribution used to create Figure 8. The individual graphs appear on columns AK-AS of the spreadsheet. The main diagram showing relative fossil count (x-axis) versus the accumulated thickness (y-axis) appears on columns AD-AH. All of the plots can be manipulated by changing the red values on the control panel on columns AB-AC. The *scale to thickness* value allows the accumulated thickness plots to be scaled to match any stratigraphic thickness. Frequency, position of maximum, and relative amplitude of the small- or package-scale cycle can be changed through the *# small cycles in grand*, the *y-axis offset*, and the *small amplitude* values under the SMALL header, respectively. Similarly, controls for the frequency, position of maximum, and relative amplitude of the grand-scale cycle are listed under the GRAND header. The *x-axis offset* value changes the position of the x-axis relative to the maximum amplitude of the grand scale cycle. The *subsidence rate* value controls the relative amount of accommodation created per unit time irrespective of base-level oscillations. The *optimum burial rate* value governs the theoretical depositional rate best suited for the burial of bone. Finally, the red markers on the main plot respond to the text entry and x-axis position under the MARKERS heading. The list of markers appears in column X. The default values on the spreadsheet are those used to produce Figure 8.

TABLE CAPTIONS

TABLE 1—Examples of the studies describing fining-upward rhythms in fluvial strata. One third of these references describe such rhythms in the context of a stratigraphic framework (sequence stratigraphy or allostratigraphy), and fewer acknowledge the presence of terrestrial fossils.

TABLE 2—Facies of the lower Horseshoe Canyon Formation, including the Drumheller Marine Tongue, following the nomenclature of Miall (1978, 1992).

TABLE 3—Distribution of facies in raw section data and from fossil sites. Facies listed in Table 2 not included here collectively comprise less than 10% of the lower HCF and contain less than 1% of HCF fossil sites. Results of correlation between facies distributions are significant: r= 0.789, two-tailed, 0.01 level of significance, n= 15.

TABLE 4—Distribution of sites and site arrangements within different facies associations in the lower HCF. The other two facies associations preserve no fossil remains.

TABLE 5—Statistical comparison of relationship between the stratigraphic dispersion of facies against the stratigraphic dispersion of fossil sites. Each statistical test of the fossil survey data (*no* indicates no relationship at the level of significance for the test) is contrasted with similar tests against ten synthetic, random fossil site distributions (listing is the number of tests resulting in a significant relationship).

TABLE 6—Statistical comparison of relationship between the stratigraphic position of bounding surfaces (described in text) and stratigraphic position of fossiliferous horizons. Each statistical test of the fossil survey data (yes indicates a relationship was present at the level of significance for the test) is contrasted with similar tests against 20 synthetic, random fossiliferous horizon distributions (listing is the number of tests resulting in a significant relationship).

Table 1, part 1

Region	*References*	*Age*	*Depositional Environment*	*Applied Stratigraphy*
Breathitt Gp, KY	Aitken and Flint, 1994, 1995	Carboniferous	shoreface to lower floodplain	sequence stratigraphy
Monongahela-Dunkard Gps, WV	Ghosh, 1987	Pennsylvanian/ Permian	lower to upper floodplain	facies architecture
Salt Wash Mbr, Morrison Fm, UT	Robinson & McCabe, 1998	Jurassic	upper to central floodplain	facies architecture
Mannville Gp, AB	Cant, 1998	early Cretaceous	upper to central floodplain	allostratigraphy
northeast NM?	Holbrook & White, 1998	early Cretaceous	upper to central floodplain	facies architecture
Dunvegan Fm, AB	Bhattacharya, 1989	late Cretaceous	estuary	allostratigraphy
Book Cliffs, UT	Van Wagoner, 1995; Kamola & Van Wagoner, 1995; Olsen et al., 1995	late Cretaceous	lagoon to lower floodplain	sequence stratigraphy
Straight Cliffs, UT	Shanley & McCabe, 1991, 1993, 1995; Shanley et al., 1992	late Cretaceous	shoreface to central floodplain	sequence stratigraphy
Judith River Fm, AB	Wood, 1985; Wood et al., 1988	late Cretaceous	central floodplain	facies architecture
Horseshoe Canyon Fm, AB	Rahmani, 1988; Ainsworth & Walker, 1994; this study	late Cretaceous	shoreface to upper floodplain	sequence stratigraphy
Wilcox Gp, TX	Breyer, 1997	?Paleogene	estuary to lower floodplain	sequence stratigraphy
Willwood Fm, WY	Davies-Vollum & Wing, 1998	Eocene	upper floodplain	facies architecture
Siwaliks, Pakistan	Badgley, 1986; Behrensmeyer, 1987; Willis & Behrensmeyer, 1994	Miocene	central floodplain	facies architecture
Ebro Basin, Spain	Nichols & Hirst, 1998	Miocene	alluvial fan	facies architecture
Mississippi River, MS	Aslan and Autin, 1998, 1999	Holocene	lower to central floodplain	facies architecture
Okavango Basin, S Af; Neuquen Basin, Argentina	Legarreta & Uliana, 1998	Holocene	alluvial fan	facies architecture

Table 1, part 2

Region	*Term for Base*	*Dominant Facies*	*Paleosol*	*Splay*	*Coal*	*Bone*
Breathitt Gp, KY	scour	mud>sand	yes	?yes	yes, few	no
Monongahela-Dunkard Gps, WV	undefined	mud>>sand	yes	yes	no	no
Salt Wash Mbr, Morrison Fm, UT	scour	sand>mud	no	?no	no	no
Mannville Gp, AB	unconformity	cgl/sand<mud	no	no	yes	no
northeast NM?	?scour	sand= mud	no	yes	no	no
Dunvegan Fm, AB	scour	sand>>mud	no	no	no	no
Book Cliffs, UT	unconformity	sand>mud	yes	?no	yes	no
Straight Cliffs, UT	unconformity	sand>>mud	no	yes	yes	yes, few
Judith River Fm, AB	?scour	sand>>mud	no	no	no	yes
Horseshoe Canyon Fm, AB	unconformity	mud>sand	yes	yes	yes	yes
Wilcox Gp, TX	unconformity	sand= mud	yes, few	no	yes	no
Willwood Fm, WY	scour	sand>mud	yes	no	no	yes
Siwaliks, Pakistan	scour	sand= mud	yes	yes	no	yes
Ebro Basin, Spain	scour	mud>sand	no	no	no	no
Mississippi River, MS	?scour	sand= mud	yes, few	yes	no	no
Okavango Basin, S Af; Neuquen Basin, Argentina	scour	sand>mud	yes	no	no	no

Table 2

Code	*Facies Description*	*Association*	*Interpretation*
C	Blocky subbituminous coal interbedded with black fissile mud, lignite lamina, partly silicified/coalified wood, *in situ* stumps, amber, bone, and sulfur coatings.	5	Peat swamp, probably brackish estuarine where sulfur is present.
Fa	Blocky to moderately fissile, pale to dark gray silty mud, with roots and plant fragments, amber, bone, slickensides, and bentonite.	5, 6	Seasonally saturated floodplain, possibly marshland.
Fe	Massive dark brown mud, granular parting, sparse plant fragments.	5	Saturated floodplain, possibly as an overbank flood.
Ff	Poorly fissile, carbonate-cemented pink or red-brown mud/silt, decimeter-thick erosion-resistant sheets or thicker lenticular bodies with sparse hash, oxide-cast plant fragments, roots, slickensides, and amber.	5	Paleosol leaching horizon.
Fg	Green or gray-green silty mud, interlaminated or mottled with very fine sand or silt in contorted enclaves or thin ripple-laminated seams, swelling clay, plant fragments, fragmentary bone and small teeth.	6	Trampled splays on dry floodplain.
Fo	Blocky red-brown or tan, massive or sparsely laminated with very fine sand or silt, with oxide-cast roots, abundant siderite nodules, and rare bone.	6	Dry floodplain.
Gb	Large blocks of tilted strata, attenuated in downstream direction.	3	Bank collapse blocks.
Gl	Lag of reworked siderite clasts, wood, bone, and mudstone intraclasts.	1, 2, 3	Lag accumulated by winnowing in channel.
Sb	Medium/fine sand with nearly horizontal bedding, occasionally interbedded with laminated mud, with burrows, coal fragments, sulfur, gypsum, and glauconite.	4	Washover fan.
Se	Horizontal or gently undulating laminae of fine/very fine sand and pale green/gray silty mud bedded in couplets; gypsum, shell debris; subtle scour beneath each sand.	4	Tide- or event-dominated middle estuary, possibly near turbidity maximum.
Sf	Fine/very fine sand in laterally extensive decimeter-thick sheets with climbing ripples, with complete to patchy carbonate cementation, burrows, and roots.	2	Splay fringe
Sl	Medium/fine sand with inclined plane beds, interbedded or draped with mud and/or hash lamination, fining and increasing mud content upward, with reworked siderite pebbles and bone on bedding surfaces.	1, 2, 3	Lateral accretion surfaces, usually from a low-sinuosity meandering channel.
Sn	Alternating horizontal laminae of fine/very fine sand and tan or gray mud; amber, plant hash and fragments, wood, bone, nodules, and rooting.	5, 6	Floodplain deposition of alternating splays and levees
So	Carbonate-cemented very fine sand/silt with breccia of complete and partial brackish-water bivalves.	4	Oyster bank debris, possibly from washover.
Sp	Medium/fine sand with planar crossbeds, reworked siderite pebbles on bedding surfaces.	2, 3	Migrating sand bars and bedforms in an active channel.
Sr	Fine/very fine sand, fining upward with ripple lamination and small trough crossbeds, commonly as winged lens-shaped bodies or sheets, with coal rip-up clasts, hash, bone, and wood on an irregular basal scour.	1, 2	Splay channel/chute fill.
St	Medium/fine sand with trough crossbedding, siderite lags, and hash lamination on bedding surfaces; in layers or in fining upward stacks; wood and bone fragments.	1, 2, 3	High-energy channel-bottom fill.

Table 3

Distribution of facies…	*Fa*	*Fe*	*Ff*	*Fg*	*Fo*	*C*	*Sl*	*Sn*	*Sr*	*St*
…from fossil sites	19%	6%	10%	8%	13%	10%	10%	7%	12%	5%
…in raw section data	30%	6%	2%	7%	7%	7%	12%	7%	7%	6%

Table 4

	(1) Plane-bedded, cross-bedded sandstone body	*(2) Terrace-forming sandstone body*	*(5) Organic-rich mudrocks*	*(6) Organic-poor mudrocks*
Total Sites	88	50	228	161
Solitary	52	28	112	69
Packed Bonebed	15	3	0	20
Sparse Bonebed	15	16	107	9
Microsite	6	3	9	16

Table 5

	Individual Facies										*Facies Associations*			
	Fa	*Fe*	*Ff*	*Fg*	*Fo*	*C*	*Sl*	*Sn*	*Sr*	*St*	*(1)*	*(2)*	*(5)*	*(6)*
Spearman Rank														
survey, 0.01 level	no	no	no	no	yes	no	no	no	no	no	no	no	no	no
survey, 0.05 level	yes	no	no	no	yes	no	yes	no	no	no	no	no	yes	no
random, 0.05 level	1	1	0	0	0	1	0	0	0	1	0	0	0	1
Kolmogorov-Smirnov														
survey, 0.05 level	no	no	no	no	no	no	no	no	no	no	no	no	no	no
random, 0.05 level	0	0	0	0	0	0	0	0	0	0	0	0	0	0
Chi-squared 2-sample														
survey, 0.05 level	no	no	no	no	no	no	no	no	no	no	no	no	no	no
random, 0.05 level	0	0	0	0	0	0	0	0	0	0	0	0	0	0

Table 6

	survey	*in 20 random*
Spearman Rank		
0.05 level	yes	0
Kolmogorov-Smirnov		
0.01 level	yes	0
0.05 level	yes	3
Chi-squared 2-sample		
0.05 level	yes	0

FIGURE CAPTIONS

FIGURE 1—General geology of the Alberta Foreland Basin in southern Alberta. The structural cross-section A-A' is generalized from Jerzykiewicz and Norris (1993). An enlargement of the field area near Drumheller, Alberta, is shown in Figure 2.

FIGURE 2—Field area around Drumheller, Alberta. Nine measured sections (dots) and eight fossil survey areas (squares) lie along two transects (B-B', C-C') on the eastern valley wall.

FIGURE 3—Stratigraphic architecture of the 29-kilometer-long B-B' dip transect of the northeastern wall of the Red Deer River Valley. Ticks refer to vertical sections on 26 photographic mosaics at which the relative position of visible contacts were measured. Vertical lines mark the positions of measured sections. Numbers in circles refer to landmarks similarly labeled in Figure 2; numbers without circles refer to coal seams, modified from Gibson (1977). Shading indicates sandstone facies. Vertical scale is approximate.

FIGURE 4—Stratigraphic architecture of the 14-kilometer-long C-C' oblique transect of the eastern wall of the Red Deer River Valley. Ticks refer to vertical sections on 9 photographic mosaics at which the relative position of visible contacts were measured. Vertical lines mark the positions of measured sections. Numbers in circles refer to landmarks similarly labeled in Figure 2; numbers without circles refer to coal seams, modified from Gibson (1977). Shading indicates sandstone facies. Long-dashed line below coal seam 10 indicates a visible change in color of deposits from red-brown to green-gray. Vertical scale is approximate.

FIGURE 5—Typical arrangement of facies within the six facies associations of the HCF. Each image is a composite of several field examples. Facies nomenclature from Table 3.

FIGURE 6—Composite section and distribution of vertebrate fossil sites in the lower HCF. Key to symbols and format as in Figure 5. Numbers right of section refer to coal seams, modified from Gibson (1977). Basal scours (solid horizontal lines in plot) and internal surfaces (dotted horizontal lines) partition the section into ten packages (letters A-J), based on facies relationships in measured sections. Stratigraphic position of fossil sites to nearest meter is based on fossil survey data. Circles represent solitary sites; triangles, microsites; crosses, sparse bonebed sites; squares, packed bonebed sites.

FIGURE 7—Typical package from the HCF. Key to symbols and format as in Figure 5. Intervals are marked by a vertical change in facies association. Thinner packages usually have thinner intervals b, e, f, and g; very thin packages do not preserve intervals above the internal surface, and the overlying basal scour truncates interval d. Base-level change interpretation discussed in text. BLR = base-level rise, BLF = base-level fall.

FIGURE 8—Modeling the stratigraphic distribution of fossils using only parameters of base-level variation in lower HCF. (A) Partial grand-scale cycle of variation in accommodation, probably reflecting subsidence throughout deposition of the lower HCF and DMT. (B) Ten package-scale cycles, probably resulting from climatically controlled pulses in sediment supply. (C) Sum of curves in A and B, showing complex variation of accommodation through time estimated for the lower HCF. (D, E) Relative proxy for depositional rate calculated from incremental variations in accommodation, assuming that at each time increment the available accommodation filled with sediment. The depositional rate is high between lowstand (solid horizontal line) and the following highstand (dashed horizontal line). (F) Depositional rate proxy with vertical axis reflecting preserved accommodation (accumulated thickness) instead of time. The model predicts the non-equal division

of thick packages by highstand markers seen in HCF packages and has a similar three-fold hierarchy in package form (4 large packages of nearly equal thickness; 3 packages of successively diminishing thickness; and 3 thin packages without highstand markers). (G) Fossil burial potential, calculated by degree of similarity between depositional rate and an optimum rate for bone burial (vertical line through curves, E-F) for each increment of preserved accommodation. The resulting distribution and shape of peaks of fossil preservation potential are very similar to the distribution and shape of fossiliferous horizons in the lower HCF (dense isolated horizons on highstands in lower packages; thinner and weaker horizons on stillstands in middle packages; and a non-fossiliferous gap at the top). Changing any one of the parameters (cycle amplitudes and offsets, optimum burial rate, subsidence rate, etc.) in this mathematical model creates a very different distribution of fossiliferous and nonfossiliferous intervals, suggesting that terrestrial vertebrate distribution may permit a semi-quantitative discrimination of various local controls on accommodation.

Figure 1

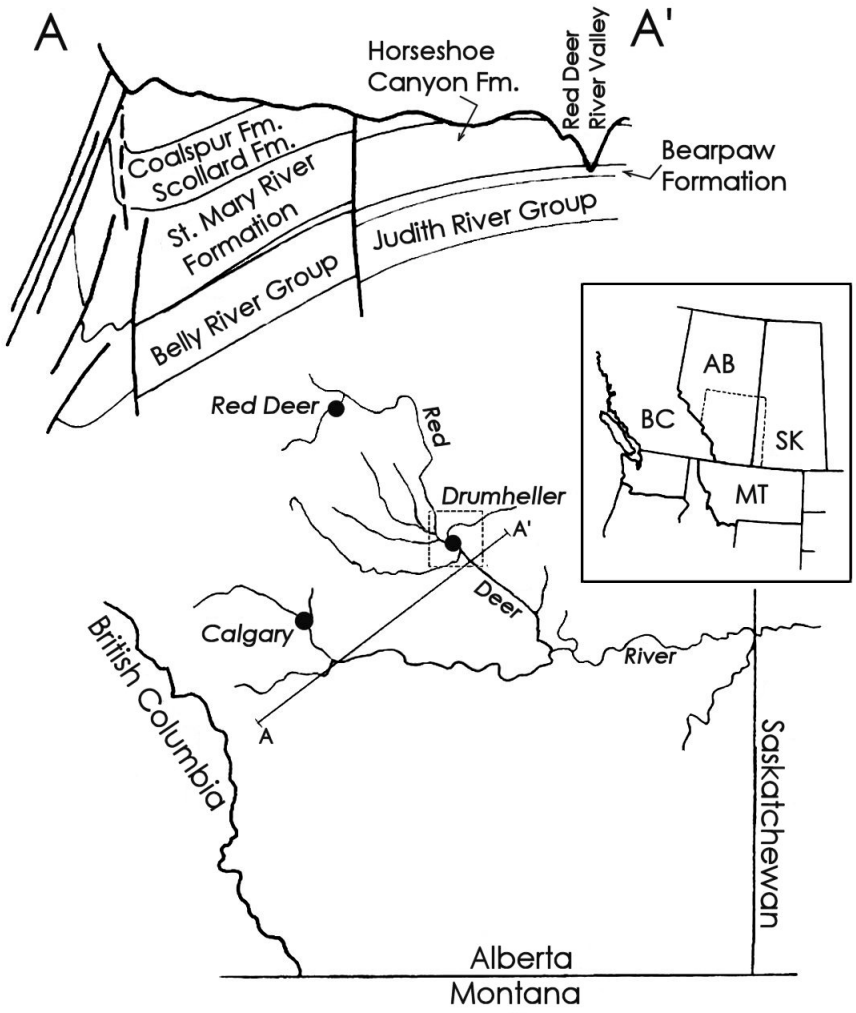
A
A'
Horseshoe
Canyon Fm.
Red Deer
River Valley
Coalspur Fm.
Scollard Fm.
St. Mary River
Formation
Bearpaw
Formation
Judith River Group
Belly River Group
AB
BC
SK
MT
Red Deer
Red
Drumheller
A'
Deer
River
Calgary
A
British Columbia
Saskatchewan
Alberta
Montana

Figure 2

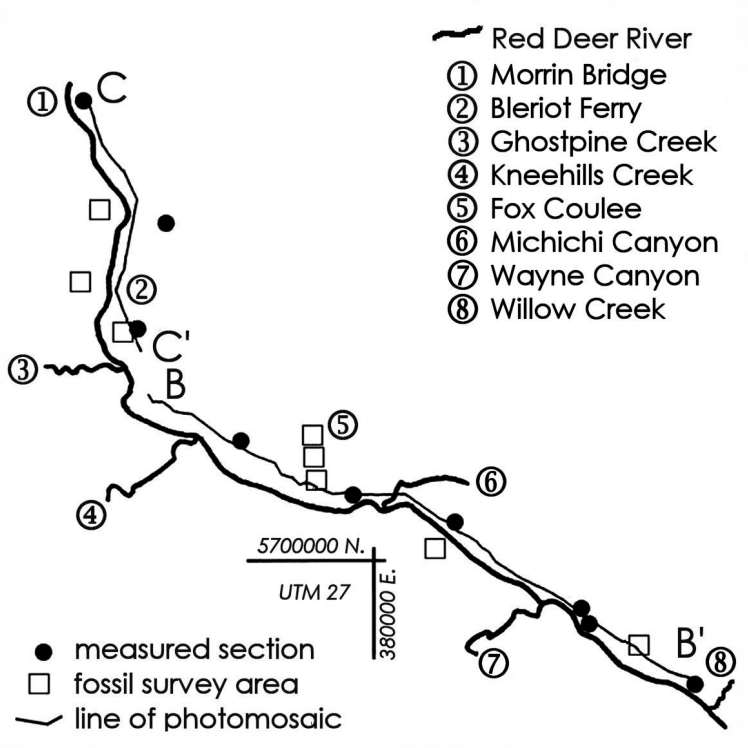
Red Deer River
① Morrin Bridge
② Bleriot Ferry
③ Ghostpine Creek
④ Kneehills Creek
⑤ Fox Coulee
⑥ Michichi Canyon
⑦ Wayne Canyon
⑧ Willow Creek
C
C'
B
B'
5700000 N.
UTM 27
380000 E.
measured section
fossil survey area
line of photomosaic

Figure 3

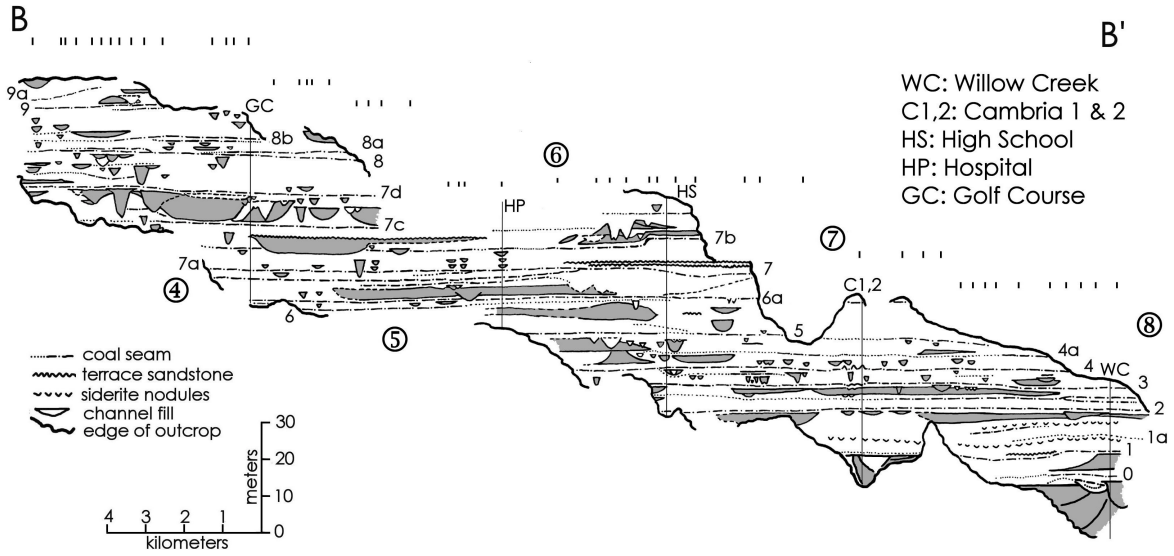
B
B'
WC: Willow Creek
C1,2: Cambria 1 & 2
HS: High School
HP: Hospital
GC: Golf Course
9a
9
GC
8b
8a
8
7d
7c
7a
HP
HS
7b
7
6a
6
5
C1,2
4a
4
WC
3
2
1a
1
0
④
⑤
⑥
⑦
⑧
coal seam
terrace sandstone
siderite nodules
channel fill
edge of outcrop
30
20
10
0
meters
4 3 2 1
kilometers

Figure 4

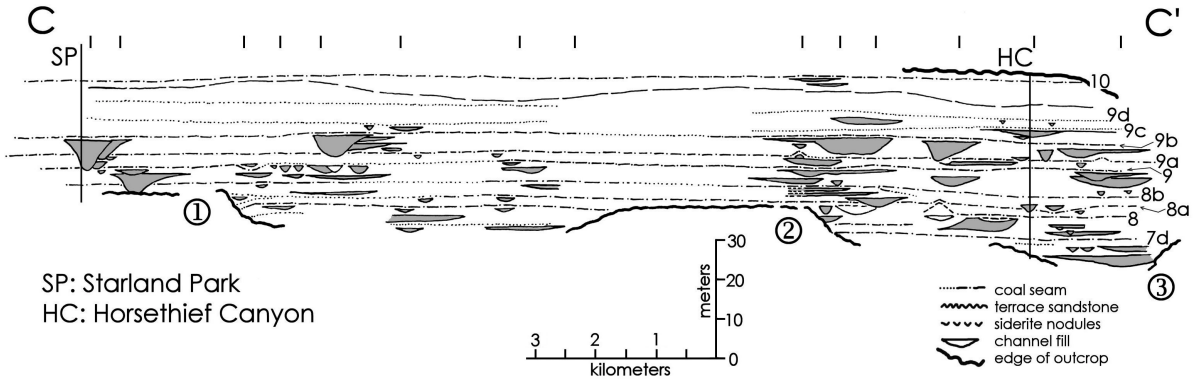
C
C'
SP
HC
10
9d
9c
9b
9a
9
8b
8a
8
7d
①
②
③
SP: Starland Park
HC: Horsethief Canyon
meters
30
20
10
0
3
2
1
kilometers
coal seam
terrace sandstone
siderite nodules
channel fill
edge of outcrop

Figure 5

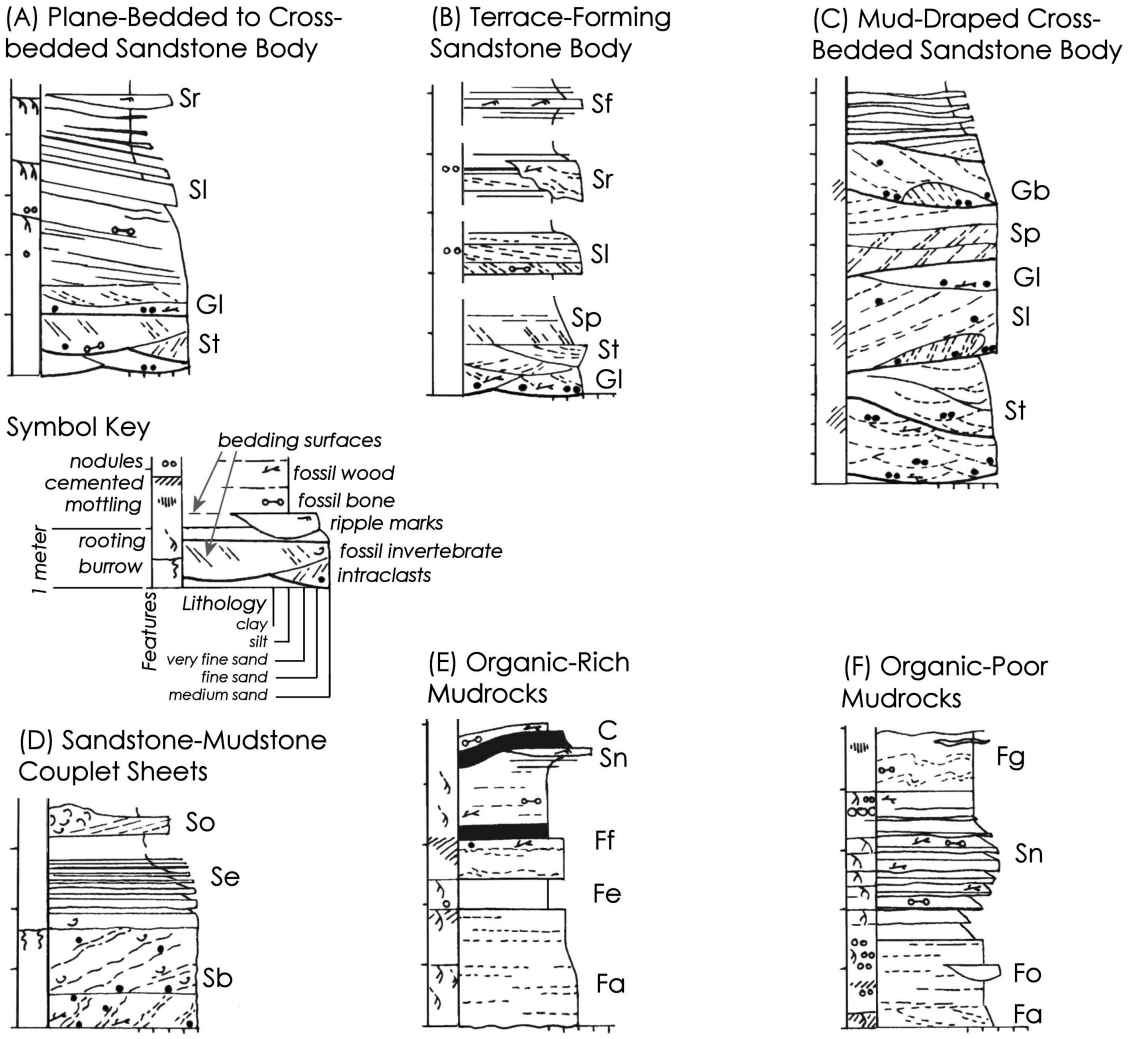
(A) Plane-Bedded to Cross-bedded Sandstone Body
Sr
Sl
Gl
St
(B) Terrace-Forming Sandstone Body
Sf
Sr
Sl
Sp
St
Gl
(C) Mud-Draped Cross-Bedded Sandstone Body
Gb
Sp
Gl
Sl
St
Symbol Key
bedding surfaces
nodules
cemented
mottling
rooting
burrow
1 meter
fossil wood
fossil bone
ripple marks
fossil invertebrate
intraclasts
Features
Lithology
clay
silt
very fine sand
fine sand
medium sand
(D) Sandstone-Mudstone Couplet Sheets
So
Se
Sb
(E) Organic-Rich Mudrocks
C
Sn
Ff
Fe
Fa
(F) Organic-Poor Mudrocks
Fg
Sn
Fo
Fa

Figure 6

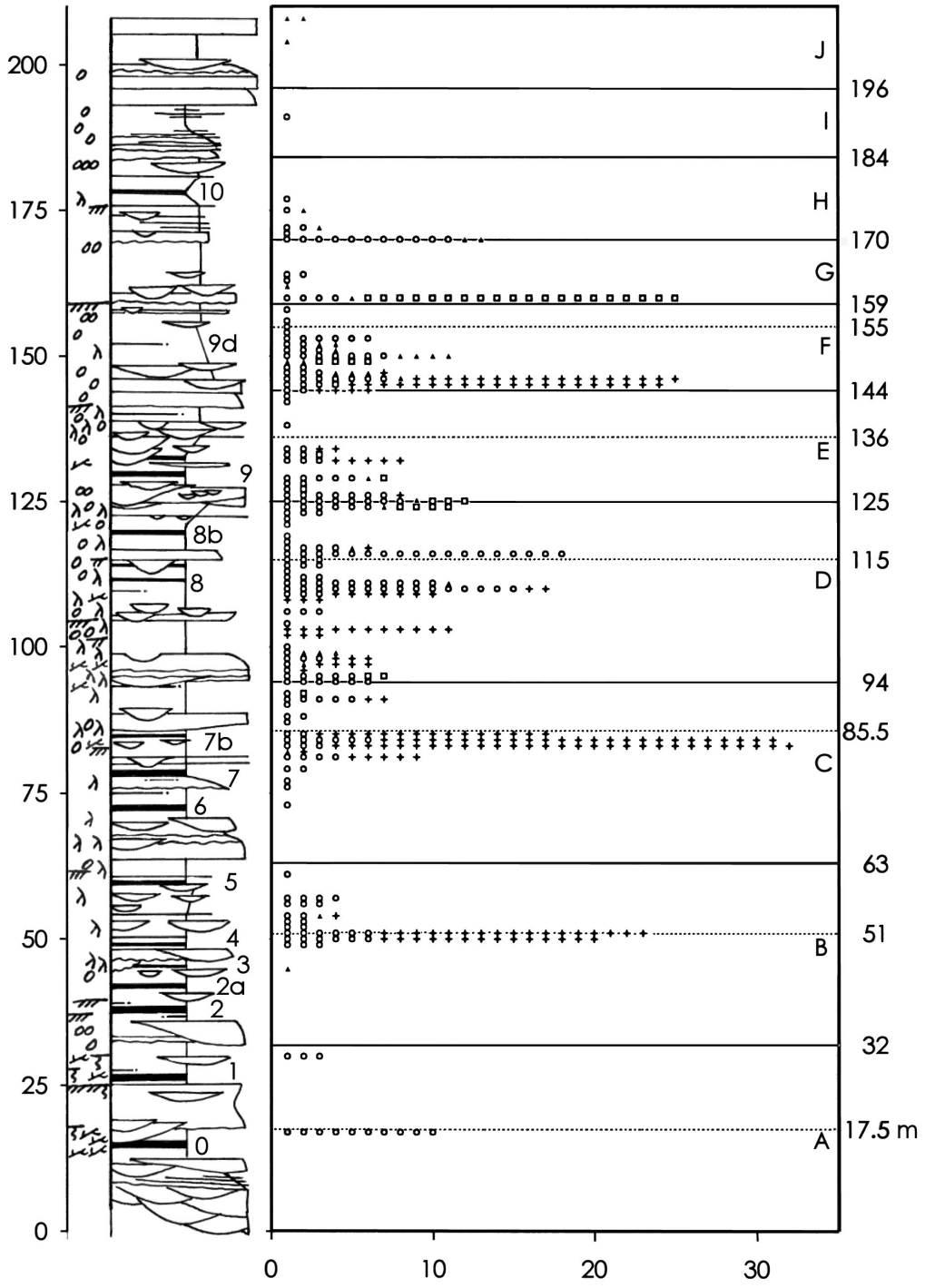
200
175
150
125
100
75
50
25
0
10
9d
9
8b
8
7b
7
6
5
4
3
2a
2
1
0
J
I
H
G
F
E
D
C
B
A
196
184
170
159
155
144
136
125
115
94
85.5
63
51
32
17.5 m
0
10
20
30

Figure 7

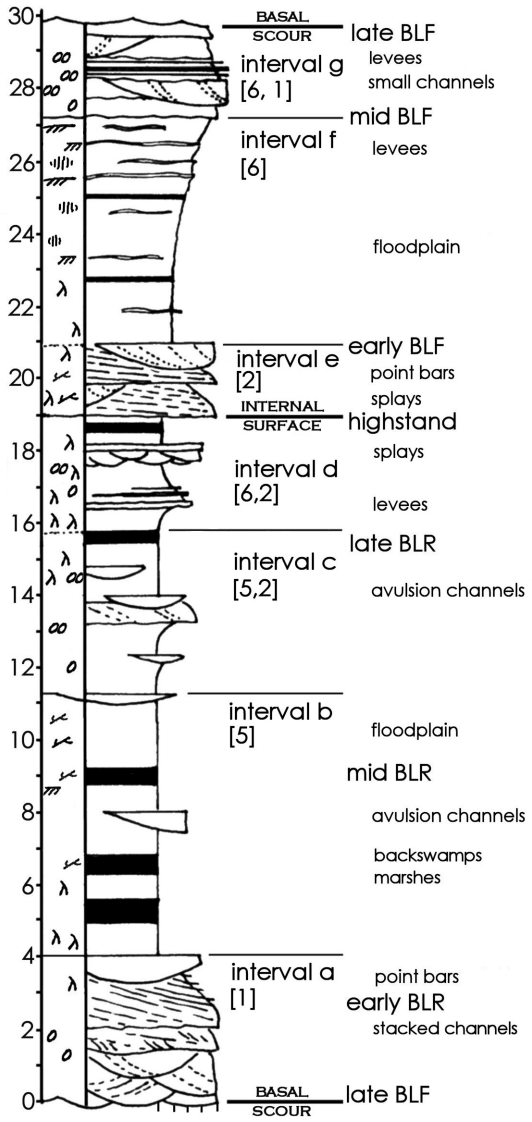
30
28
26
24
22
20
18
16
14
12
10
8
6
4
2
0
BASAL SCOUR
late BLF
levees
small channels
interval g
[6, 1]
mid BLF
interval f
[6]
levees
floodplain
early BLF
interval e
[2]
point bars
splays
INTERNAL SURFACE
highstand
splays
interval d
[6,2]
levees
late BLR
interval c
[5,2]
avulsion channels
interval b
[5]
floodplain
mid BLR
avulsion channels
backswamps
marshes
interval a
[1]
point bars
early BLR
stacked channels
BASAL SCOUR
late BLF

Figure 8

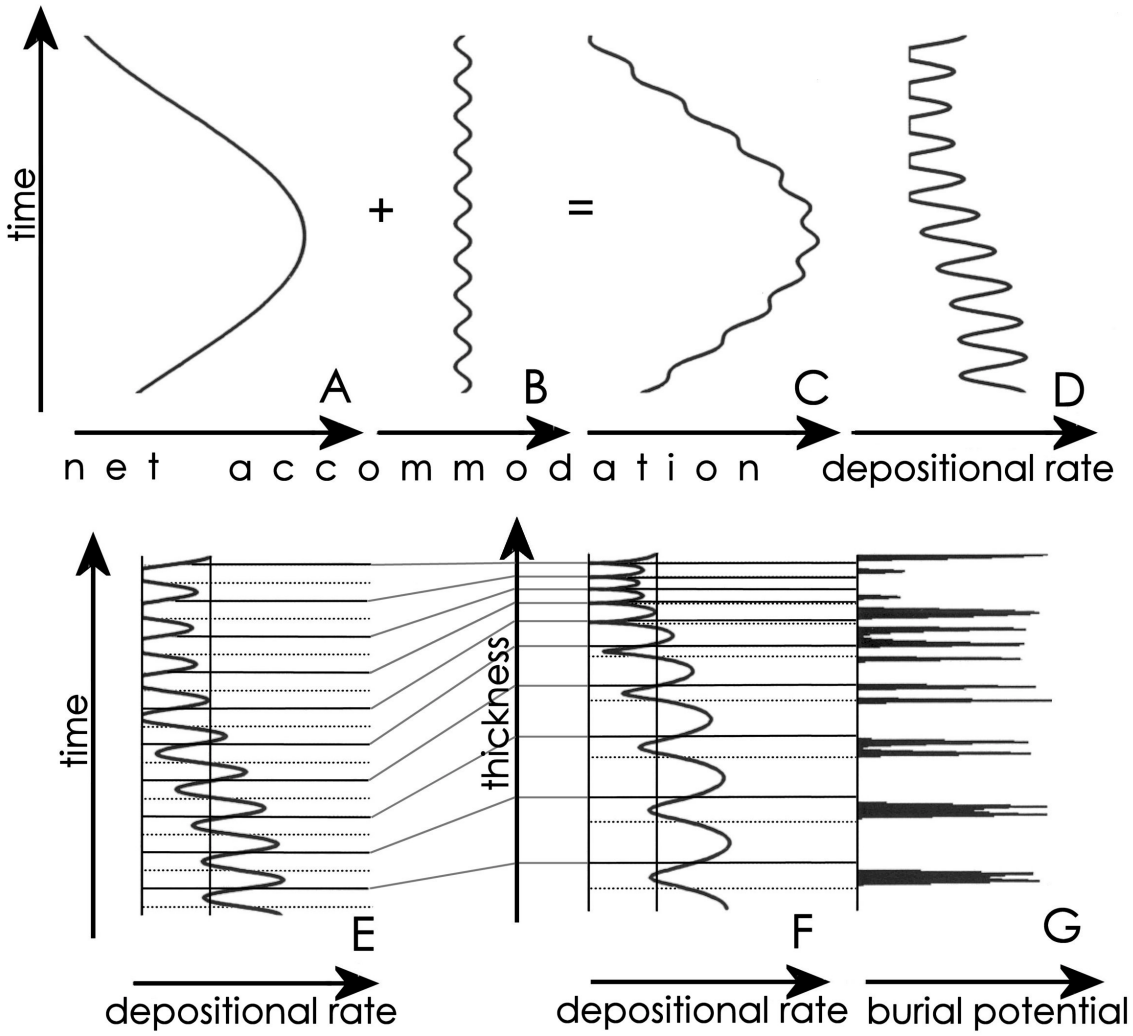
time
+
=
A
B
C
D
net accommodation
depositional rate
time
thickness
E
F
G
depositional rate
depositional rate
burial potential

CHAPTER TWO

Reflections of Surface Water, Seasonality and Climate in Stable Oxygen Isotopes From Tyrannosaurid Tooth Enamel

STRAIGHT, WILLIAM H

Marine, Earth, and Atmospheric Sciences Department,

Box 8208, North Carolina State University, Raleigh, NC 27695

BARRICK, REESE E

Marine, Earth, and Atmospheric Sciences Department,

Box 8208, North Carolina State University, Raleigh, NC 27695

EBERTH, DAVID A

Royal Tyrrell Museum of Palaeontology, Box 7500,

Drumheller, AB T0J 0Y0, Canada

In Press

Straight, W.H., Barrick, R.E., Eberth, D.A., in press. Reflections of surface water, seasonality and climate in stable oxygen isotopes from tyrannosaurid tooth enamel. Palaeogeography Palaeoclimatology Palaeoecology.

Abstract

Patterns of isotopic variation in enamel of eight *Albertosaurus* teeth from the Campanian/Maastrichtian Horseshoe Canyon Formation, Alberta, were measured by serial sampling along the growth axis. Cycles in the isotopic values appear to correlate to published tooth growth rates for tyrannosaurids. Tyrannosaurid dinosaur teeth of ~50 mm in length provide ideal repositories of terrestrial climatic information as each records a full annual cycle of body water isotopic variation. The relatively thin enamel precludes problems associated with time-averaging associated with complex growth patterns found in thick mammalian enamel. The most consistent and striking pattern associated with all of the teeth are two relatively closely spaced subequal maxima. These appear to be associated with onset of a seasonal episode of high humidity after the activation of the "amount effect," where the influence of ambient temperature on surface water (and body water) $\delta^{18}O$ ends while temperatures remain above 20º C. Teeth within a single fossiliferous horizon show the same general isotopic pattern and range. A notable difference in pattern shape and magnitude of isotopic variation between tyrannosaurid teeth from several stratigraphic intervals of the lower Horseshoe Canyon Formation section indicates a climatic changes from strong seasonality (high annual temperature range with distinct precipitation and humidity maxima during each year) at the base of the section to milder seasonality at the top.

Keywords: isotope, oxygen, dinosaur, enamel, paleoclimate, amount effect

1. Introduction

Biogenic phosphate minerals such as bone, dentine, and enamel are now regularly used as recorders of paleoenvironment (see Barrick, 1998, for review). Biogenic phosphates derive their phosphate $^{18}O/^{16}O$ signal ($\delta^{18}O_p$) from the body water reservoir $\delta^{18}O$. Isotopically, this reservoir is a combination of three oxygen sources: ingested water (drinking water and water in food), food solids, and atmospheric oxygen (Fig. 1; Bryant and Froelich, 1995; Kohn, 1996; Barrick, 1998). Of the three inputs to the body water reservoir, drinking (meteoric) water dominates the reservoir isotopic ratio and varies with temperature (Luz and Kolodny, 1989; D'Angela and Longinelli, 1990) and evaporative enrichment (Kohn, 1996). Food and food water

isotopic ratios are related to meteoric water but are also modified by changes in relative humidity through the evapotranspirative enrichment of leaves (Cormie et al., 1994). Deciphering an animal's $\delta^{18}O_p$ signal is also complicated by the effect of the animal's thermoregulatory strategy. In most heterotherms, $\delta^{18}O_p$ is also influenced by changes in body temperature (Barrick et al., 1992, 1993, 1996; Fricke and Rogers, 2000; but see Barrick et al., 1999) whereas in homeotherms bone forms at a constant temperature and preserves the variation in body water $\delta^{18}O$ alone (D'Angela and Longinelli, 1990; Bryant et al., 1994; Barrick and Showers, 1995; Barrick et al., 1996). Therefore, phosphates of homeotherms are manufactured containing an oxygen isotope record related to surface water and humidity (Kohn, 1996).

Bone is often remodeled in vivo and susceptible to overprinting by the addition of secondary, external phosphate after burial, both processes which can disrupt the record of body water $\delta^{18}O$. Tooth enamel is more dense, more crystalline, and less organic than bone and is hence more resistant to post-depositional modification (Lucas and Prévôt, 1991). Early studies reported phosphate $\delta^{18}O$ from tooth enamel of bears (Reinhard et al., 1996), elephants (Ayliffe et al., 1992, 1994), horses (Bryant et al., 1994, 1996; Sanchez-Chillon et al., 1994), and dinosaurs (Fricke and Rogers, 2000; Jensen, 2000; Jensen et al., 2000), using whole teeth to produce a single isotopic value, usually because the analytical technique required samples of up to 200 mg. Serial sampling of a single tooth, in which samples are collected as a series of bands or spots paralleling growth lines from tooth root to crown (Hillson, 1986), has been employed for isotopic studies of carbon and oxygen in teeth (Lee-Thorp et al., 1997; Cerling et al., 1998; Hobson and Sease, 1998; Balasse et al., 2001) and has worked on thickly enameled or very large teeth of beaver (Stuart-Williams and Schwarcz, 1997), zebra, gazelle (Kohn et al., 1996, 1998), horse (Cerling and Sharp, 1996; Sharp and Cerling, 1998; Feranec and MacFadden, 2000), bison (Gadbury et al., 2000), sheep (Fricke and O'Neil, 1996), rhinos (Dettman et al., 2001), Miocene gomphotheres (Fox and Fisher, 2001), Paleocene pantodonts (Fricke et al., 1998), and in the tusks of elephants (Koch et al., 1989, 1998). Each of these studies revealed seasonal variation in enamel $\delta^{18}O$ in tooth enamel phosphate and/or enamel carbonate. Until recently, however, the combination of enamel phosphate oxygen isotopic analysis with high-resolution isotopic sampling has been unavailable. New wet chemistry and preparation techniques, transformation of enamel to silver phosphate (Dettman et al., 2001), and pyrolysis mass spectrometry (Koziet, 1997; Showers et al., 2002), have substantially reduced the minimum

sample size required for analysis of $\delta^{18}O_p$. High-resolution serial sampling may now be applied to small and/or thinly enameled teeth, such as those of theropod dinosaurs.

Here, enamel from eight teeth of the tyrannosaurid theropod *Albertosaurus* from latest Campanian Horseshoe Canyon Formation of south-central Alberta has been serially sampled and analyzed isotopically to search for a seasonality signal in $\delta^{18}O_p$. Results are compared to published estimates of tooth growth rate in theropod dinosaurs (Erickson, 1996a) and results compared to theoretical both within and between several stratigraphic intervals from the same succession.

2. Methods

2.1 Collection of Dinosaur Teeth

Eight nearly complete adult *Albertosaurus* teeth used in this study were collected during a stratigraphic and taphonomic survey in the lower Horseshoe Canyon Formation (Straight and Eberth, 2002; Fig. 2). The 210-m thick succession of fossil-rich fluvial sediments of the lower Horseshoe Canyon Formation were deposited as a part of a clastic wedge on the Western Interior Seaway during the final two m.y. of the Campanian (Catuneanu and Sweet, 1999). The succession includes nearly 15 m of coal, almost 80 m of carbonaceous mudrocks, and a fossil record of subtropical plants, including fossilized remains of palms, cypress, and ferns, indicating a wet, seasonally warm climate during the late Campanian. The coals and carbonaceous mudrocks are more abundant toward the base of the formation, and the stratigraphic data indicate a general decrease in surface wetness through the time recorded by the succession (Straight and Eberth, 2002).

Vertebrate fossils of the lower Horseshoe Canyon Formation are preserved in laterally continuous, chronostratigraphic fossiliferous horizons of one to four meters in thickness, separated by intervals of generally less fossiliferous strata (Straight and Eberth, 2002). Like most of the fossils in the lower Horseshoe Canyon Formation, the tyrannosaurid teeth used in this study came from floodplain mudrocks or siltstones, with no evidence of reworking, pre-burial weathering, of post-burial alteration. Stratigraphic position of fossils from the survey and the horizons containing them is described in terms of meters above formation base (m AFB; Fig. 2). The eight teeth from the survey represent five important fossiliferous horizons in the lower Horseshoe

Canyon Formation and were analyzed isotopically to assess $\delta^{18}O_p$ variation in one taxon through time. Tooth H021 represents a sparse fossiliferous horizon at 17 m AFB in fluvial deposits reflecting a transition to fluvial control on deposition. Three teeth, F010, F007b, and F027, come from the most fossiliferous horizon in the section between 83 and 84.5 m AFB. One tooth, B148, comes from a thin horizon at 129 m AFB. Two teeth, D039 and D011, come from two closely spaced fossiliferous horizons between 146 and 151 m AFB, respectively. The last tooth, G008, comes from fluvial strata at 170 m AFB in an interval informally termed the Drumheller Marine Tongue.

2.2 Growth and Sampling of Dinosaur Teeth

Sediment was removed from the fossil teeth by a sonic bath, and fossil preparatory tools were used to remove additional museum preservative, adhesive, or resistant matrix from the enamel surface. Samples were collected using a carbide bit in a low-speed rotary drill. Each sample of 1 to 4 mg of powder was collected from a shallow groove in the enamel, usually down to the surface of the dentine, nearly parallel to lines of cross-section (Fig. 3).

The rationale for this sampling pattern comes in part from previous work involving serially sampled mammal teeth (Fricke and O'Neil, 1996) and in part from histological studies describing the growth of theropod teeth (Erickson, 1996a; Sander, 1999). Teeth of *Albertosaurus* are posteriorly curved cones of dentine covered by a 150-µ m-thick sheath of enamel (Figure 3; Sander, 1999), composed of 99% inorganic carbonate hydroxyapatite or dahllite (Hillson, 1986; Lucas and Prévôt, 1991; Rink and Schwarcz, 1995). Tooth growth commences at the tip with a cone of dentine extending rootward by the daily addition of a layer of dentine, in *Albertosaurus* averaging 15 µ m thick, inside the previous growth, forming the lines of von Ebner (Erickson, 1996a; Dean, 2000). Where the dentine cone extends the length of the tooth, enamel forms a circular band (incremental line or regular striation of Retzius) inclined toward the tooth tip from the enamel-dentine junction (Sander, 1999; Dean, 2000). Incremental lines in dentine (lines of von Ebner) and enamel (short-period lines, regular striae of Retzius) both represent daily growth and thus form in tandem, although individual lines may not be continuous from one material to the other (Fig. 3; Dean, 2000). The transverse bands of enamel are visible as thin color bands and/or as surface undulations in the enamel of tyrannosaur and

other coeval theropod teeth among the survey specimens collected from the lower Horseshoe Canyon Formation (Fig. 4). Where such features were visible on the teeth used in this study, they were used as guides for sample grooves. Sampling trenches were kept narrow, about 1 mm in width, to minimize time-averaging through the inclusion of numerous incremental lines. In teeth with thicker enamel, the apical cant of incremental lines results in time-averaged samples even in serial analysis (Hoppe, 2001), but in tyrannosaurids the thin enamel and the subordination of incremental lines to parallel, columnar crystallites perpendicular to the enamel surface (Sander, 1999) minimize the degree of time-averaging with sampling depth.

Enamel powder was prepared for analysis following the method detailed in the data repository for Dettman et al. (2001). Samples were dissolved in 1 ml 2M HF to liberate the phosphate anion. Solids were removed, the remaining solution diluted to 10 ml, and then 0.8 ml of 20% NH_4OH (6% by assay) and 1 ml of 2M $AgNO_3$ were added to instantly precipitate a cloud of brilliant yellow Ag_3PO_4 particles. With centrifuging the Ag_3PO_4 mud flocculates, and with drying turns into bright yellow powder. Phosphate yields for samples over 2.0 mg were 100±5%, whereas phosphate recovery degrades for smaller enamel samples. This loss of phosphate occurs because as the smaller samples dry they adhere to the sides of the centrifuge tube rather than forming a pellet as in larger samples. This incomplete recovery does not correlate with $\delta^{18}O_p$ in standards.

Silver phosphate samples averaging 0.5 mg were packed in 3.5 × 5 mm silver capsules, then thermochemically decomposed at 1450° C in an automated Finnegan MAT Delta Plus TCEA (at either North Carolina State University or the University of Arkansas Stable Isotope Lab) connected to a continuous-flow GC mass spectrometer under an anoxic atmosphere (Koziet et al., 1997; Kornexl et al., 1999a; Showers et al., 2002). Results were compared to a CO reference gas to get a raw $\delta^{18}O_p$ value and corrected against two or three reference standards, including NBS 120c (Florida Phosphate Rock, 21.6‰, prepared using the same technique as the enamel), NBS 8542 (sucrose, 36.4‰; Farquhar et al., 1997; Kornexl et al., 1999b), and NBS 127 (BaSO4, 9.4‰). Isotopic data are reported in standard delta notation (Tables 1 and 2), based on the relation between each sample and standard mean ocean water (SMOW),

$$\delta^{18}O = [({}^{18}O / {}^{16}O_{sample}) / ({}^{18}O / {}^{16}O_{standard})] - 1 \times 10^4 \quad (1).$$

2.3 Diagenesis

Stable isotope geochemistry on biological apatite as a paleoenvironmental recorder has been repeatedly challenged on the grounds that the process of fossilization results in diagenetic alteration. Recent theoretical studies conclude that stable isotopic records in biogenic phosphate are typically diagenetically destroyed (Sanchez-Chillon et al., 1994; Hubert et al., 1996;) or altered either by partial dissolution of phosphate during recrystallization of apatite crystals (Iacumin et al., 1996a), by microbial reprecipitation (Ayliffe et al., 1994; Kolodny et al., 1996; Blake et al., 1997), or through interaction with groundwater and/or other sources of phosphate (Wang and Cerling, 1994; Iacumin et al., 1996b).

However, diagenetic disruption of isotopic signals in continental vertebrate fossils is extremely unlikely. The model of fossils as francolite pseudomorphs of bone (Hubert et al., 1996; Kolodny et al., 1996) is derived from a study of the process of phosphatization of marine carbonate deposits to form phosphorites (Shemesh et al., 1988; Jarvis, 1992; Blake et al., 1997). In the marine environment, microbes deposit phosphate minerals derived from PO_4 in organic material buried within a carbonate mineral matrix (Jarvis, 1992). The minor amount of skeletal phosphate present is overprinted by diagenetic phosphatic cements, which preserve isotopic characteristics of the depositional environment. By contrast, fossil bone and teeth in most fluvial rocks are preserved as hydroxyapatite or carbonate hydroxyapatite instead of francolite, due to the relative immobility and rarity of both fluorine and phosphate in fluvial sediments (Pate et al., 1989; Lucas and Prévôt, 1991; Person et al., 1995; Barker et al., 1997). X-ray diffraction and histological studies of bone, enamel, and dentine from fossils from lower Horseshoe Canyon Formation fossil surveys, including teeth used in this study, show uniform preservation as carbonate hydroxyapatite (Straight and Eberth, 2002). Microbial modification of bone is rare in terrestrial soils, where most organic constituents in bone are lost to photolysis during weathering (Koch et al., 2000) and most alteration involves addition of trace elements rather than removal of phosphate (Bocherens et al., 1994; Kohn et al., 1999). In cases where microbial reprecipitation of bone mineral does occur, the reduction of organic material does not disrupt the PO_4 anion in preexisting phosphate minerals (Jarvis, 1992), wherein the paleoecological $\delta^{18}O$ signal is preserved. Such reprecipitation produces a distinctive, easily detectable morphology in fossil bone (Koch et al., 2000; Nielsen-Marsh and Hedges, 2000) and produces diagenetic phosphate cement proportional to the mass of organic material from

which it was derived, relatively small compared to the mass of bone phosphates. The low organic mass and low porosity of tooth enamel and the relatively large size of microbes capable of metabolizing skeletal phosphate indicate that microbially mediated diagenetic phosphate within tooth enamel is highly unlikely (Kohn et al., 1999).

Diagenetic homogenization that nevertheless maintains histological characters (Hubert et al., 1996) is frequently invoked to explain isotopic variation seen in skeletal phosphate $\delta^{18}O_p$ (Ayliffe et al., 1992, 1994; Sanchez-Chillon et al., 1994; Iacumin et al., 1996a, 1996b); a more parsimonious interpretation is that variation arises from intricately recorded biological signals (interbone and intrabone variation *sensu* Barrick and Showers, 1994, 1995; Barrick et al., 1996; and intratooth variability in Hobson and Sease, 1998, Kohn et al., 1998; Feranec and MacFadden, 2000; Dettman et al., 2001; this study) undetected by past analytical and sampling techniques.

3. Results

Results for enamel $\delta^{18}O_p$ are tabulated (Table 1; Appendix) and graphically displayed (Fig. 5) with the vertical axis serving as both an isotopic variation axis and for relative stratigraphic position; the horizontal axis shows distance from tooth tip to reflect the passage of time and tooth growth. All patterns feature two subequal maxima; longer patterns feature two unequal minima. G008, D039, D011, and B148 feature low-amplitude variation, whereas F010, F027, F007b, and H021 feature a high-amplitude $\delta^{18}O_p$ signal. The graph for each tooth (Fig. 5) also features a two-point running average line to smooth out analytical error, to clearly separate the isotopic profiles, and to display isotopic trends within each pattern.

4. Discussion

4.1 Growth Rate

Recovery of a complete twin-peaked annual $\delta^{18}O_p$ cycle from a tyrannosaurid tooth requires a tooth crown with a ~55 mm long sheath of enamel. Slightly more than half of full tooth length is root in

tyrannosaurids, hence the isotopic results imply that a 11 cm tooth with root represents two years' growth. This result contrasts with estimates from Johnston (1979) of eight years' growth period for tyrannosaurid teeth, but his interpretation has been criticized. The more recent work of Erickson (1996a, 1996b) found virtually identical daily incremental growth lines in dentine of mammalian, dinosaur, and crocodilian teeth. The addition of a daily incremental line with a mean thickness of 15 μm to a growing tyrannosaurid tooth (Erickson, 1996a) results in between 51 and 62 mm growth per year for tyrannosaurids, and between 51 and 53 mm per year for *Albertosaurus*. Erickson's (1996a) estimate of 519 days for growth of an average tooth in an adult *Albertosaurus* indicates that average complete tooth (crown + root) should be 78 mm long, with a corresponding crown length of ~39 mm. Fourteen complete *Albertosaurus* crowns (tooth sans root) recovered from the survey in the lower Horseshoe Canyon Formation (Straight and Eberth, 2002) feature an average crown length of 36 mm. *Albertosaurus* tooth size and oxygen isotopes from this study are consistent with growth rate estimates from Erickson (1996a). Tooth length of smaller dinosaurs precludes seasonal climate analysis as only a very short part of an annual cycle is recorded. Similar problems occur when analyzing highly worn teeth.

4.2 Correlation with Body Water Models

Longinelli and Nuti (1973) first empirically derived an equation correlating the isotopic oxygen values from biogenic phosphates in invertebrates to environmental temperatures and water oxygen isotope values,

$$T(^{o}\,C) = 111.4 - 4.3(\delta^{18}O_p - \delta^{18}O_w) \qquad (2).$$

Kolodny et al. (1983) empirically confirmed the correlation between temperature and phosphate $\delta^{18}O_p$ values, demonstrating that fish body water and environmental water $\delta^{18}O$ values are in equilibrium. Luz and Kolodny (1985, 1989) validated the equation for mammals, showing that bone $\delta^{18}O_p$ values are in equilibrium with body temperature and body water $\delta^{18}O$ values rather than with environmental temperatures and meteoric water $\delta^{18}O$ values. Many studies have found variable relationships between body water and meteoric water $\delta^{18}O$ values depending upon diet, humidity and physiology (e.g., Longinelli, 1984, Luz et al., 1984, D'Angela and Longinelli, 1990; Bryant et al., 1996, Kohn, 1996).

Kohn (1996) created a comprehensive model for predicting the effects of diet and physiological adaptation on body water and bone $\delta^{18}O$ values. For carnivores, the predicted relationship between bone or enamel $\delta^{18}O_p$ and surface water $\delta^{18}O$ values is:

$$\delta^{18}O_p = 21.3\text{-}3.0h + 0.74(\delta^{18}O_{sw}) \quad (3),$$

where *h* is relative humidity. The correlation between surface water $\delta^{18}O$ and body water $\delta^{18}O$ values for carnivores at 75% relative humidity is:

$$\delta^{18}O_{bw} = 0.74(\delta^{18}O_{sw}) + 1.47 \quad (4).$$

Prior to interpreting the isotopic patterns in tyrannosaurid teeth with respect to climatic factors, the general relationship for carnivores and surface water $\delta^{18}O$ in equations (3) and (4) must be demonstrated valid for carnivorous dinosaurs. Applying a typical range of relative humidity values (30 to 80%) and the range of measured $\delta^{18}O_p$ values from the tyrannosaur teeth to Equation (3), surface water $\delta^{18}O$ derived from enamel in this study fall between – 7.2‰ to – 15.5‰, usually below -12‰. These results are consistent with an independent determination of surface water $\delta^{18}O$ from this region of Alberta from Campanian turtle bone phosphate, showing a range from – 9.5‰to – 11.5‰(Barrick et al., 1999).

4.3 Influences of Ecology and Physiology on Isotopic Pattern

In homeothermic carnivores such as tyrannosaurids (Barrick and Showers, 1994), isotopic changes in body water are a reflection of changes in local surface water for two reasons. First, the body water $\delta^{18}O$ of homeotherms is not influenced by environmental temperature. Second, the carnivore's body water reservoir includes both drinking water consumed by the carnivore and drinking water from the body water of prey (Kohn, 1996). No trophic level effect has been demonstrated in $\delta^{18}O$ of body water for predators' assimilation of prey (i.e., no fractionation has been shown between food water and body water $\delta^{18}O$ values in predators). Most predators manufacture their body water primarily through drinking, whereas prey herbivores gain a large proportion of body water from foliage (Kohn, 1996). The $\delta^{18}O_p$ of homeothermic predators should therefore provide a better record of surface water $\delta^{18}O$ than that of herbivorous and/or heterothermic animals.

Sharp and Cerling (1998) found a relationship between body mass in some modern mammal species and enamel $\delta^{18}O_p$, in which the annual record of $\delta^{18}O_p$ from enamel is attenuated relative to that for coeval surface water $\delta^{18}O$ cycle. This signal dampening, as well as a delay in isotopic extremes, results from the long retention time of body water in very large animals (Nagy and Peterson, 1988). Precise effects of body mass on isotopic value, attenuation, and delay for dinosaurs, including the 3000-kg *Albertosaurus* used in this study, are not known. In this study, however, all teeth come from animals of at least subadult size, i.e., animals that had lived long enough to manufacture, wear out, and shed at least one set of teeth, probably >2 years (Erickson, 1996a). Hence the effect of body mass on enamel $\delta^{18}O_p$, if any, for these eight teeth should be approximately consistent.

4.4 Influences of Climate on Isotopic Pattern

Surface water $\delta^{18}O$ is critical to several models designed to reconstruct mean annual or mean monthly temperature. Enamel $\delta^{18}O_p$ values from several types of mammals have been used to approximate paleotemperature by first transforming $\delta^{18}O_p$ into surface water $\delta^{18}O$ through metabolic relationships (Bryant and Froelich, 1996; Kohn, 1996) and then transform it again using a relationship between surface water $\delta^{18}O$ and temperature (Dansgaard, 1964; Gat, 1980, Rozanski, 1993; Fricke and O'Neil, 1999),

$$\delta^{18}O = 0.69T - 13.6 \qquad (5).$$

Temperature and humidity vary on a regional scale due to elevation, latitude, and proximity to shorelines. Both influence surface water $\delta^{18}O$, with high temperature and low humidity each promoting enriched $\delta^{18}O$ values, with temperature the stronger of the two controls. However, above a threshold temperature, further increases in temperature do not impact meteoric water $\delta^{18}O$ due to the *amount effect*, defined as a relative depletion of precipitation $\delta^{18}O$ values by ~1.5‰ per 100 mm of precipitation (Dansgaard, 1964; Rozanski, 1993; Fricke and O'Neil, 1999). Typically, falling rain is progressively enriched by evaporation as it falls, but in air above a threshold temperature, enrichment of rainfall by evaporation ceases as the air through which the rain falls becomes saturated. Equation (5) implies that for an air temperature of 30° C, surface water should be + 6‰ but such precipitation values are never found (Rozanski, 1993; Fricke and O'Neil, 1999; Bowen and

Wilkinson, 2002). Instead, based on the most positive precipitation values measured empirically from sites around the world, Equation (5) is truncated above approximately 20º C (Rozanski, 1993; Bowen and Wilkinson, 2002), at and above which precipitation does not exceed 0‰, even at locations with extreme warmth for some or all of the year. This depletion and the absence of precipitation $\delta^{18}O$ values in excess of 0‰ are consequences of the amount effect. Kohn (1996) shows that surface water $\delta^{18}O$ at both New Delhi and Rio de Janeiro never exceeds 0‰ in spite of temperatures in excess of 20º C for at least nine months out of the year. During New Delhi's summer when mean monthly temperatures remain over 30º C, surface water $\delta^{18}O$ drops from 0‰ to -6‰. Given that atmospheric saturation could occur with less evaporation under lower temperature, the threshold temperature for the engagement of the amount effect may be less than 20º C at high altitude, at high latitude, or during winter months.

Above the threshold temperature, humidity becomes the critical control on precipitation $\delta^{18}O$. Precipitation falling into nearly saturated air rapidly engages the amount effect and thus retains its original, relatively depleted $\delta^{18}O$ value of the precipitation as it leaves the cloud. Consequently, locations for which summer corresponds to the annual humidity maximum may have their lowest $\delta^{18}O$ values during the hottest months. At Rio de Janeiro, where relative humidity is 80% all year, the annual signal is completely reversed relative to the predictions of Equation (6), with southern-hemisphere summer months of January to March having the lowest surface water $\delta^{18}O$ (Kohn, 1996). By contrast, highly arid regions such as the eastern Sahara feature the most positive $\delta^{18}O$ values for precipitation, nearly 0‰ (Bowen and Wilkinson, 2002), because the dry air cannot become saturated by the amount of precipitation falling through it. Due to the amount effect in climates regularly exceeding 20º C, neither surface water $\delta^{18}O$ nor enamel $\delta^{18}O_p$ proxies can be converted reliably to temperature.

However, as surface water responds to climatologic controls, and given that carnivore enamel $\delta^{18}O$ tracks surface water $\delta^{18}O$, comparisons of isotopic patterns from carnivore teeth should still reveal relative changes in the seasonal climate regime over several time scales. For comparative purposes, Figure 6 shows eight hypothetical plots of mean monthly surface water $\delta^{18}O$ for combinations of seasonality (high and low amplitude changes) and mean annual temperature (0, 3, 6, and 9 months with mean monthly temperature above

the amount effect threshold). For both types of seasonality, the annual $\delta^{18}O$ pattern shows two subequal maxima, reflecting the start and stop of amount effect influence, and a minimum between them associated with peak humidity. With relatively higher mean annual temperature, the amount effect is engaged for more months of the year (vertical axis, Fig. 6). Figure 6 suggests that at locations when mean temperature always exceeds the amount effect threshold, isotopic patterns will be the reverse of those predicted by Equation (5), consistent with Kohn's (1996) data from Rio de Janeiro.

4.5 Pattern Interpretation

The tyrannosaurid tooth enamel $\delta^{18}O_p$ data compare closely to hypothetical surface water curves of Figure 6. In each pattern, two maxima are interpreted as the timing for the engagement and cessation of the influence of the amount effect. The intervening minimum is interpreted as the point of maximum annual humidity and strongest influence over surface water and tooth enamel $\delta^{18}O$ by the amount effect. The bimodal annual isotopic maximum has been detected in teeth of gazelles (Kohn et al., 1998) and possibly explains the bifurcated maxima and dissimilar minima of a $\delta^{18}O_p$ seasonality record extracted from an elephant tusk (Koch et al., 1998). Narrowing of incremental lines associated with each minima in the tusk suggests reduced growth rate due to thermal stress (Koch et al., 1998); under this interpretation the animal suffers thermal stress during summer heat as well as during winter cold.

The patterns from the tyrannosaurids in the survey can be divided into two groups based on amplitude, with H021, F007b, F027, and F010 showing high (>1.4‰) amplitudes and B148, G008, D011, and D039 showing relatively lower amplitudes (<1.4‰). If the spacing between the maxima on a cyclic pattern represents the period of the year during which the amount effect is generally engaged (i.e., the period of the year during which the average temperature exceeds 20° C), each tooth can be compared to a specific hypothetic surface water trend in Figure 6 by converting the spacing between the isotopic maxima from millimeters of enamel to days, using established growth rates for tyrannosaurids. For example, the separation of the two maxima for F010 is 20 mm, which given expected growth rates correlates to 130 days of amount effect influence during the year (Fig. 6); the same period for low-amplitude tooth D011 corresponds to 80 days. Applying this conversion to the eight teeth patterns, teeth below 130 m AFB (H021, F007b, F010, F027, and

B148) reflect 4 to 7 months per year above the amount effect threshold, whereas teeth above 130 m AFB (D011, D039, and G008) reflect 2 to 4 months above the amount effect threshold (Fig. 6).

Isotopic results from tyrannosaurid enamel can be compared between teeth from the same fossiliferous horizon. Three teeth (F027, F007b, and F010) come from a fossiliferous horizon between 83 and 84.5 m AFB. All three teeth have high-amplitude cyclic signals and the highest isotopic ranges from the lower Horseshoe Canyon Formation, indicating a period of high seasonality (high annual temperature range with episodic precipitation and/or high humidity during only part of the year). By contrast, two teeth (D039, D011) from a fossiliferous horizon between 146 and 150 m AFB just below the transition to the Drumheller Marine Tongue feature low-amplitude cyclic signals interpreted as recording low seasonality (mild annual temperature and humidity range with relatively evenly distributed precipitation events through the year), with amplitudes of 1.36 and 0.97‰ respectively, although the isotopic range of D011 may be underestimated due to its size.

Isotopic results from tyrannosaurid teeth can also be compared stratigraphically and correlated with changes in stratigraphic architecture, sedimentology, and paleoenvironment. Independent stratigraphic sections and sedimentological analyses indicate that a significant change in depositional setting occurs above Coal Seam 9 (Straight and Eberth, 2002; Eberth, 2002; "SB" in Fig. 2). Above this boundary, coal and organic mudrocks are less common, rooted horizons are more common, and all facies are generally thinner than similar examples below the boundary. Preserved channels and levees are thinner, narrower, and finer-grained above the boundary than below. Organic-rich mudrocks interpreted as wetland facies are significantly less common above the boundary, and clay-rich paleosol facies are more common. The stratigraphic data indicate a transition from a wet climate, in which the amount effect likely played a role in surface water $\delta^{18}O$ values, to a drier climate, in which the amount effect would have been less important or inactive. Isotopic evidence from the tyrannosaurid teeth in this study is consistent with these changes; teeth from below the boundary all exhibit high-amplitude isotopic patterns interpreted as reflecting high seasonality, whereas those from above the transition all exhibit low-amplitude isotopic patterns consistent with mild seasonality.

Considered in terms of maximum value (Table 1, Fig. 7), the teeth fall into two groups: H021, F010, F007b, and D011 all have maxima at or above 12.6‰, whereas F027, B148, D039, and G008 have maxima at or less than 12.0‰. Overlap between the two groups depends upon a single measurement, probably an outlier,

in the F027 pattern (Fig. 7). In each group, mean $\delta^{18}O_p$ trends upsection toward more positive values. The trends of both groups follow a similar slope and are separated by ~2.5‰ One explanation for this non-stratigraphic grouping is that the data set contains teeth from two types of tyrannosaur, consistent with faunal lists which indicate that up to four types of tyrannosaurs occur in the lower Horseshoe Canyon Formation, including *Aublysodon*, two forms of *Albertosaurus*, and *Daspletosaurus* (Braman, 1988; Braman et al., 1995; Eberth et al., 2001). No unequivocal means yet exists to distinguish between individual species of tyrannosaur by dental morphology (Farlow et al., 1991; Baszio, 1997), as both the animals and the teeth they produce strongly overlap in size and design. A second explanation is that some of the tyrannosaurs fossilized in the lower Horseshoe Canyon Formation drink in one of two different regimes of mean annual temperature. If so, the groups could represent local niche partitioning (e.g., two water sources, such as non-local river water versus local, evaporatively-enriched ponded water) or migratory behavior in one or both groups of animals. The parallel trends of isotopic enrichment are consistent with both groups experiencing equivalent climate change, probably related to an increase in mean annual temperature.

4.6 Sampling Technique

Previous studies incorporated several sources of isotopic variability and error inherent in techniques in which isotopic analysis of enamel resulted in one $\delta^{18}O_p$ value for each tooth (Bryant et al., 1994; Iacumin et al., 1996a; Reinhard et al., 1996; Fricke and Rogers, 2000; Jensen et al., 2000). Measurement of $\delta^{18}O_P$ from enamel homogenized by stripping a whole tooth does not adequately represent an annual mean unless the preserved growth period is exactly a year. Otherwise, the result will be biased toward the isotopic value of the last season of enamel growth (Fig. 8). Thus, single-value analyses of a collection of unrelated teeth will result in a range of values. A single enamel $\delta^{18}O_p$ measurement from stripped tooth enamel formed in nine months may vary from the actual annual mean by ± 14% of the annual seasonal isotopic range (Fig. 8). For example, in a tooth influenced by a 2‰ seasonal cycle, a whole-tooth measurement of enamel $\delta^{18}O_p$ will vary by 0.57‰ From enamel formed over six months, the variation increases to ± 30%, and from enamel grown over three months, ± 43%. Enamel grown in periods of over a year can produce $\delta^{18}O_p$ variation of ± 10% of the annual range (Fig. 8).

Stripping enamel from several teeth from different individuals of one species will not necessarily reveal the annual isotopic mean, particularly in mammals in which teeth are formed at a specific time during the animal's life. Mineralization of permanent molar (M1) among equids begins just before a late-spring birth and lasts eight months (Nowak, 1991; Bryant et al., 1996). Consequently, most equid M1 teeth record the relatively enriched body water isotopic ratios experienced between early spring and mid winter. Therefore, a single-value measurement for each M1 in a population will generally over-estimate the actual annual mean. This problem is further compounded by tooth wear, particularly in herbivores, destroying the oldest enamel, truncating the preserved isotopic record, and commensurately increasing the potential range of isotopic variability. Theropod teeth are shed before developing significant wear and are continuously replaced, and consequently are less affected by these problems. However, conic or tapering teeth from theropod dinosaurs and canines from mammalian predators possess more enamel near the root than near the tip, biasing measurement of $\delta^{18}O_p$ in a homogenized sample toward the last enamel formed.

Serial sampling avoids these sources of variability by reducing the time-averaging of the preserved isotopic record. The serial sampling technique therefore presents several new opportunities for isotopic treatment of fossil remains, including the stratigraphic applications employed in this study. Serial sampling provides a new test for diagenesis, as a cyclic signal in $\delta^{18}O_p$ is unlikely to have been caused by or survived diagenetic alteration. In animals in which several teeth are formed at the same time or continuously replaced, enamel isotopic records should preserve an overlapping, self-checking isotopic record of body water $\delta^{18}O$. The enamel record in teeth from dental batteries of dinosaurs (Patchus et al., 2001) or the tusks of elephants (Ayliffe et al., 1992, 1994; Koch et al., 1996) may allow a multi-year record of meteoric water changes to be assembled. Cross-sections of large dinosaur bones bear lines of arrested growth (LAGs; Sander, 2000; Curry, 1999), which if serially sampled may yield a multi-year proxy for meteoric water and humidity.

5. Summary

Seasonal variations in the body water $\delta^{18}O$ of the theropod dinosaur *Albertosaurus* can be reconstructed by serially sampling enamel from unaltered teeth. The sampling technique used here avoids error associated with time-averaging associated with single whole tooth analyses or thick enamel. The

continuous replacement and the thin enamel of dinosaur teeth make them ideal for retrieving high resolution seasonal isotopic data. The patterns of these isotopic records are consistent with previously published tooth growth rates for *Albertosaurus*. Two general patterns arise from the isotopic data, consistent with evidence of changing climate regimes in the stratigraphic section of the lower Horseshoe Canyon Formation. The patterns are differentiated by the magnitude of the isotopic variation across the tooth and the shape of a double peak that likely arises from a seasonal jump in humidity. In addition, the eight teeth analyzed herein fall into two non-stratigraphic groups possibly associated with a taxonomic and/or ecological difference. Although the isotopic patterns in the enamel reflect variations in surface drinking water, these values cannot be accurately transformed into mean monthly or seasonal temperatures as the relationship between temperature and meteoric water isotope values is invalid above approximately 20^{o}C at which point humidity has the strongest effect upon meteoric isotope values. However, the interaction between temperature and humidity do generate predictable patterns in the seasonal variations of meteoric isotope values. Recognition of these patterns in the stratigraphic record can lead to an understanding of shifts in general climate regime. These climate patterns may then be correlated to patterns of sediment accumulation or faunal/floral turnover within the stratigraphic record.

Acknowledgements

The authors would like to thank Bernard Genna for analyzing specimens at the North Carolina State University Stable Isotope Facility and Julia Cox for sample analysis at the University of Arkansas Stable Isotope Laboratory. The assistance of Jonathan Perry and Patty Ralrick with field collection was invaluable. Comments and criticisms from Dale Russell, Alan Coulson, Matt Kohn, Jennifer Griffiths, Pennilyn Higgins, and an anonymous reviewer have improved this work. This project was supported in part by the 1st Annual Heaton Student Support Grant through the Royal Tyrrell Museum of Palaeontology in Drumheller, Alberta, by grants to RTMP from numerous petroleum companies throughout southern Alberta, and by a Rikleo Fund Research Grant.

References

Ayliffe, L.K., Lister, A.M., Chivas, A.R., 1992. The preservation of glacial-interglacial climatic signatures in the oxygen isotopes of elephant skeletal phosphate. Palaeogeography, Palaeoclimatology, Palaeoecology, 99,179-191.

Ayliffe, L.K., Chivas, A.R., Leakey, M.G., 1994. The retention of primary oxygen isotope compositions of fossil elephant skeletal phosphate. Geochimica et Cosmochimica Acta, 58(23),5291-5298

Balasse, M., Bocherens, H., Mariotti, A., Ambrose, S.H., 2001. Detection of dietary changes by intra-tooth carbon and nitrogen isotopic analysis: an experimental study of dentine collage of cattle (*Bos taurus*). Journal of Archaeological Science, 28,235-245.

Barker, M.J., Clark, J.B., Martill, O.M., 1997. Mesozoic reptile bones as diagenetic windows. Bulletin of the Geologic Society of France, 168(5),535-545.

Barrick, R.E., 1998. Isotope paleobiology of the vertebrates: ecology, physiology, and diagenesis. The Paleontological Society Papers, v. 4: Isotope Paleobiology and Paleoecology, pp. 101-137.

Barrick, R.E., Showers, W.J., 1994. Thermophysiology of *Tyrannosaurus rex*: Evidence from Oxygen Isotopes. Science, 265,222-224.

Barrick, R.E., Showers, W.J., 1995. Oxygen isotope variability in juvenile dinosaurs (*Hypacrosaurus*): evidence for thermoregulation. Paleobiology, 21(4),552-560.

Barrick, R.E., Fischer, A.G., Kolodny, Y., Luz, B., Bohaska, D., 1992. Cetacean bone oxygen isotopes as proxies for Miocene ocean composition and glaciation. Palaios, 7,521-531.

Barrick, R.E., Fischer, A.G., Bohaska, D., 1993. Paleotemperatures versus sea level: oxygen isotope signal from fish bone phosphate of the Miocene Calvert Cliffs, Maryland. Paleoceanography, 8(6),845-858.

Barrick, R.E., Showers, W.J., Fischer, A.G., 1996. Comparison of thermoregulation in four ornithischian dinosaurs and a varanid lizard from the Cretaceous Two Medicine Formation: Evidence from oxygen isotopes. Palaios, 11,295-305.

Barrick, R.E., Fischer, A.G., and Showers, W.J., 1999. Oxygen isotopes from turtle bone: Application for terrestrial paleoclimate? Palaios, 14(2),186-191.

Baszio, S., 1997. Investigations on Canadian dinosaurs: systematic paleontology of isolated dinosaur teeth from the latest Cretaceous of south Alberta, Canada. Courier Forschungsinstitut Senckenberg, 196, 33-77.

Blake, R.E., O'Neil, J.R., Garcia, G.A., 1997. Oxygen isotope systematics of biologically mediated reactions of phosphate: I. microbial degradation of organophosphorus compounds. Geochimica et Cosmochimica Acta, 61(20),4411-4422.

Bocherens, H., Brinkman, D., Dauphin, Y., Mariotti, A., 1994. Microstructural and geochemical investigations on Late Cretaceous archosaur and crocodilian teeth from Alberta, Canada. Canadian Journal of Earth Science 21,783-792.

Bowen, G.J., Wilkinson, B., 2002. Spatial distribution of $\delta^{18}O$ in meteoric precipitation. Geology, 30(4),315-318.

Braman, D.R., Eberth, D.A., 1988. Paleontology and geology of the Edmonton Group (late Cretaceous to early Paleocene), Red Deer River Valley, Alberta, Canada. Society of Vertebrate Paleontology 48th Annual Meeting Field Guidebook. Occasional Paper of the Tyrrell Museum of Palaeontology no. 8, Drumheller, Alberta, pp. 1-25.

Braman, D.R., Johnston, P.A., Haglund, W.A., 1995. Upper Cretaceous paleontology, stratigraphy, and depositional environments at Dinosaur Provincial Park and Drumheller, Alberta. Canadian Paleontology Conference Field Trip Guidebook no. 4. Geological Association of Canada, St. John's, Newfoundland, pp. 1-119.

Bryant, J.D., Froelich, P.N., 1995. A model of oxygen isotopic fractionation in body water of large mammals. Geochimica et Cosmochimica Acta, 59(21),4523-4537.

Bryant, J.D., Luz, B., Froelich, P.N., 1994. Oxygen isotopic composition of fossil horse tooth phosphate as a record of continental paleoclimate. Palaeogeography, Palaeoclimatology, Palaeoecology, 107,303-316.

Bryant, J.D., Froelich, P.N., Showers, W.J., Genna, B.J., 1996. A tale of two quarries: Biologic and taphonomic signatures in the oxygen isotope composition of tooth enamel phosphate from modern and Miocene equids. Palaios, 11(4),397-408.

Catuneanu, O., Sweet, A.R., 1999. Maastrichtian-Paleocene foreland-basin stratigraphies, western Canada: a reciprocal sequence architecture. Canadian Journal of Earth Sciences, 36,685-703.

Cerling, T.E., Harris, J.M., MacFadden, B.J., 1998. Carbon isotopes, diets of North American equids, and the evolution of North American C4 grasslands. In: Griffiths, H., (ed.), Stable Isotopes, BIOS Scientific Publishers Ltd. Oxford. pp. 363-379.

Cerling, T.E., Sharp, Z.D., 1996. Stable carbon and oxygen isotope analysis of fossil tooth enamel using laser ablation. Palaeogeography, Palaeoclimatology, Palaeoecology, 126,173-186.

Cormie, A.B., Luz, B., Schwarcz, H.P., 1994. Relationship between the hydrogen and oxygen isotopes of deer bone and their use in the estimation of relative humidity. Geochimica et Cosmochimica Acta, 58,3439-3449.

Curry, K., 1999. Ontogenetic histology of *Apatosaurus* (Dinosauria, Sauropoda): new insights on growth rates and longevity. Journal of Vertebrate Paleontology, 19,654-665.

D' Angela, D., Longinelli, A., 1990. Oxygen isotopes in living mammal' s bone phosphate: further results. Chemical Geology, 86,75-82.

Dansgaard, W., 1964. Stable isotopes in precipitation. Tellus, 16,436-468.

Dean, M.C., 2000. Incremental markings in enamel and dentine: what they can tell us about the way teeth grow. In: Teaford, MF, MM Smith, and MWJ Ferguson, (eds.), Development, Function, and Evolution of Teeth. Cambridge University Press, Cambridge, pp. 119-130.

Dettman, D.L., Kohn, M.J., Quade, J., Ryerson, F.J., Ojha, T.P., Hamidullah, S., 2001. Seasonal stable isotope evidence for a strong Asian monsoon throughout the past 10.7 m.y. Geology, 29(1),31-34.

Eberth, D.A., 2002. Taphonomic modes of large dinosaurs in the Horseshoe Canyon Formation (Campanian-Maastrichtian) of southern Alberta, Canada. Journal of Vertebrate Paleontology, Abstracts of Papers, 62nd Annual Meeting, Norman, Oklahoma, 22(3s), 50A-51A.

Eberth, D.A., Currie, P.J., Brinkman, D.B., Ryan, M.J., Braman, D.R., Gardner, J.D., Lam, V.D., Spivak, D.N., Neuman, A.G., 2001. Alberta's dinosaurs and other fossil vertebrates: Judith River and Edmonton groups (Campanian-Maastrichtian). In: Hill, C.L., (ed.), Society of Vertebrate Paleontology, 61st Annual Meeting Field Trip Guidebook. Museum of the Rockies Occasional Paper no. 3, Bozeman, Montana, pp. 49-75.

Erickson, G.M., 1996a. Incremental growth lines of von Ebner in dinosaurs and the assessment of tooth replacement rates using growth line counts. Bulletin of the National Academy of Sciences, 93,14623-14627.

Erickson, G.M., 1996b. Toothlessness in American Alligators, *Alligator mississippiensis*. Copeia, 3,739-743.

Farlow, J.O., Brinkman, D.L., Alber, W.L., Currie, P.J., 1991. Size, shape, and serration density of theropod dinosaur lateral teeth. Modern Geology, 16,161-198.

Farquhar, G.D., Henry, B.K., Styles, J.M., 1997. A rapid on-line technique for determination of oxygen isotope composition of nitrogen-containing organic matter and water. Rapid Communications in Mass Spectrometry, 11,1554-1560.

Feranec, R.S., MacFadden, B.J., 2000. Evolution of the grazing niche in Pleistocene mammals from Florida: evidence from stable isotopes. Palaeogeography, Palaeoclimatology, Palaeoecology, 162,155-169.

Fox, D.L., Fisher, D.C., 2001. Stable isotope ecology of a late Miocene population of *Gomphotherium productus* (Mammalia, Proboscidea) from Port of Entry Pit, Oklahoma, USA. Palaios, 16(3),279-293.

Fricke, H.C., O'Neil, J.R., 1996. Inter- and intra-tooth variation in the oxygen isotope composition of mammalian tooth enamel phosphate: implications for paleoclimatological and paleobiological research. Palaeogeography, Palaeoclimatology, Palaeoecology, 126,91-99.

Fricke H.C., Clyde, W.C., O'Neil, J.R., Gingerich, P.D., 1998. Evidence for rapid climate change in North America during the latest Paleocene thermal maximum: oxygen isotope compositions of biogenic phosphate from the Bighorn Basin (Wyoming). Earth and Planetary Science Letters, 160,193-208.

Fricke, H.C., O'Neil, J.R., 1999. The correlation between $^{18}O/^{16}O$ ratios of meteoric water and surface temperature: its use in investigating terrestrial climate change over geologic time. Earth and Planetary Science Letters, 170,181-196.

Fricke, H.C., Rogers, R.R., 2000. Multiple taxon-multiple locality approach to providing oxygen isotope evidence for warm-blooded theropod dinosaurs. Geology, 28(9),799-802.

Gadbury, C., Todd, L., Jahren, A.H., Amundsen, R., 2000. Spatial and temporal variations in the isotope composition of bison tooth enamel from the early Holocene Hudson-Meng Bonebed, Nebraska. Palaeogeography, Palaeoclimatology, Palaeoecology, 157,79-93.

Gat, J.R., 1980. The isotopes of hydrogen and oxygen in precipitation; in Handbook of environmental isotope geochemistry, volume 1. Elsevier, New York Amsterdam. pp. 21-47.

Gibson, D.W., 1977. Upper Cretaceous and Tertiary coal-bearing strata in the Drumheller-Ardley region, Red Deer River Valley, Alberta. Geological Survey of Canada Paper 76-35:1-41.

Hobson, K.A., Sease, J.L., 1998. Stable isotope analyses of tooth annuli reveal temporal dietary records: an example using stellar sea lions. Marine Mammal Science, 14,116-129.

Hillson, S. 1986. Teeth. Cambridge University Press. pp. 376.

Hoppe, K.A., Amundsen, R., 2001. Patterns of tooth enamel formation in hypsodonty teeth: Implications for isotopic microsampling. 61st Annual Meeting, Abstracts of Papers, Journal of Vertebrate Paleontology, 21,63.

Hubert, J.F., Panish, P.T., Chure, D.J., Prostak, K.S., 1996. Chemistry, microstructure, petrology, and diagenetic model of Jurassic dinosaur bones, Dinosaur National Monument, Utah. Journal of Sedimentary Research, 66,531-547.

Iacumin, P., Bocherens, H., Mariotti, A., Longinelli, A., 1996a. Oxygen isotope analyses of co-existing carbonate and phosphate in biogenic apatite: a way to monitor diagenetic alteration of bone phosphate? Earth and Planetary Science Letters, 142,1-6.

Iacumin, P., Cominotto, D., Longinelli, A., 1996b. A stable isotope study of mammal skeletal remains of mid-Pleistocene age, Arago cave, eastern Pyrenees, France: Evidence of taphonomic and diagenetic effects. Palaeogeography, Palaeoclimatology, Palaeoecology, 126,151-160.

Jarvis, I., 1992. Sedimentology, geochemistry and origin of phosphatic chalks: the Upper Cretaceous deposits of NW Europe. Sedimentology, 39,55-97.

Jensen, M.L., Sharp, Z.D., Lucas, S.G., 2000. Migrating Cretaceous theropods? Evidence from oxygen isotope geochemistry, Canada and New Mexico. In: Lucas, S.G., Heckert, A.B., (eds.), Dinosaurs of New Mexico. New Mexico Museum of Natural History and Science Bulletin 17,91.

Jensen, M.L., 2000. Oxygen isotope analysis of sympatric late Cretaceous crocodile and theropod tooth enamel: Evidence for ectothermic theropod dinosaurs. M.S. Thesis, University of New Mexico, Albuquerque, New Mexico.

Johnston, P., 1979. Growth bands in dinosaur teeth. Nature, 278(5075):635-636.

Koch, P.L., Fisher, D.C., Dettman, D.L., 1989. Oxygen isotope variation in the tusks of extinct proboscideans: A measure of season of death and seasonality. Geology, 17,515-519.

Koch, P.L., Hoppe, K.A., Webb, S.D., 1998. The isotopic ecology of late Pleistocene mammals in North America, Part 1. Florida. Chemical Geology, 152,119-138.

Koch, P.L., Behrensmeyer, A.K., Stott, A.W., Tuross, N., Evershed, R.P., Fogel, M.L., 2000. The effects of weathering on the stable isotope composition of bones. Ancient Biomolecules, 3,117-134.

Kohn, M.J.. 1996. Predicting animal $\delta^{18}O$: accounting for diet and physiological adaptation. Geochimica et Cosmochimica Acta, 60(23),4811-4829.

Kohn, M.J., Schoeninger, M.J., Valley, J.W., 1996. Herbivore tooth oxygen isotope compositions: Effects of diet and physiology. Geochimica et Cosmochimica Acta, 60(20),3889-3896.

Kohn, M.J., Schoeninger, M.J., Valley, J.W., 1998. Variability in oxygen isotope compositions of herbivore teeth: reflections of seasonality or developmental physiology? Chemical Geology, 152,97-112.

Kohn, M.J., Schoeninger, M.J., Barker, W.W., 1999. Altered states: Effects of diagenesis on fossil tooth chemistry. Geochimica et Cosmochimica Acta, 63(18):2737-2747.

Kolodny, Y., Luz, B., and Navon, O., 1983. Oxygen isotope variations in phosphate of biogenic apatites, I. Rechecking the rules of the game: Earth and Planetary Science Letters 64,398-404.

Kolodny, Y., Luz, B., Sander, M., Clemens, W.A., 1996. Dinosaur bones: fossils or pseudomorphs? The pitfalls of physiology reconstruction from apatitic fossils. Palaeogeography, Palaeoclimatology, Palaeoecology, 126,161-171.

Kornexl, B.E., Gehre, M., Hoffling, R., Werner, R.A., 1999a. On-line $\delta^{18}O$ measurement of organic and inorganic substances. Rapid Communications in Mass Spectrometry, 13:1685-1693.

Kornexl, B.E., Werner, R.A., Gehre, M., 1999b. Standardization for oxygen isotope ratio measurement—still an unsolved problem. Rapid Communications in Mass Spectrometry, 13:1248-1251.

Koziet, J., 1997. Isotope ratio mass spectrometric method for the on-line determination of oxygen-18 in organic matter. Journal of Mass Spectrometry, 32, 103-108.

Lee-Thorp, J.A., Manning, L., Sponheimer, M., 1997. Problems and prospects for carbon isotope analysis of very small samples of fossil tooth enamel. Bulletin of the Geological Society of France, 168(6),767-773.

Lucas, J., Prévôt, L.E., 1991. Phosphates and Fossil Preservation. In: Allison, P.A., Briggs, D.E.G, (eds.), Taphonomy: Releasing the Data Locked in the Fossil Record, Volume 9 of Topics in Geobiology. Plenum Press, New York, pp. 389-409.

Longinelli, A., Nuti, S., 1973. Revised phosphate-water isotopic temperature scale: Earth Planetary Science Letters, 19,373-376.

Longinelli, A., 1984. Oxygen isotopes in mammal bone phosphate: A new tool for paleohydrological and paleoclimatological research?: Geochimica et Cosmochimica Acta, 48,385-390.

Luz, B., Kolodny, Y., Horowitz, M., 1984. Fractionation of oxygen isotopes between mammalian bone-phosphate and environmental drinking water: Geochimica et Cosmochimica Acta, 48,1689-1693.

Luz, B., Kolodny, Y., 1985. Oxygen isotope variations in phosphate of biogenic apatites IV: Mammal teeth and bones. Earth and Planetary Science Letters, 75, 29-36.

Luz, B., Kolodny, Y., 1989. Oxygen isotope variation in bone phosphate. Applied Geochemistry, 4,317-323.

Nagy, K.A., Peterson, C.C., 1988. Scaling of water flux rate in animals. University of California Publications in Zoology, 120:1-172.

Nielsen-Marsh, C.M., Hedges, R.E., 2000. Patterns of diagenesis in bone I: the effect of site environments. Journal of Archaeological Science, 27,1139-1150.

Nowak, R.M., 1991. Walker's Mammals of the World, 5th Edition. Johns Hopkins University Press, Baltimore London. 1627 p.

Patchus, R., Straight, W.H., Barrick, R.E., Showers, W.J., Genna, B., 2001. Biologic and ecologic information from oxygen and carbon isotope records in hadrosaur tooth enamel. 61st Annual Meeting, Abstracts of Papers, Journal of Vertebrate Paleontology, 21,87-88.

Pate, F.D., Hutton, J.T., Norris, K., 1989. Ionic exchange between soil solution and bone: Toward a predictive model. Applied Geochemistry, 4:303-316

Person, A., Bocherens, H., Saliege, J.F., Paris, F., Zeitoun, V., Gerard, M., 1995. Early diagenetic evolution of bone phosphate: an X-ray diffractometry analysis. Journal of Archaeological Science, 22,:211-221.

Reinhard, E., de Torres, T., O'Neil, J.R., 1996. $^{18}O/^{16}O$ ratios of cave bear tooth enamel: a record of climate variability during the Pleistocene. Palaeogeography, Palaeoclimatology, Palaeoecology, 126,45-59.

Rink, W.J., Schwarcz, H,P., 1995. Tests for diagenesis in tooth enamel: ESR dating signals and carbonate contents. Journal of Archaeological Science, 22,251-255.

Rozanski, K., Araguas-Araguas, L., Gonfantini, R., 1993. Isotopic patterns in modern global rainfall. Geophysical Monograph, 78,1-36.

Sanchez-Chillon, B., Alberdi, M.T., Leone, G., Bonadonna, F.P., Stenni, B., Longinelli, A., 1994. Oxygen isotopic composition of fossil equid tooth and bone phosphate: an archive of difficult interpretation. Palaeogeography, Palaeoclimatology, Palaeoecology, 107,314-328.

Sander, M., 1999. The microstructure of reptilian tooth enamel: terminology, function, and phylogeny. Muncher Geowissenshaftliche Abhandlungen, Reihe A-38, 102 p.

Sander, M., 2000. Longbone hisotology of Tendaguru sauropods: implications for growth and biology. Paleobiology, 26,466-488.

Sharp, Z.D., Cerling, T.E., 1998. Fossil isotope records of seasonal climate and ecology: straight from the horse's mouth. Geology, 26(3),219-222.

Shemesh, A., Kolodny, Y., Luz, B., 1988. Isotope geochemistry of oxygen in phosphate and carbonate of phosphorite francolite. Geochimica et Cosmochimica Acta, 52:2565-2572.

Showers, W.J., Barrick, R.E., Genna, B., 2002. Isotopic analysis of dinosaur bones. Analytical Chemistry 74,142a-150a.

Stuart-Williams, H.L., Schwarcz, H.P., 1997. Oxygen isotopic determination of climatic variation using phosphate from beaver bone, tooth enamel, and dentine. Geochimica et Cosmochimica Acta, 61(12),2539-2550.

Straight, W.H., Eberth, D.A., 2002. Testing the utility of vertebrate remains in recognizing patterns in fluvial deposits: An example from the lower Horseshoe Canyon Formation, Alberta. Palaios, 17(5), 472-490.

Wang, Y., Cerling, T.E, 1994. A model of fossil tooth and bone diagenesis: implications for paleodiet reconstruction from stable isotopes. Palaeogeography, Palaeoclimatology, Palaeoecology, 107,281-289.

APPENDIX CAPTION

APPENDIX. Enamel phosphate $\delta^{18}O$ data from eight tyrannosaurid teeth from the lower Horseshoe Canyon Formation. Asterisks indicate that the isotopic values is an average of two* or three* * replicate analyses.

Appendix, Part 1

H021		F010		F027		F007b	
elev mm from tip	17 m $\delta^{18}O$ (‰)	elev mm from tip	83 m $\delta^{18}O$ (‰)	elev mm from tip	83 m $\delta^{18}O$ (‰)	elev mm from tip	84.5 m $\delta^{18}O$ (‰)
32.2*	11.91	44.5*	13.03	54.0	10.04	62.0	11.49
30.7	12.50	42.9*	12.97	50.1	10.19	58.9	12.05
29.4	12.58	41.0*	13.38	48.8*	10.13	56.2	12.08
28.0	12.39	39.4*	13.04	47.4	9.70	52.9	12.76
26.5	11.54	38.0*	12.45	46.0	9.97	49.1	12.64
25.4	12.03	36.0	12.80	44.8	10.06	46.6	11.35
21.9	11.79	34.3*	12.82	43.8	10.83	43.7	12.16
20.4	12.21	32.5*	12.65	42.0	9.79	40.5	12.18
18.9	11.71	31.0*	12.84	41.1	10.20	38.5	13.61
17.0	12.19	29.5	12.53	39.9	9.74	34.7	12.36
15.4	12.46	28.0*	13.19	38.7	10.41	31.6	12.12
11.6	12.66	26.5**	12.88	37.5*	10.19	28.4	12.25
9.2*	12.13	24.8*	13.01	36.7	9.62	25.5	11.16
7.6	11.39	23.2*	13.22	34.9	9.32	22.4	11.77
6.0	11.67	21.3*	13.60	33.4	9.17	19.2	11.39
3.8	11.21	19.7*	13.18	32.3	10.70	15.7	11.67
2.0	11.93	18.0*	12.68	29.8	9.98	11.4	12.33
0.0	11.78	15.7*	12.70	28.5	10.53	8.2	11.86
		14.0*	12.87	27.8	10.56	4.2	13.46
		12.1*	12.57	26.7	10.89	0.0	11.25
		9.2	12.42	25.5*	11.07		
		7.3**	12.36	23.8	10.49		
		5.8*	12.42	22.2	10.96		
		3.8*	12.09	19.3	11.02		
		2.3*	11.78	16.5	10.79		
		0.0*	11.67	14.8	11.76		
				13.2	10.64		
				11.5	10.28		
				10.0	10.77		
				8.5	9.65		
				7.0*	10.81		
				5.7	10.41		
				3.9	10.04		
				3.0	9.85		
				1.2	9.58		
				0.0	9.87		

Appendix, Part 2

B148		D011		D039		G008	
elev	129 m	elev	146 m	elev	150 m	elev	170 m
mm from tip	$\delta^{18}O$ (‰)	mm from tip	$\delta^{18}O$ (‰)	mm from tip	$\delta^{18}O$ (‰)	mm from tip	$\delta^{18}O$ (‰)
30.2	10.48	22.6	12.86	44.8	11.18	32.3	11.29
28.1	10.03	20.9	13.58	42.0	10.29	31.2*	11.63
26.6	10.71	18.9	13.21	41.0	10.38	30.1	11.74
24.6	11.10	17.2	12.67	39.8	10.72	28.5	11.35
22.7	10.54	15.8	13.23	38.3	10.64	26.7	11.87
21.3	10.88	14.4	13.06	36.5	11.55	24.3	11.35
18.0	10.49	12.7	13.29	33.2	11.13	22.8	11.44
14.1	10.43	11.2*	13.27	31.9	11.02	20.3	11.15
12.4	10.41	10.0	13.02	30.5	10.73	18.3*	11.29
10.7	10.32	8.6	13.64	29.1	10.69	16.1	11.91
9.2	9.84	7.0*	13.56	27.6	10.21	14.1	11.79
7.7	9.85	5.3	13.29	26.4	10.69	12.3	11.59
5.5	9.92	3.7	13.49	25.0	10.44	10.1	12.03
4.0	10.61	2.0	13.31	23.4	10.40	7.9	11.57
1.7	10.48	0.0	13.37	22.2*	10.67	5.4	11.47
0.0	9.85			19.2	10.73	2.7*	11.50
				18.0	10.19	0.0	11.53
				16.6	10.81		
				14.4	10.54		
				13.1	10.47		
				11.7	10.55		
				10.0*	10.49		
				8.1	10.59		
				6.5	10.41		
				4.9	10.68		
				3.8	10.27		
				2.1	10.67		
				0.0*	10.83		

TABLE CAPTION

TABLE 1. Stratigraphic position and isotopic summary for tyrannosaurid teeth used in this study. *Elevation* lists each tooth's stratigraphic level above the basal contact of the Horseshoe Canyon Formation in meters.

Table 1

	elevation (m AFB)	length	max $\delta^{18}O$	$\delta^{18}O$ range
H021	17 m	32 mm	12.66‰	1.45‰
F010	83 m	45 mm	13.60‰	1.93‰
F027	83 m	54 mm	11.76‰	2.60‰
F007b	84.5 m	62 mm	13.61‰	2.45‰
B148	126 m	30 mm	11.10‰	1.26‰
D011	146 m	23 mm	13.64‰	0.97‰
D039	150 m	45 mm	11.55‰	1.36‰
G008	170 m	32 mm	12.03‰	0.87‰

FIGURE CAPTIONS

FIGURE 1. Fluxes of oxygen contributing to isotopic ratio of body water reservoir in theropod dinosaur (modified from Bryant and Froelich, 1995).

FIGURE 2. Location and stratigraphic relationships for theropod tooth collection sites in the Horseshoe Canyon Formation of Alberta, Canada. The *PM* column indicates the paleomagnetic record for the Edmonton Group (Eberth, 2002). The base of the Horseshoe Canyon Formation is the baseline for both thickness (*m*, in meters) and the numerical hierarchy for major coal seams (Gibson, 1977; Straight and Eberth, 2002); Coal Seam 13 within the Scollard Formation is also known as the Nevis Coal Seam and marks the Cretaceous-Paleocene (K-T) boundary. Intervals dominated by kilometer-wide sandstone units >10m thick are labeled as *SS*. Sequence boundaries (*SB*) indicate changes in facies and architecture of deposits; their positions are approximate.

FIGURE 3. Incremental growth bands and structure of a theropod tooth. (A) Cut-away section revealing incremental bands (lines of von Ebner) in dentine (cones expanding toward tooth root) and in the enamel sheath (striae of Retzius; enamel thickness exaggerated for clarity). (B) Incremental bands on enamel surface produce gently arcing growth lines transverse to tooth length. (C) Sampling pattern used on tooth RTMP1.

FIGURE 4. Visual cues guiding sample collection in the surface texture (A) or color (B,C) on fossil theropod teeth. (A) *Albertosaurus* and (B) *Saurornitholestes*, both from lower Horseshoe Canyon Formation. (C) Tyrannosaurid tooth from Dinosaur Provincial Park. Scale bars are 5 mm.

FIGURE 5. Enamel oxygen isotope data from eight serially-sampled tyrannosaurid teeth. Patterns distributed to avoid overlap; horizontal and vertical scale consistent within but not between individual tooth patterns. Small numbers display boundary isotopic values in per mil, boxed numbers display distance of last sample from tooth tip in millimeters. Gray points indicate two averaged measurements of the same sample, black

points indicate three. Large bold values under sample names indicate elevation above the base of the Horseshoe Canyon Formation. Lines are two-point running averages of data to clearly separate profiles while displaying similarities among isotopic trends between patterns.

FIGURE 6. Hypothetical variations of surface water $\delta^{18}O$ over eighteen months for high- and low-seasonality environments. Vertical variation reflects the difference given the length of time (center, in months) during which temperatures exceed the amount effect threshold (AE). Results from tyrannosaur teeth are compared to hypothetical patterns and placed by matching signal amplitude and spacing between maxima (in parentheses, converted from millimeters to days given growth rate estimates).

FIGURE 7. Isotopic range versus elevation for the eight tyrannosaurid teeth. Elevation (x-axis) is recorded as meters above formation base (AFB). Teeth fall into two non-stratigraphic groups, separated by ~2.5‰and both trending upsection toward more positive mean $\delta^{18}O_p$. The overlap between F010, F007b and F027 (slightly exploded along the x-axis for clarity) represents the only point of contact between the two groups and depends on one possibly anomalous point on the F027 pattern. These groups could reflect two distinct species of tyrannosaurids and/or some form of ecological separation (niche partitioning, migration, difference in diet, etc.).

FIGURE 8. Effects of single-measurement techniques on tooth enamel isotopic results. A hypothetical simple seasonal variation of surface water oxygen isotopes varies cyclically by 2‰over a year. Sample teeth, positioned under the portion of the seasonal curve their enamel integrates and to right of their growth period in months, show effects of time-averaging on isotopic results. The value inside each tooth indicates the divergence from annual average (AA) for a single isotopic measurement of enamel; the cross above the midpoint of each tooth shows the measurement relative to surface water curve. Values to the right of each tooth indicate the maximum isotopic range, out of the 2‰annual range and as a percentage of the annual range, between teeth formed over a period of months listed to the left of each tooth. Conical or tapering teeth and/or a more complex seasonality curve will result in more complex isotopic variability in teeth.

Figure 1

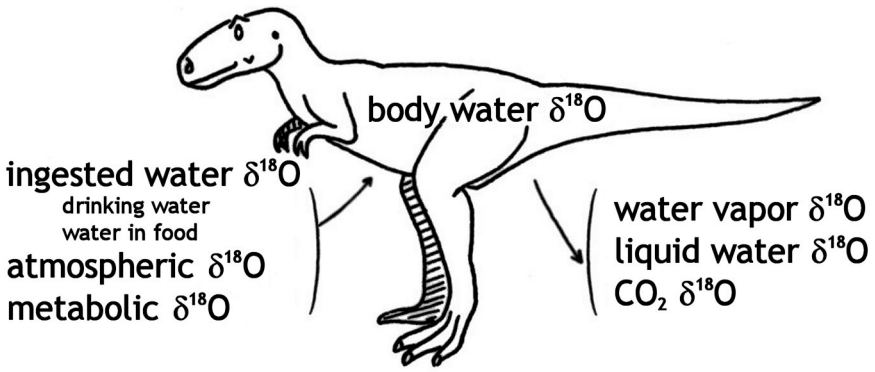
body water $\delta^{18}O$
ingested water $\delta^{18}O$
drinking water
water in food
atmospheric $\delta^{18}O$
metabolic $\delta^{18}O$
water vapor $\delta^{18}O$
liquid water $\delta^{18}O$
CO_2 $\delta^{18}O$

Figure 2

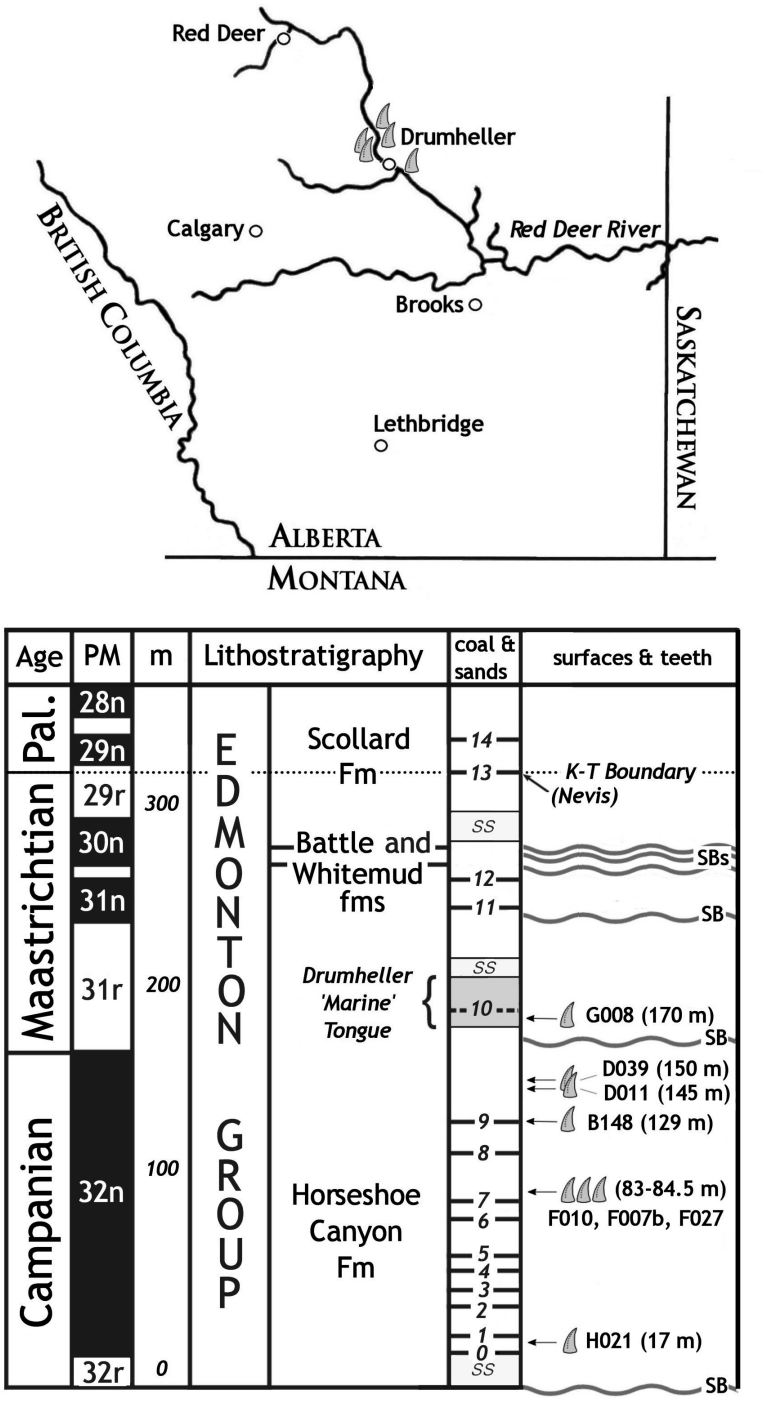
Red Deer
Drumheller
Calgary
Red Deer River
Brooks
Lethbridge
BRITISH COLUMBIA
SASKATCHEWAN
ALBERTA
MONTANA
Age
PM
m
Lithostratigraphy
coal & sands
surfaces & teeth
Pal.
Maastrichtian
Campanian
28n
29n
29r
30n
31n
31r
32n
32r
300
200
100
0
EDMONTON GROUP
Scollard Fm
Battle and Whitemud fms
Drumheller 'Marine' Tongue
Horseshoe Canyon Fm
14
13
12
11
10
9
8
7
6
5
4
3
2
1
0
SS
K-T Boundary (Nevis)
SBs
SB
G008 (170 m)
D039 (150 m)
D011 (145 m)
B148 (129 m)
(83-84.5 m)
F010, F007b, F027
H021 (17 m)

Figure 3

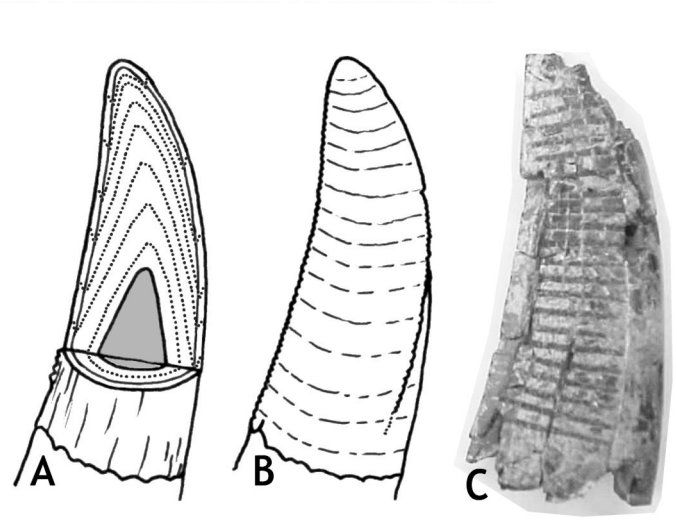

Figure 4

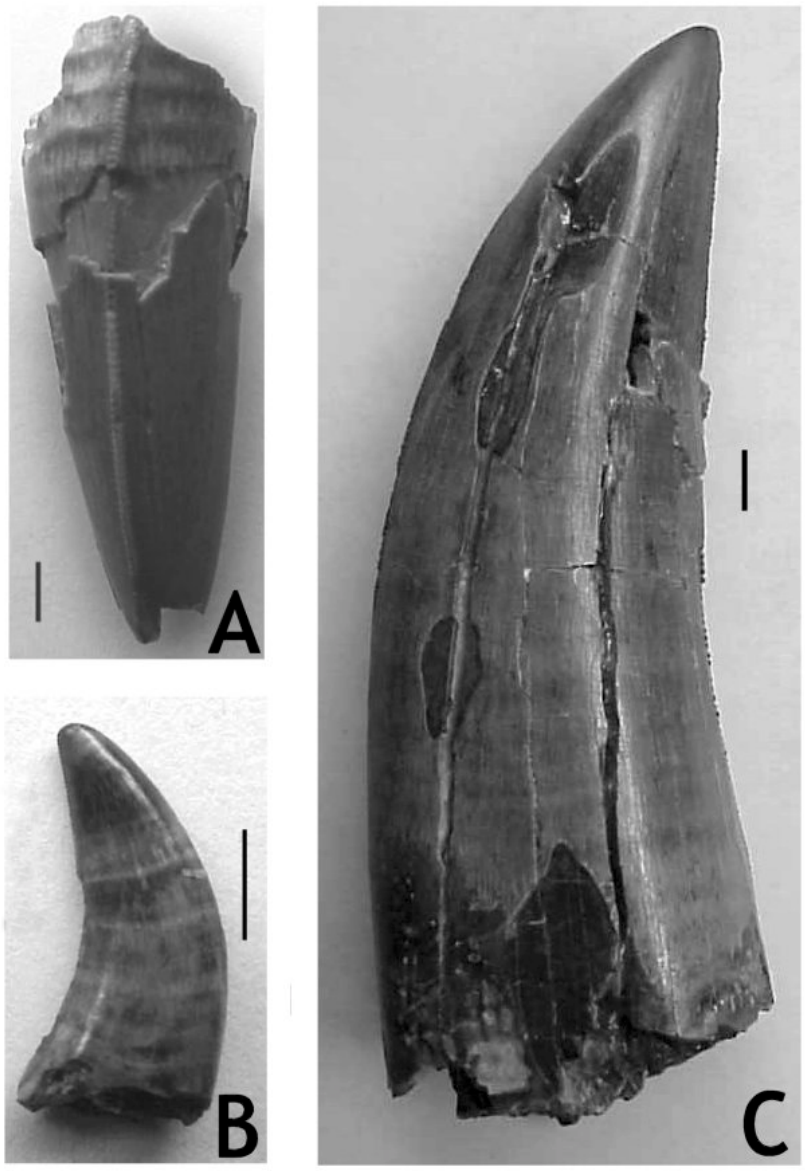

Figure 5

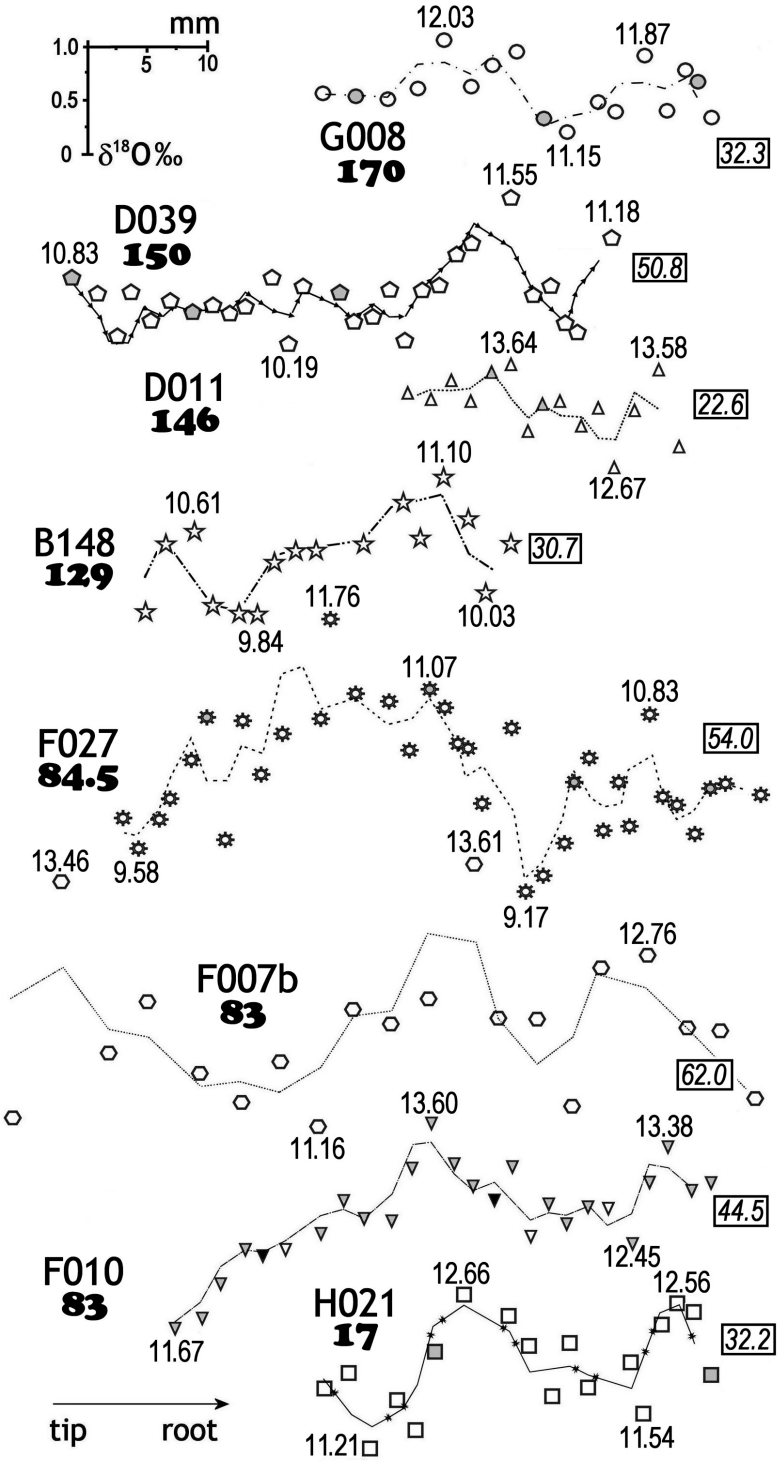
mm
1.0
0.5
0
5
10
δ18O‰
G008
170
12.03
11.87
11.15
11.55
32.3
D039
150
10.83
11.18
50.8
10.19
D011
146
13.64
13.58
22.6
12.67
B148
129
11.10
10.61
30.7
11.76
10.03
9.84
F027
84.5
11.07
10.83
54.0
13.46
9.58
13.61
9.17
F007b
83
12.76
62.0
11.16
13.60
13.38
44.5
12.45
F010
83
11.67
H021
17
12.66
12.56
32.2
11.21
11.54
tip
root

Figure 6

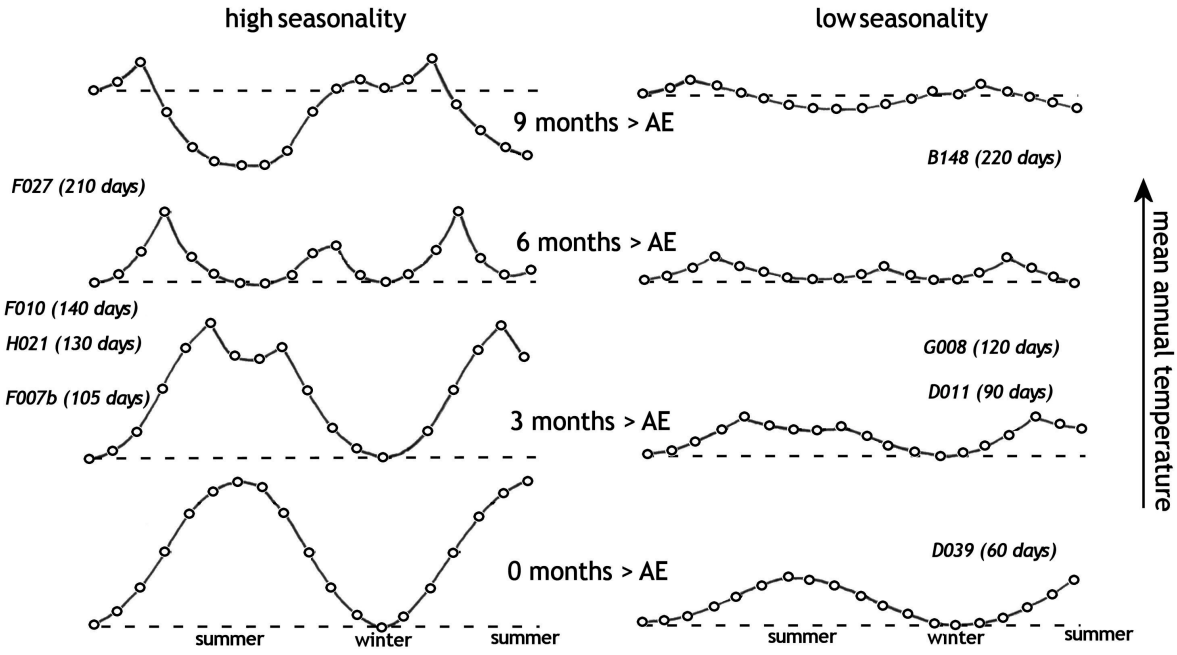
high seasonality
low seasonality
9 months > AE
B148 (220 days)
F027 (210 days)
6 months > AE
F010 (140 days)
H021 (130 days)
G008 (120 days)
F007b (105 days)
D011 (90 days)
3 months > AE
D039 (60 days)
0 months > AE
summer
winter
summer
summer
winter
summer
mean annual temperature

Figure 7

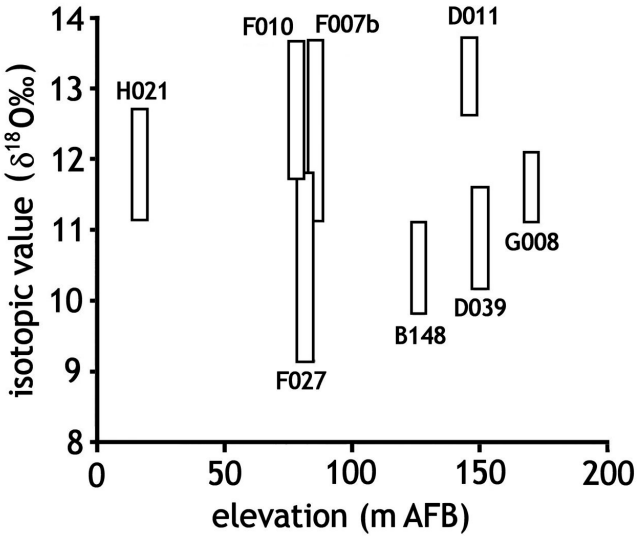
14
13
12
11
10
9
8
isotopic value (δ18O‰)
0
50
100
150
200
elevation (m AFB)
H021
F010
F007b
F027
D011
B148
D039
G008

Figure 8

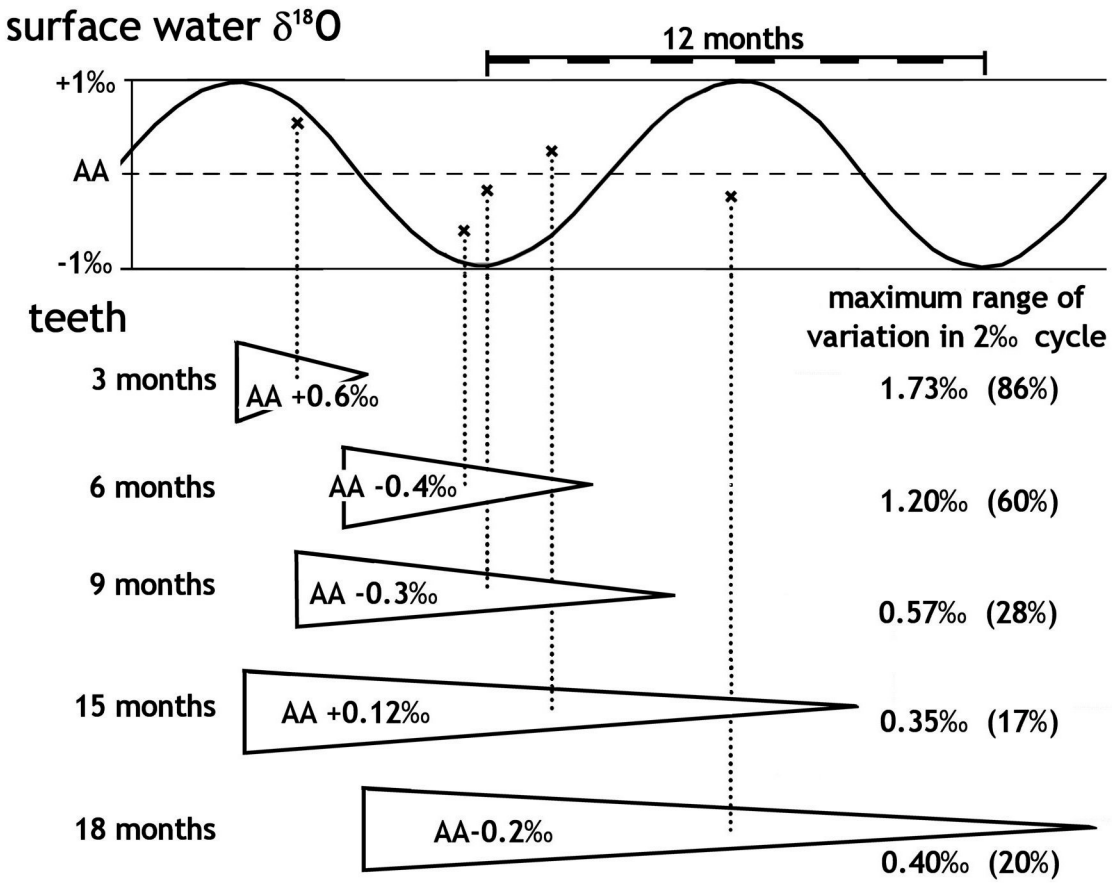
surface water δ18O
12 months
+1‰
AA
-1‰
teeth
maximum range of variation in 2‰ cycle
3 months
AA +0.6‰
1.73‰ (86%)
6 months
AA -0.4‰
1.20‰ (60%)
9 months
AA -0.3‰
0.57‰ (28%)
15 months
AA +0.12‰
0.35‰ (17%)
18 months
AA-0.2‰
0.40‰ (20%)

CHAPTER THREE

Taphonomy of the Lower Horseshoe Canyon Formation (Latest Campanian), Alberta, Canada: Attritional Accumulations of Bone as a Response to Variations of Base-Level and Depositional Rate

WILLIAM H. STRAIGHT

Marine, Earth, and Atmospheric Science Department,

North Carolina State University, Raleigh, NC 27695

DAVID A. EBERTH

Royal Tyrrell Museum of Palaeontology, Box 7500, Drumheller, AB T0J 0Y0, Canada

JONATHAN M. G. PERRY

Department of Biology, Anthropology, and Anatomy, Duke University, Durham, NC, 27708

PATRICIA E. RALRICK

Museum Studies Program, University of Nebraska State Museum, Lincoln, NE, 68588

for submission to *Palaios*

A survey of vertebrate fossil taphonomy was conducted in conjunction with a high-resolution stratigraphic study of the 210-meter thick lower Horseshoe Canyon Formation spanning the last 2 million years of Campanian deposition in southern Alberta, Canada. The fossil record indicates a pair of overlapping ecosystems, a dinosaur fauna dominated by hadrosaurs, ceratopsians, and tyrannosaurs and an aquatic fauna of fish, turtles, champsosaurs, and skates, that persisted essentially without change through the end of the Campanian. Taphonomically, bone in the LHCF is well-preserved, with abrasion, fracture, and hydraulic sorting relatively rare and fine-sediment scouring, fungal mottling, and pedogenic corrosion common, consistent with attritional accumulation. Taphonomy of the LHCF differs from other attritional accumulations; rather than the typical channel-bound hydraulically sorted bonebeds, dispersed fossil sites cluster stratigraphically in laterally extensive, facies-independent horizons, predominantly in fine-grained floodplain facies. This "floodplain-fill" mode of preservation results from a balance between bone supply, sediment supply, and accommodation, reflecting external controls of subsidence and climate and internal controls of population and community structure. Bone preservation and fluvial architecture are thus linked by the interplay of sediment supply and accommodation, or mean aggradation rate. Bone can be buried whenever the mean aggradation rate matches a relatively low depositional rate optimum for bone burial for at least 10^4 years. During the deposition of the lower Horseshoe Canyon Formation, small-scale cycles in base-level achieved this balance as base-level approached or departed from a stillstand. The resulting "trickle fill" of minimal accommodation across the floodplain produced widespread sparsely fossiliferous horizons, associating them with lithostratigraphic stillstand surfaces and making them analogous to fossiliferous condensed sections in marine successions.

INTRODUCTION

Since the introduction of the study of taphonomy by Efremov (1940), research into the "transition, in all details, of organics from the biosphere into the lithosphere or geological record" (Lyman, 1994:1) has focused on three key perspectives important to paleontologists: processes, localities, and geologic formations. Process research follows the steps of bone alteration from death (Haynes, 1988), decomposition (Weigelt,

1927, translated 1989; Dodson, 1971; Coe, 1978), and disarticulation (Toots, 1965a; Hill and Behrensmeyer, 1984) through surface weathering (Tappen and Peske, 1970; Behrensmeyer, 1978; Fiorillo, 1988; Tappen, 1994), scavenging and insect boring (Erickson and Olson, 1996; Dominguez-Rodrigo, 1999; Paik, 2000), trampling (Hill, 1979; Andrews and Cook, 1985; Fiorillo, 1987) to fluvial transport and accumulation (Voorhies, 1969; Dodson, 1973; Korth, 1979; Behrensmeyer, 1988; Blob, 1997). Analytical and theoretical studies derived from process data include numerical and statistical methods for taphonomy (Badgley, 1986a; Behrensmeyer, 1991; White et al., 1998) and several interpretations of time measurement through taphonomic interpretation (Behrensmeyer, 1978, 1982; Lyman and Fox, 1989; Behrensmeyer and Chapman, 1993; Graham, 1993; Aslan and Behrensmeyer, 1996). Locality-scale research involves either isolated fossil-rich sites (e.g. Lawton, 1977; Behrensmeyer et al., 1979; Brinkman, 1990; Cook, 1995; Eberth and Brinkman, 1997; Hungerbuhler, 1998; Hadly, 1999; Fiorillo et al., 2000; Ryan et al., 2001) or very thin stratigraphic intervals (e.g. Smith, 1993, 1995; Therrien and Fastovsky, 2000; Eberth et al., 2000), studied for their excellent preservation, environmental interpretation, and/or paleoecological significance. By contrast, formation-scale research comprises efforts to describe and interpret both general faunal composition and patterns of evolution or broad ecological change (e.g., Beland and Russell, 1978; Dodson et al., 1980a; Bown and Kraus, 1981; Badgley, 1986b; Wood et al., 1988; Sheehan et al., 1991, 2000; Nadon, 1993; Morgan et al., 1995).

However, interpretation of vertical taphonomic variation in fluvial successions has been hindered by the lack of a clear chronostratigraphic context. Techniques available for interpretation of marine and paralic successions use laterally extensive stratigraphic surfaces as chronostratigraphic markers (Posamentier and Vail, 1988; Van Wagoner et al., 1988; Galloway, 1989), across which there are usually distinct changes in facies and fossil character (e.g. Kidwell, 1986, 1988, 1989; Banerjee and Kidwell, 1991; Brett, 1995, 1998; Siggerud and Steel, 1999; Courville and Collin, 2002). Such surfaces, which partition marginal marine strata into chronostratigraphic intervals, have been difficult to trace into fluvial successions. However, recent researchers of fluvial vertebrate taphonomy have developed similar techniques to describe stratigraphic-taphonomic variation, using numerical models (Holland, 1995), broad biostratigraphic trends (Brinkman et al., 1998; Sheehan et al., 2000), or fluvial architecture changes (Bown and Kraus, 1993; Smith, 1993; Willis and Behrensmeyer, 1994, Rogers and Kidwell, 2000). In the present work, data from a survey of fossil remains in

the latest Campanian lower Horseshoe Canyon Formation are described both in formational terms and in the context of a previously described chronostratigraphic framework (Straight and Eberth, 2002). In addition, the taphonomic characteristics of the formation are compared to similar studies and to theoretical models relating architecture and taphonomy to depositional rate.

HORSESHOE CANYON FORMATION

The Horseshoe Canyon Formation is one of five formations of the Edmonton Group of south-central Alberta, Canada, recording the last incursions and final retreat of the Western Interior Seaway during the late Campanian and Maastrichtian. Underlain by the marine Bearpaw Formation and covered by the fully fluvial Whitemud, Battle, and Scollard formations, the Horseshoe Canyon Formation comprises a pair of eastward-thinning clastic wedges of transitional estuarine and fluvial rocks. Between the wedges are estuarine and shallow marine mudrocks informally termed the Drumheller Marine Tongue (DMT), deposited during the final transgression of the Bearpaw Sea and correlated with the Campanian-Maastrichtian boundary (Catuneanu and Sweet, 1999). The Red Deer River cuts the nearly horizontal succession of the lower Horseshoe Canyon Formation (LHCF) and Drumheller Marine Tongue into dissected badlands and steeply sloping valley walls (Figure 1).

Since the earliest paleontological exploration in 1884, the badlands around Drumheller, Alberta, have yielded abundant isolated, associated, and articulated vertebrate skeletal remains, particularly those of dinosaurs (Russell and Chamney, 1967; Braman and Eberth, 1988). Previous studies of the lower Horseshoe Canyon Formation have divided the succession into three informal members on the basis of fossil abundance and/or lithology (Srivastava, 1968; Braman and Eberth, 1988; Hamblin, 1998; Eberth et al., 2001). Recent high-resolution stratigraphic analysis of the LHCF (Straight and Eberth, 2002) refined the three-way subdivision, describing a basal fossil-poor, coal-rich member 95 meters thick; a middle fossil-rich, coal-poor member 65 meters thick; and an upper fossil-poor, coal-poor member 50 meters thick (Figure 2). In addition, the analysis reveals that the 210-meter-thick succession of strata, deposited over ~2 million years, is subdivided by laterally discontinuous scours under broad sheets of sandstone into ten chronostratigraphic bodies of strata (herein termed packages) of between 11 and 31 meters thickness. These packages formed as a

response to regional cyclic changes in base-level; each basal scour records a lowstand of regional base-level. Many of the packages are also internally subdivided, often unequally, by an internal surface corresponding to a highstand of regional base-level and are thus composed of two successive chronostratigraphic sheets of strata: a lower interval recording a relative rise in base-level (herein referred to as a *rise-interval*) and an upper interval recording a relative fall in base-level (herein referred to as a *fall-interval*). Each package also records an evolution of channel morphology: (1) laterally migrating low-sinuosity meandering channels during lowstand; (2) anastomosing channels avulsing into flooded backswamps during base-level rise; (3) channel abandonment and coalescence, resulting in dissected floodplain borders, during highstand; (4) incising meandering channels and soil development on stable floodplains during base-level fall. Stillstands generated the lithostratigraphic surfaces in each package, but these surfaces are laterally discontinuous and hard to recognize in the field. The surfaces are more easily detected using vertebrate fossils.

Fossil sites are non-randomly distributed throughout the section (Figure 3A), clustering stratigraphically into horizons 1 to 4 meters thick. The stratigraphic position of these horizons significantly correlate with the position of both basal scours and internal surfaces (Figure 2). The coal-rich basal member includes packages A, B, and C, each of which is 31 meters thick and split into nearly equal halves by an internal surface. Major fossil-bearing horizons in each of these packages are present just beneath the internal surface, whereas the remaining strata are virtually non-fossiliferous. The coal-poor, fossiliferous middle member includes packages D, E, and F; each package and fall-interval is thicker than the one above. Several fossiliferous horizons occur in each package; in each case, the richest horizon occurs just under the internal surface (D) or just above the basal scour (E, F). In addition, rocks throughout the member yield numerous isolated fossils. The coal-poor, non-fossiliferous upper member (the DMT) includes packages G, H, I, and J. These packages average 13 m thick and have no obvious internal surface. The upper member is nearly nonfossiliferous, but in the lower packages, thin fossiliferous horizons are found on or above the basal scour. This detailed stratigraphic framework makes the LHCF an ideal succession to search for changes in faunal diversity, taphonomy, and paleoecology through time.

METHODS

Fieldwork

A survey of exposed fossil remains was conducted as part of a stratigraphic, taphonomic, and paleoclimatologic study of the LHCF exposures around Drumheller (Straight and Eberth, 1998, 2002; Straight et al., 2003; Figure 1). Seven areas, each of 250,000 square meters, were selected for the survey of surface fossils to minimize forms of stratigraphic bias: each site features minimal local slumping, low slope with few slope breaks, and light ground cover. Survey areas were also chosen in areas with limited previous surface collection, although one area bordered an excavation active during the survey.

The position of each fossil-bearing site (herein defined as 1 m^2 of exposure) was measured geographically by GPS and stratigraphically by relation to at least two stratigraphic markers, usually coal beds or thin bench-forming sheet sandstones. For each specimen, documentation included, where possible, the taxon, usually to family level, the identity of the skeletal element, and color and associated post-depositional mineralization. For each site, documentation included fractures and surface marks, surface wear and removal, and associated facies. Describing each taphonomic character for each specimen found during the survey at first appeared preferable, but taphonomic information such as weathering, surface damage, and rounding was frequently detectable at sites in the field at which reconstruction and/or identification of fragmentary remains was impossible. Given that bone modification can begin only after the bone is defleshed and in contact with the local depositional environment, modification data were associated with each depositional site rather than with the taxon or skeletal element.

Fragments and fossils of less than 5 mm in longest dimension were excluded from the survey to prevent the overemphasis on fragmentary, often unidentifiable material, and to focus the study on the distribution of macrofossils. In addition, taphonomic information from such tiny fossils is severely limited. However, the lower size limit means that the fossil content in some sites, particularly microsites (*sensu* Brinkman, 1990), is underrepresented in the survey. For example, at one microsite, a handful of sediment scattered on white paper revealed fossil seeds, tiny teeth, and fossilized insect fragments, all smaller than the minimum inclusion size.

Although several techniques for counting individuals from a bonebed have been devised (Shotwell, 1955; Grayson, 1978; Badgley, 1986a, b), each specimen found in this survey has been treated as representing an individual. The primary reason for this approach is the extreme dispersal and complete disarticulation of remains. The majority of LHCF sites contained a single bone or two specimens of demonstrably different species. Even shed teeth were found widely enough dispersed both laterally and vertically to justify the conclusion that they had only a small likelihood of coming from the same animal. For this survey of stratigraphic variation of taphonomy, an estimate of population per chronostratigraphic interval was deemed less useful than counts of sites or specimens.

The bulk of the material was left *in situ*, but approximately 60 dinosaur teeth were collected for geochemical analysis (Straight et al., 2001, 2003). Although available, collection material from the Royal Tyrrell Museum of Palaeontology and other institutions are not included in the survey because collection records rarely include facies relationships or high-resolution stratigraphic and geographic reference data and because collections generally emphasize well-preserved and/or articulated specimens instead of typical preservation. All data collected from the survey are on file at the Royal Tyrrell Museum of Palaeontology.

Standardization and Statistics

Several methods of standardization are employed to compare the taphonomy in intervals of dissimilar site richness and/or thickness. Raw data are presented as counts of sites or specimens (Figures 3A, 4A). Most survey data are reported as a percentage of the number of all sites or specimens of a specific characteristic in an interval. Standards include (a) interval thickness (e.g., sites per meter, Figure 3B), (b) the number of sites or specimens in the interval (e.g., percentage of teeth among specimens per interval, Figure 5A), and (c) the number of specimens in the interval with the same characteristic (e.g., percentage of hadrosaurid teeth among teeth per interval, Figure 5B). Rank-abundance as demonstrated by Brinkman (1990) was used for stratigraphic comparisons of fauna between intervals (Figure 6A). Pie charts are used to show the composition of the assemblage as a whole (e.g. skeletal components, Figure 5E; faunal groups, Figure 6B). Many characteristics of fossils documented during the survey, such as facies association and fossil configuration, can be used to subdivide sites or specimens into three categories. Each set of three categories

provide axes for graphical display of faunal group data (e.g., faunal groups by configuration, Figure 6C) in the form of ternary taphograms as described by Kowalewski et al. (1995).

Statistical tests applied to survey data include t-tests for similarity of means and Pearson correlations for pairwise comparison. Relationships between the stratigraphic distributions of two characteristics are tested by the same battery of three non-parametric statistical tests previously used to compare fossil occurrence and stratigraphic boundaries in this section (Straight and Eberth, 2002): the Spearman Rank correlation for its ability to analyze ordinal data; and the Kolmogorov-Smirnov and χ^2 tests for similarity of means and dispersion. All tests were conducted at the 0.05 level of significance; in most instances in which the hypothesis tested was accepted, it also passed at the 0.01 level of significance.

IDENTITY OF FOSSIL REMAINS

Taxonomic identification during the field surveys could not be refined to the degree available in faunal lists based on museum collections built over the last 35 years (Russell and Chamney, 1967; Braman and Eberth, 1988; Braman et al., 1995; Eberth et al., 2001) but survey results are consistent with these studies. Eleven faunal groups (*sensu* Wood et al., 1988; also similar to guilds of Baszio, 1997a,b) were each represented in the LHCF by ten or more specimens described during the survey: hadrosaurids, tyrannosaurids, ornithomimids, dromaeosaurids, troodontids, ceratopsians, ankylosaurians, champsosaurs, fish, turtles, and skates (Figure 6B). Five crocodilian teeth teeth were found, and although sharks, amphibians, lizards, pterosaurs, and mammals are known from the LHCF (Eberth et al., 2001), no identifiable remains of these types of animals were encountered during the present survey.

Two general patterns of stratigraphic distribution are present in the survey data (Figures 3A, 3C). Dinosaur fossils are concentrated in the strata from package B to package G, but are sparse or absent in the basal and top packages of the section. By contrast, remains of fish, turtles, skates, and champsosaurs are common in package A and in the top member (packages G-J), but less often recovered from the strata in between.

Hadrosaur remains are the most abundant fossils in the LHCF (Table 1; Figure 6A), represented by disassociated vertebrae, limb and pelvic bones, ribs, and fossilized tendons, particularly in a small

monospecific bonebed packed with two dozen exposed (and probably many more still covered) elements in package G. Hadrosaurid femora, usually over 100 cm in length, represent most of the longest complete bones found in the LHCF (Figure 7A). Worn nubs of hadrosaur teeth constitute less than 20% of hadrosaur remains in most intervals, but the ratio of hadrosaur bone to teeth varies through the section (Figures 5B, 7B, 7C).

Tyrannosaur remains are evenly distributed throughout the LHCF (Figure 6A). Skeletal elements assigned to the tyrannosaurids include mostly long bones, vertebrae, and tarsals, but more than half the tyrannosaurid fossils are shed teeth, identified as *Albertosaurus* by comparison with published examples of tooth shape and denticle counts (Farlow et al., 1991; Baszio, 1997a). The proportion of tyrannosaurid teeth among all teeth declines upward through the section (Figure 5C).

Ceratopsians are represented by bones of the cranial frill, horn cores, ribs, and shed teeth. Ribs and vertebrae occur only in rise-intervals, and three ceratopsian bone fragments are the only vertebrate remains found in middle- and upper-estuary facies (Straight and Eberth, 2002). The rank-abundance of ceratopsian fossils decreases up-section to package F, then increases through the upper member (Figure 6A).

Ornithomimid unguals and fragmentary dermal scutes of ankylosaurs constitute a tiny fraction of the fossils in the middle member. Teeth of small maniraptoran dinosaurs identified as *Troodon* and *Saurornitholestes* (Farlow et al., 1991; Baszio, 1997a; Peng et al., 2001; Sankey et al., 2002) are preserved exclusively in rise-intervals, increasing in both relative and rank-abundance from the base of the section to the top of the middle member (Figure 5D). A single crushed hollow bone found at one survey area was attributed to *Troodon*.

Ganoid scales, fish teeth and dental plates, disc-shaped vertebrae, and *Myledaphus* teeth, common constituents of fossil concentrations in the middle and top members, are similar to microvertebrate material described from the Judith River Group (Brinkman, 1990; Peng et al., 2001; Figure 6A). Turtle carapace fragments and crocodilian teeth are found sparsely throughout the section, and champsosaur vertebrae and long bones occur in the basal and middle members.

FOSSIL CONFIGURATIONS

Fossils occur in four different configurations (*sensu* Koster, 1987). Solitary sites, each of which contains a single, usually fragmentary bone, are laterally separated from adjacent sites by 20 meters or more (Table 2). Although most of the specimens are oriented with long axis roughly horizontal, some specimens in fine-grained sediments are subvertically oriented. Bone orientation is therefore non-random (Toots, 1965b) and consistent with bones trampled or churned by rooting into soft sediment.

Sparse bonebed sites contain one or two elements and lie within a few meters of another site on the same stratigraphic level. Sparse bonebeds extend laterally up to 100 meters and frequently contain large and relatively complete but disarticulated fossil elements.

Each packed bonebed site contains two or more bones lying in contact. These rare, relatively dense fossil concentrations generally extend laterally less than 10 meters. One packed bonebed in package G includes eight such sites, each containing three or more elements. Two separate packed bonebeds contain associated partial skeletons, both of hadrosaurs, in the rise-intervals of packages D and F. Although articulated skeletal material would qualify as packed bonebeds under this definition because they would contain two or more bones lying in contact, no such material was found during the survey.

The remaining sites are microsites containing small fragments of bone, fish scales, and shed teeth. In the LHCF, microsites associated with channel or lateral accretion facies occur with a sparse pebble lag of reworked siderite nodules and mudstone clasts, whereas microsites associated with silty mudrock facies are often supplemented by invertebrate steinkerns, fossilized seeds, and small coprolites but lack a pebble lag. These two types of microsites are consistent with previous descriptions of concentrations of microvertebrate material and bone pebbles (Behrensmeyer, 1988; Brinkman, 1990). Microsites incorporating reworked nodules and clay clasts have been interpreted as lag formed in a channel concentrated from reworking of floodplain sediments (Eberth, 1990). Examples of partly reworked bank-collapse blocks with downstream-attenuated aprons of reworked siderite clasts are present in the LHCF sandy channel fills (Straight and Eberth, 2002). Microsites without reworked clay or nodule clasts have been interpreted as part of abandoned channel infill, distal splay, or pond deposition (Lehman, 1982; Eberth, 1990; Blob and Fiorillo, 1996).

Of seventeen facies defined from the lower Horseshoe Canyon Formation (Straight and Eberth, 2002), ten yield 99% of the fossil remains found in the survey. Non-fossiliferous facies in the LHCF occur in associations interpreted as upper and lower estuary deposits (Rahmani, 1989; Ainsworth, 1991, 1994; Eberth, 1995, 1996), where deposition occurred under marine influence. The ten fossiliferous facies fall into four associations interpreted as fully fluvial deposition (Straight and Eberth, 2002): (1) ribbon-form, plane-bedded to crossbedded sand bodies, representing sand-filled channels and point-bars in a low-sinuosity fluvial system (Figure 8A); (2) laterally-thinning sheet-form ripple-marked sand bodies, interpreted as proximal floodplain deposits made by crevasse-splays (Figure 8B); (3) organic-rich drab mudrocks, recording deposition in a saturated proximal floodplain backswamps (Figure 8C); and (4) organic-poor siltstones and mudrocks, deposition on a seasonally dry distal floodplains (Figure 8D).

In the LHCF, 73% of fossil sites occur in fine-grained mudrocks of the floodplain (Table 2). The proportion rises to 95% if specimens in small splay channels and siltstones are included in the proximal floodplain category. The proportion of specimens in each facies association for each taxonomic group is displayed as a taphogram, combining the backswamp and splay facies into a proximal floodplain association (Figure 8E). Vertebrate remains in the LHCF fall into two major groups. In the first group, remains of the dinosaurs, turtles, and champsosaurs are concentrated in the proximal floodplain facies. In the second group, fossils of ornithomimids, fish, and skates are generally found in distal floodplain facies. In the LHCF, channel and point-bar sandstones contain few sites, but are comparatively rich in packed bonebeds and solitary sites. All four facies associations feature a similar distribution of the fossil configurations (Figures 3C, 3D, 3E).

Hadrosaur remains are concentrated in bonebeds, other dinosaurs and the champsosaur fossils are dominantly solitary, and remains of freshwater vertebrates are concentrated in microsites (Figure 6C). The abundance of fossil sites and of specimens increases up-section through the basal and middle members through package F (Figure 4C, 4E, 7B), although package E represents a break in this pattern. Fossil sites are rare above package F, with several intervals virtually nonfossiliferous. The ratio of specimens to sites (Figure 4B) decreases from 1.7 in the basal member of the section, approaches 1.2 in package C, and then increases to 3.0 in the uppermost packages.

Rise-intervals contain 82% of all fossil sites and over 95% of the bonebed sites (Figure 3E). In such intervals, fossiliferous horizons are composed of a mix of sparse bonebed and solitary sites (Figure 4C), particularly in packages C and F. In the relatively less fossiliferous fall-intervals, notably in package D, most sites are dispersed and contain only one specimen. In the intervals of the basal and middle members, microsites are rare, comprising less than 15% of the sites in each interval except in package A (Figure 3D). Above package F, microsites become the dominant configuration (Figure 4D) but are not significantly more common than in lower packages.

BONE MODIFICATION

Three broad types of bone modifications were encountered during the taphonomic survey of the LHCF (Tables 3, 4). Changes in mineralization include alteration of bone composition, usually by the addition of minerals or trace elements or by the nucleation of mineral nodules on bone surfaces. Abrasion includes modification in which slight incisions into the outer (cortical) bone create an array of markings of varying length, depth, distribution, and density across the surface of the bone. Bone destruction involves the removal of significant amounts of bone material, either by breakage or dissolution. Broadly, abrasion modifications are the most common features among fossils from the LHCF, represented in some form in nearly all of the sites.

Mineralization

Most fossil bone mineralization in the LHCF resulted in deep brown, red-brown, or vitreous black calcium hydroxyapatite (Straight and Eberth, 2002), which weathers in modern exposures to pale hues of pink, gray, tan, brown, blue, and white. Enamel occasionally turns amber yellow but like dentine is usually deep brown or black. Where modern exposure has scattered fragments of a bone or tooth, the reassembled specimen is often a mosaic of hues. Specimen color is statistically independent of facies, facies association, and package.

However, at sites in which specimens are partially or completely encrusted by mineral concretions (Figure 9A), fossil hue is more predictable. Bone covered by concretions of siderite is common in the LHCF. Such concretions formed rapidly enough in saturated fine-grained sediments to envelop palm fruits, seeds,

conifer cones, flowers, and fern corms without compressional distortion (Aulenback and Braman, 1991; Aulenback and LePage, 1998). Nodules associated with fossil bone has been interpreted as a consequence of the decomposition of bone organic matrix after burial, creating a microenvironment chemically favorable for the precipitation of iron or calcium carbonate (Bao et al., 1998). Where protected by siderite, bone in the LHCF is typically a streaky reddish-brown inside and out. Bone exposed by modern erosional removal of nodular overgrowths usually turns lavender or purplish-blue.

A rind of white clay is associated with bone in the rare cases in which bone occurs in coals or carbonaceous mudrocks. Bone inside the clay rind is typically vitreous, black, and brittle, breaking with a glassy fracture. Based on their association with coals (including a sparse bonebed inside Coal Seam 4a) and their bituminous appearance, these vitreous bones are often described informally as "coalified," but XRD and isotopic tests (Straight and Eberth, 2002; Straight et al., 2003) indicate that carbonization has not occurred. Although the exterior of these specimens appears fibrous or corroded and the surrounding clay rind contains small free bone fragments, the vitreous bone is well-preserved hydroxyapatite, with Haversian canals visible in reflected light on clean breaks and polished sections. Mineral overgrowths of both siderite and clay are evenly distributed throughout the fluvial members but are rare in the DMT. In addition, a few hollow limb elements were found with internal voids partially filled by small crystals of quartz or calcite.

Abrasion

Abrasion among fossils in the LHCF is relatively mild, usually appearing as shallow marks or patina on surface cortical bone. Cortical bone polished to glass-like smoothness is common among sites of the middle member (packages D-F) but does appear, if less commonly, on fossils throughout the section (Figure 9B). Some of the largest bones in the survey, such as femurs, dorsal vertebrae, and ribs, feature irregular patches of polish. Although similar polish has been described from experimentally reworked tyrannosaur teeth (Argast et al., 1987), none of the teeth found during the survey is polished as smoothly or completely as the cortical bone of mid- to large-sized bones. Polish has been interpreted as a consequence of movement of unconsolidated mud around the bone (Brain, 1967), either as the bone settles downward or is churned into the sediment by trampling (Olsen and Shipman, 1988), rooting, or invertebrate reworking.

The cortical bone of some fossils and, less commonly, the enamel of some teeth feature patches where groups of shallow straight microscopic striations, each 0.1 mm in width and depth, cross-cut one another. These “brushmarks” have no preferred orientation and are easily viewed under 10× magnification but are occasionally visible to the naked eye. Similar marks on dinosaur bone have been interpreted as a result of bioturbation in low-clay mud (Rogers, 1989). The incidence of brushmarks become more common up-section (Figure 9C) and are regarded as a consequence of settling through or being churned into silty floodplain sediments.

Larger grooves, single irregular curvilinear gouges across the surface of the bone, appear on numerous specimens from the basal (packages A-C) and middle (packages D-F) members (Figure 9D). These grooves are consistent with the coarse, widely-spaced marks attributed to trampling (Fiorillo, 1984, 1987; Andrews and Cook, 1985).

Cortical bone and tooth enamel are in places mottled with pale-colored broad (0.5 mm) shallow sinusoidal or dendritic grooves on specimens with a distribution closely correlated to the incidence of polish (Table 4). Mottles are common on bone throughout the section (Figure 9E). The mottles on most such specimens are concentrated on one side and the discolored bone or enamel is relatively soft and has a bleached appearance. Similar mottles, called “root etching” (Lyman, 1994), have been attributed to plant roots or fungal growth (Behrensmeyer, 1978; Andrews and Cook, 1985; Tappen, 1994) and may indicate which side of the element faced upward during and after burial (Andrews, 1995).

Pits and punctures appear in specimens concentrated in the middle member, particularly in the rise interval of package F. A rare form of pitting is a short deep irregular cavity flanked on some specimens by evenly spaced, parallel 0.4-mm-wide U-shaped grooves in the bone surface or across fossil tendons. Such marks are consistent with the spacing and shape of tyrannosaurid tooth denticles and have been attributed to bite marks (Erickson and Olson, 1996; Tanke and Currie, 1998; Chure et al., 1998; Jacobsen, 1998). A more common variety, shallow round irregular depressions in surface bone, may be simple punctures attributable to the bite of scavengers such as tyrannosaurids, small theropods, or crocodilians. However, some of these rounded holes, which appear rarely in the LHCF (<1% of sites) as irregular tubes 3 to 8 mm in diameter penetrating several centimeters of cortical bone, may be related to insect borings. Prior to preparation, these

tubes were filled with sediment and bone powder, matching descriptions of insect-bored dinosaur bone (Paik, 2000). The few specimens bearing these types of modifications are bone fragments from sites in packages C and D. Because it is not possible to determine how much of the bone was actually destroyed by insects relative to other forms of bone destruction, borings are tentatively grouped with abrasion. However, insects are known to play leading roles in decomposition (Coe, 1978) and bone destruction (Tappen, 1994) in certain environments.

Destruction

Bone destruction, caused by processes removing significant amounts of bone material, is much less obvious among LHCF fossils than are other types of modification. Rounding of bone elements involves the removal of thin processes or the reduction of protrusions, edges, or ends. In the fossil survey, two specimens bearing coarsely scoured flat bevels were associated with sparse siderite pebble lags at the base of sandy channel fills, but most of the rounded specimens are small elements such as phalanges, vertebrae, and fragmentary skull elements and are typically found in microsites. Rounded fossils are uncommon in the microsite-poor horizons of the basal and middle members. Rounding is usually associated with fluvial transport of bone, although experiments comparing the performance of green and fossil bones in rock tumblers indicates that green bone does not fracture, break, or round during extensive transport (Andrews, 1995; Coulson et al., 2002). Instead, most rounding related to transport occurs on weathered (Andrews, 1995) or fossilized bone (Bartlett et al., 2003). Consequently, rounding of LHCF fossils may be a result of transport after reworking. Alternatively, rounding may be an extension of scouring abrasion such as polish and brushmarking that results from the extensive trampling of sediment encasing the specimen (Olsen and Shipman, 1988).

Some specimens show patchy or complete removal of surface bone, exposing fibrous or cancellous bone underneath. Such surface removal is characteristic of the vitreous black bone associated with carbonaceous mudrocks and clay rinds described above. Similarly, cortical bone that appears uneven or frosted but that is not stripped to the cancellous interior is generally associated with sites at which siderite concretions cover parts of the specimens. This corrosion is interpreted as chemical weathering associated with

burial in acidic forest soil, marsh mud, or peat, or possibly as damage caused by bacteria during decomposition and mineralization.

Rapid surface erosion, swelling clays, and modern vegetation on LHCF exposures cause extensive breakage to almost all large near-surface fossils prior to and after exposure, making the differentiation of ancient from modern fractures impossible. Spiral, stepped, and splintering fractures are absent in the bones of the LHCF, but modern erosion has replicated the perpendicular, longitudinal, and flake fractures that occur prior to burial (Lyman, 1994). During the present survey, fissures in specimens were attributed to modern disintegration if they featured sharp-edged fractures, irregular breakage faces, notable color changes, and/or numerous tiny slivers of bone in fissures. Fissures that display rounding of the fracture margin or mineral coatings deposited on fracture surfaces were attributed to ancient fracturing. Ancient fractures were detected on specimens at 6% of the sites, most of them solitary sites in the upper and middle members and, very rarely, bonebed sites.

The weathering of fossils at each site was evaluated by comparing sample modification to a scale empirically devised for the weathering of large animal bones in modern assemblages (Miller, 1975; Behrensmeyer, 1978; Fiorillo, 1988; Smith, 1993). Due to modern disintegration of fossil bone at the surface, fractures such as split lines are difficult to recognize in exposed remains and thus may have gone undetected, causing weathering data to be skewed slightly toward milder stages. However, most intact fossil elements from the LHCF are attributed to weathering stage 0 (36% of sites) or 1 (46%). At 10% of the sites, at least one specimen or fragment bears the mosaic cracking pattern characteristic of weathering stage 2. Although the most weathered material is evenly spread throughout the section, the basal member (package B in particular) contains a relatively high percentage of weathered remains.

A typical bone sample from the LHCF (Figure 10) features a pattern of short irregular longitudinal marks (1 to 4 cm long, 1 mm wide) penetrating less than 2 mm into polished cortical bone and filled with gray calcite. These tiny veins have no surface relief and are incised by other types of abrasions. More calcite veins appear on one side than on the other, and where they are most numerous they occur with a few small round pits. The distribution of these mineral-filled fissures is consistent with the early stages of longitudinal split lines associated with the weathering of bone (Tappen and Peske, 1970; Behrensmeyer, 1978). However, the

calcite veins are much smaller features than longitudinal split lines for weathering stage 1 (Lyman, 1994) and show no evidence of the surface flaking or roughness associated with higher stages of weathering.

Stratigraphic Variation

Non-parametric statistical tests were used to compare the stratigraphic distribution of taphonomic modifications in order to determine which, if any, types of modifications can be correlated. Many of the taphonomic features are statistically unrelated, but the tests do reveal correlations in three groups of modification types (Tables 3, 4). In one group, the stratigraphic distributions of polish, mottling, and rounding closely correspond to one another. These three types of modifications are relatively concentrated in the sites of packages at the bottom (A,B) and top (F,G,H) of the fluvial succession, with a minimum concentration in package C. Correlations also define a second group comprising fractures, pits, and brushmarks, each of which is rare in the basal (packages A-C) and upper (packages G-J) members and abundant in package F. The Spearman Rank Test supports a link between the first and second groups. Finally, correlations define a third group of modifications including grooves, corrosion, and mineral encrustation, which are all evenly distributed through the basal and middle members but depleted in the upper member. The Spearman Rank test includes cortical bone removal in this group. No correlations linked weathering to other types of modification.

The same statistical tests revealed no unequivocal correlations between faunal groups and modification distributions: only four relationships passed one of the three tests, and none passed more than one. However, when the same set of tests were used to compare facies with modifications, the first and second modification groups distinctly correlate with the distribution of splay channels. Fractures and pits, members of the second group of modifications, match the distribution in the LHCF of dry floodplain facies and narrow mudstone-filled channels. The distribution of third group of modifications corresponds to the distribution for two facies representing wet floodplain soils in the LHCF.

ELEMENT DISTRIBUTION

Among the 752 fossil elements described during the survey, 653 (87%) were identifiable skeletal elements (Figure 5E). Isolated teeth, limbs, and ribs are equally abundant, each comprising a quarter of the

assemblage. A fifth of the assemblage includes vertebra, bones of the pelvic or shoulder girdles, bones of the feet, and skull elements and jaws, including the relatively large parietal and squamosal elements of chasmosaurine ceratopsians. The relatively small residual portion of the assemblage includes dermal armor, turtle scutes, and fragments of caudal chevrons, all relatively rare fossils in the LHCF.

Accumulations of bone frequently are associated with other types of fossilized material. Fossilized wood, leaves, and conifer cones are common, particularly in more coarse-grained facies. Fragmentary fossilized tendons, probably from hadrosaurids, are common constituents of microsites. In addition, two types of coprolites appear in the LHCF. Large subcircular or irregular "pats" ~30 cm in diameter are encrusted by white clay and replete with coalified woody debris and/or small bone fragments. These coprolites are commonly found in the upper parts of sandstone- or siltstone-filled channels and given their size were likely produced by dinosaurs. Small ~1 cm long cylindrical coprolites appear in silty mudstone microsites of the upper member are consistent with modern turtle feces. Only coprolites containing bone were documented during this study.

TRANSPORT

An important consideration in any taphonomic reconstruction is whether the bones have been fluvially transported. To test hydraulic equivalency between fossils and enclosing sediment, Behrensmeyer (1975a) compared bones to quartz spheres of equal mass. Given an estimated density of 1.5 g/cm^3 (Boaz and Behrensmeyer, 1976; Martin, 1999), a small bone such as a fish osteoderm or troodontid tooth will move as a quartz sphere 4 mm in diameter, much larger than the largest grain size observed in the LHCF. However, this comparison assumes that the sediment available to the region represents the coarsest material the stream flow can carry. In the LHCF, reworked siderite nodules of ~1 cm diameter occur as sparse lag on bedding surfaces in sand-filled channels; these nodules would have mobilized in flows capable of moving quartz spheres ~1.5 cm in diameter. Large channel fills in the LHCF preserve both reworked nodule lags and bank-collapse blocks with tilted relict bedding and a closely associated apron of reworked nodules, indicating that flow velocity in the channels rarely but occasionally reached levels capable of transporting smaller bones and teeth. Although the size distribution of bone is similar among most fossiliferous facies associations (Figure 7A), small elements

are relatively sparse in the channel association. A similar lag of nodules, wood, and bone occurs in the LHCF in some small splay channels, where flow velocity was briefly high enough to incise into floodplain deposits. If splay or avulsion deposition involved relatively high-density flows of mud rather than water, they could have acted to concentrate microvertebrate material in traps on the floodplain.

Other estimators of fluvial transport depend on the relative mobility of bones in flow conditions. Studies of flow transport of coyote and sheep bones in a flume (Voorhies, 1969) resulted in a system of three skeletal element groups based on their relative mobility under a current. Voorhies Groups, expanded by further flume and settling-rate studies to five groups (Dodson, 1973; Behrensmeyer, 1975a, 1975b; Boaz and Behrensmeyer, 1976; Korth, 1979; Coard and Dennell, 1995; Coard, 1999) and restricted by locality studies to elements of a single taxa (Lehman, 1982; Smith, 1993; Blob, 1997), have been used to discriminate fluvially transported assemblages from assemblages formed by other types of dispersal. Although Voorhies Groups have been used to interpret degree of transport for non-mammalian fossil assemblages (Lawton, 1977; Smith, 1993; Holz and Barbarena, 1994; Fiorillo et al., 2000), flume studies show that transport groupings for non-mammalian animals such as turtles are different from those of mammals of similar size (Blob, 1997; Table 5). Most studies conclude that for bones of mammals, the Voorhies Groups are “generally stable” regardless of size (Lyman, 1994), but when the list of elements comprising Group I (containing the most transportable elements) is compared between sheep, pig, horse, and hippo, the only common element type is phalanges (Table 5). Vertebrae and ribs, elements that Voorhies included in Group 1, fall into other groups for small or large herbivorous mammals (Dodson, 1973; Behrensmeyer, 1975b; Korth, 1979), indicating that Voorhies Groups are taxon-specific.

Significant differences between mammal and archosaur skeletal anatomy suggest that Voorhies Groups will be inadequate for studies of dinosaur taphonomy. In dinosaurs, vertebrae and ribs occur in a greater range of sizes and configurations than in mammals. Also in dinosaurs, femora are shorter and metapodials longer relative to tibiae than in mammals (Holtz, 1995). Skulls, girdles, and jaws of most dinosaurs disarticulate more easily and more completely than their mammalian homologues, and the sacrum in dinosaurs is generally larger than in mammals. In order to better represent the differences between mammalian and archosaurian skeletal configuration, Lehman (1982) inferred new transport groups for ceratopsians. In the

process, he reclassified seven of the sixteen types of elements described by Voorhies (1969) and subdivided four other element types into ten new types to reflect the greater disarticulation of dinosaurian homologues. Half of the element types he added are not in the same group as their mammalian counterparts. Lehman (1982) contrasted his inferred Group 1 (Table 5) and Group 3 elements to characterize degree of transport for ceratopsian remains in the Campanian Aguja Formation. His comparison produced a flow-transport ratio that compares visceral elements (vertebrae and ribs) to appendage elements (limbs, hip and shoulder girdles, sacrum, and skull). This ratio, which approached 1:1 in living dinosaurs, should be skewed toward appendage elements in lag assemblages whereas winnowed assemblages should be relatively rich in visceral elements. In the LHCF, the visceral : appendage ratio for most taxonomic groups is nearly 1:1 (Table 6), but for ceratopsians this ratio is skewed toward appendage elements. For hadrosaurid remains this ratio varies by interval through the LHCF, indicating a skew toward appendage elements in packages of the upper member (Figure 7D). This indication that bone accumulations in the LHCF were sorted by fluvial transport is at odds with our hydraulic equivalency and taphonomic modification data, which are not consistent with transport by flow conditions.

However, Lehman (1982) concluded that ceratopsian bone distribution in the Aguja was characteristic of carcass flotation rather than of transport of disarticulated bones in flow. The sequence of disarticulation during carcass flotation and drift suggests another comparison similar to Lehman's flow-transport ratio, comparing bones of the extremities (radial elements such as skull, feet, and limb bones) to bones of the body core (thoracic elements such as ribs, girdles, and vertebra) elements. This "flotation ratio" of radial to thoracic elements, which is also nearly 1:1 in complete dinosaur skeletons, indicates that the disarticulation sequence rather than hydraulic segregation groupings should be reflected in bone distribution where carcass flotation was more common than carcass transport by flow. Standing water represents a better chance at flotation, burial, and preservation for potential fossils than does floodplain exposure. Floating carcasses drop radial elements close to the death site and release thoracic elements further down flow, probably over relatively short distances (Weigelt, 1927, translated 1989). In the present study, the flotation ratio for each taxa across the assemblage (Table 6) is nearly 1:1, but a stratigraphic breakdown of hadrosaur remains by interval for both transport ratios (Figure 7E) supports a trend toward radial elements (feet, limbs, skull) in the upper member.

Hydraulic inequivalence and the suite of common taphonomic modifications observed in the LHCF argue against frequent high-flow transport for such carcasses, but carcass drift during decomposition may have occurred.

Loose teeth are common elements in most dinosaur-bearing strata, in some cases thirty times more common than other hardparts (Martin, 1999). Using stratigraphic variation in the abundance of isolated dinosaur teeth, Brinkman et al. (1998) detected faunal change over time in the Oldman and Dinosaur Park formations. Badgley (1986a, b) measured the ratio of isolated teeth and vertebra to detect flow-winnowed bone accumulations, but as in Voorhies Groups this ratio is based on mammalian skeletal anatomy. Unlike mammalian dentition, dinosaur teeth were serially replaced throughout life (Erickson, 1996) and available in a wide range of counts and dental configurations. Thus the number of fossil teeth shed by dinosaurs depended on individual lifespan and consequently does not have a consistent relationship to the number of its vertebra or to the conditions of tooth accumulation. In addition, skeletal elements of dinosaurs dispersed from the point of death, whereas shed dinosaur teeth were disseminated across the entire habitat range of the animal and only secondarily concentrated in places where the animals congregated and fed. Although transport ratios based on dinosaur teeth must be viewed with caution, they may be useful in estimating the degree of reworking associated with a concentration of fossils. Dinosaur teeth are generally small enough to move in flow but are resistant to abrasion (Argast et al., 1987) and therefore can survive repeated reworking. The discovery of "Paleocene" dinosaur teeth in the Hell Creek Formation has been attributed to such reworking (Eberth, 1990). In the LHCF, 63% of loose teeth occur in floodplain microsites (Figure 5F) and represent an increasing proportion of remains up-section (Figure 5A; Table 6). These vertical variations in the concentration of fossil teeth in the LHCF parallel lithostratigraphic indications of a relative reduction in accommodation and an associated increase in reworking of sediments through time.

INTERPRETATION

Depositional Environment

Previous studies interpret the lower Horseshoe Canyon Formation as deposits on a low-relief coastal-margin floodplain (Braman and Eberth, 1988; Ainsworth, 1991; Braman et al., 1995; Straight and Eberth, 1998). Results from this survey are consistent with that interpretation. The basal member records estuarine influence, the middle member is fully fluvial, and the top member includes the return of marine environments during the last incursion of the Bearpaw Sea. The floodplain was covered by a diverse temperate forest containing conifers, angiosperms, palms, ferns, and herbaceous plants. Low areas adjacent to the main channel were marshes, peat swamps, or ephemeral ponds filling abandoned channel reaches. Soil development began on higher ground, but the rapid influx of sediment inhibited long-term pedogenesis. Active channels alternated between laterally migrating low-sinuosity meandering and anastomosing forms, filling abandoned channels and backswamps with woody peat from forest litter and mud from avulsions and splays (Straight and Eberth, 2002). Two ecosystems coexisted the coastal plain during the latest Campanian: a dinosaurian fauna thrived around the river and on the proximal floodplain, and a freshwater fauna of fish, skates, turtles, and ornithomimid dinosaurs lived in and around ponds on the distal floodplain (Figure 8E).

Attritional Accumulation

Following a study of modern bone accumulations, Haynes (1988) concluded that the mode of mortality (attritional versus catastrophic) could not be determined for fossil bonebeds on the basis of monospecificity, scavenging, weathering, articulation, sedimentary setting, or other types of taphonomic modifications. However, where such characteristics co-occur, they have been used to interpret the cause of death and accumulation for specific localities (e.g., Voorhies, 1969; Lawton, 1977; Fiorillo, 1988; Hungerbühler, 1998; Fiorillo et al., 2000; Ryan et al., 2001). Based on three characteristics—the dominance of solitary sites, the lateral continuity and facies independence of sparse bonebeds, and the quantity of co-occurring microvertebrate material—the mode of accumulation in the LHCF is interpreted to be attritional. Remains from mass mortality events are unlikely to be buried in configurations that cross multiple facies

boundaries, as bonebeds do in the LHCF, because events produce deposits comprising a relatively small number of facies and occur over periods of time too short to permit the formation of distinct facies contacts. Empirical studies show mass mortality localities are relatively depleted in bones of small animals, attributed to causes including a relatively rapid decomposition rate, complete destruction by scavengers, or relatively low mortality during events that kill large animals (Voorhies, 1969; Behrensmeyer, 1978; Behrensmeyer et al., 1979; Haynes, 1988). In contrast, small-animal remains in LHCF microsites comprise at least 21% of specimens, consistent with models of attritional accumulation (Behrensmeyer and Chapman, 1993). Density of fossil sites in the LHCF sparse bonebeds in places reaches 1 bone per 3 m^2, matching Behrensmeyer's (1983) estimates of average buried bone frequency from millennial-scale attritional accumulation in Amboseli. Nevertheless, fossil accumulations with a lower density of bone than the solitary "bone background" of the LHCF can result from mass mortality events (Haynes, 1988) and if some of the skeletal scatter is a consequence of carcass flotation, then the cause of mortality becomes even less certain. Although our survey results are consistent with attritional mortality and autochthonous accumulation for bone in the LHCF, this interpretation must be viewed as tentative.

Taphonomic modification to bone in the LHCF can be summarized as minimal rounding, mild abrasion, and no weathering, characteristic taphonomy for a lake-strewn wetland (Cook, 1995). The dispersion and modification of bone in floodplain facies of the LHCF is similar to bone distribution and taphonomy in attritional settings, including the Permian Teekloof Formation in the Karoo Basin (Smith, 1993), the late Jurassic Morrison Formation (Dodson et al., 1980a, b), the late Cretaceous Hell Creek Formation (White et al., 1998), the Eocene paleosols of the Willwood Formation (Bown and Kraus, 1981), and to modern attritional settings (Coe, 1978; Hill and Behrensmeyer, 1984). Sparse scavenging, complete disarticulation, and under-representation of caudal vertebrae, metapodials, phalanges, and cranial elements are all consistent with decomposition in water or marshy ground (Weigelt, 1927, translated, 1989; Hill, 1979; Lehman, 1982). The association of fractures, pits, and brushmarks is interpreted as reflecting relatively long-term exposure on a continuously or seasonally wet forest floor. Although disintegration is retarded by shade and moisture, bone instead may be pitted by fungus, invertebrates, and plants (Tappen, 1994) or scoured during and after burial by churning of the sediment. The association of polish, mottling, and rounding is interpreted as symptomatic of

burial on a seasonally wet floodplain. Polish and subtle rounding of bone results from the movement of bone relative to enveloping fine-grained sediment (Brain, 1967). Solitary elements were occasionally trampled into the unconsolidated muddy sediment, putting grooves into the cortical surfaces (Behrensmeyer et al., 1986; Fiorillo, 1987).

Once bones were buried, decomposers such as roots and fungus etched their cortical surfaces while decomposition of bone organics supported chemically favorable conditions, such as high pH and high pCO_2, for the precipitation of siderite and other mineral phases. In places, seeds, flowers, tendons, and coprolites were also mineralized rapidly enough to arrest destruction by burial and decomposition. Siderite nodules formed in low-organic silty mudrocks associated with oxide-coated root casts, slickensides, and desiccation cracks, all characteristic of periodically dry sediments. The association of trampling features with mineralization is interpreted as indicating that sediment churning was an important mode of burial for potential fossils in these relatively dry facies.

Burial was not necessarily permanent, especially for microvertebrate material and shed teeth. Churning of floodplain sediment by trampling or root action often exhumed bone and other remains both before and during fossilization. Migrating channel meanders undercut and reworked blocks of floodplain sediments, concentrating some fossilized elements in channel lags. Avulsions and splay channels also locally incised the floodplain surface, excavating and reprocessing fossils. During periods of soil development, erosion by runoff and deflation could also have exhumed fossil remains, resulting in microsites (particularly channel-fill concentrations) without indications of transport.

Lack of hydraulic sorting, survival of coprolites, and lack of abrasion have all been interpreted as indicators of minimal fluvial transport (Cassiliano, 1997). Such indicators are also present in the LHCF, indicating that transport of bone and other potential fossils by moving water was not an important taphonomic control during deposition of the LHCF. Channel facies typically associated with episodic or catastrophic burial of carcasses in this case received bone by reworking floodplain deposits. However, carcass flotation may have assisted decomposition, trampling, and scavenging to produce the wide-spread low-density veneer of bones in floodplain mudrocks with a corresponding rarity of articulated or associated skeletons.

Depositional Changes Through Time

Lithofacies variation in the LHCF has been ascribed to two scales of base-level variation (Straight and Eberth, 2002), patterns that are recapitulated in the taphonomy. A grand-scale cycle of base-level, resulting in the formation of the clastic wedge over ~2 million years, can be considered in three phases of changing mean aggradation rate, coinciding with the tripartite division of the formation: (1) an early, rapid aggradational phase records increasing accommodation to a maximum during the fall-interval of package C; (2) a middle, waning aggradation phase indicates decreasing accommodation; and (3) a late, relatively low aggradation phase records bypass and transgression.

During the early phase, impounded water was common in peat bogs and marshes of the backswamps, and carcass flotation played a role in disseminating bones of at least the hadrosaurid dinosaurs, which represent half the fossils in package C (Figure 7B). Bones buried during the peak of accommodation represent autochthonous burial, with distal elements dropped near the death site during decomposition, resulting in transport ratios skewed toward body core elements (Figures 7D, 7E). Incidence of cortical bone damage associated with mottling, trampling, and rounding declined during the early phase because bones did not spend long periods of time exposed at the surface. Rapid and deep burial of the largest bones (Figure 7A) prior to the decomposition of their organic matrix promoted local formation of nodule growth (Figure 9A), but microsite formation was inhibited as small bones and teeth were dispersed in thick sheets of saturated organic-rich mud.

After the peak of aggradation, concentrators such as surface erosion, reworking, and periods of relatively low depositional rate became more common. Brushmarks, polish, and marks on cortical bone formed more commonly during the middle phase as sediment supplied to the floodplain became more silty and as lower depositional rates resulted in shallowly buried bones experiencing sediment churning by plant rooting, trampling, and other surface disruption (Figures 9B, 9C). Smaller elements such as teeth were less easily swamped by abundant sediment and remained at the surface long enough to form microsite concentrations (Figures 4B, 4D, 5A). As a result of lower deposition rates of the middle phase, most bones were exposed or shallowly buried for longer periods of time, allowing organic decomposition to run to completion and more frequently subjecting bones to exhumation and pedogenic weathering.

During the late phase of base-level change, the transgression of the Bearpaw Sea brought marine influence back to the region. Hadrosaurid remains in the complex channel fills of the DMT are scattered body-core elements, suggesting that floating carcasses shed limbs, heads, and tails before reaching the marine margin. Bone is rare in the upper member of the LHCF (Figures 3A, 4A) because the late-phase sediment bypass and seasonally dry floodplain sediments impeded burial; a few dinosaur teeth in microsites from the upper member feature advanced stages of weathering. Large bones exposed by local erosion of floodplain soils were broken up by plant roots or weathered away, but small fragments and teeth could have been released and concentrated by surface flow events into depressions or ponds where they supplemented native freshwater microvertebrate remains, explaining the dominance of microsites in the upper member (Figures 4B, 4D).

Individual packages were created by a smaller scale cycle of base-level change, which added a periodic variation to the mean aggradation rate. During periods of small-scale base-level rise and highstand, splays and avulsions regularly supplied sheets of fine-grained sediment to areas of the floodplain. This sediment in addition to a steady supply of bone and volumes of accommodation available on the floodplain preserved accumulated bone on the floodplain as laterally continuous, relatively fossiliferous horizons (Figure 2). During package-scale base-level fall, the incision of coalescing, laterally-mobile channels reduced sediment export to the floodplain. Local overbank events buried small transportable fragments and teeth in floodplain traps, but laterally extensive horizons of buried bone did not form. Hence, almost all of the sites and specimens in the LHCF are concentrated in rise-intervals (Figures 3A, 3B, 4E) adjacent to the internal surface, a trend echoed in distribution of small theropod teeth (Figure 5D).

Faunal Change Through Time

Evidence for changes in community structure or population during the deposition of the LHCF is scarce and equivocal. Tyrannosaurid remains comprise ~10% of the remains in many intervals of the basal and middle members, but the proportion of tyrannosaurid teeth among all shed teeth declines through the succession (Figure 5C). The rank-abundance of ceratopsians, champsosaurs, and turtles each decline up to package F, whereas most of the small theropod remains occur in the middle member (Figure 6C). These trends probably result from the up-section increase in microsite abundance (Figure 3D), which contain fewer

than half of the tyrannosaurid teeth found during the survey, but more than 70% of all other teeth. Rarity of microsites could also explain the sparse distribution of smaller vertebrates in the basal member, because their remains are seldom found except in microsites. Remains of small theropods occur only in rise-intervals (Figure 5D), which could indicate that dromaeosaurs had an affinity for marshy terrain. However, the thin-walled hollow bones of small maniraptoran theropods are rarely recovered; all specimens but one of these animals from the LHCF are small shed teeth. They fall within the hydraulic equivalency range for high-flow events and often exhibit advanced weathering stages in microsites. Variations in the tooth-to-bone ratio among hadrosaurs (Figure 7C) appears to show an intermediate-scale cyclicity. This pattern reflects microsite abundance, although a similar pattern also appears in the maximum element size per interval. Although changes in depositional character from one member or package to the next make detailed faunal change difficult to discern, the results from this survey provide no compelling evidence for major faunal changes in the lower Horseshoe Canyon Formation up to the Campanian-Maastrichtian boundary.

DISCUSSION

The Floodplain Fill Mode

Behrensmeyer (1988) described two types of attritional bone accumulation, a channel-lag assemblage and a channel-fill assemblage. The channel-lag assemblage, in which bone is preserved on lower bedding surfaces and in crossbed troughs in sand-filled channels, is common in the sand-dominated Campanian Dinosaur Park Formation (Dodson, 1971; Koster and Currie, 1987; Wood et al., 1988; Eberth, 1990; Ryan et al., 2001), in which high-diversity packed bonebeds occur on lateral accretion surfaces in multistory amalgamated sandstones, and in the Campanian Two Medicine Formation (Lorenz, 1981; Rogers, 1989, 1990; Rogers and Kidwell, 2002) and the Maastrichtian Javelina Formation (Lehman, 1987, 1990; Straight, 1996), in which remains typically form hydraulically concentrated lags in channel bases. Both types of accumulations represent multiple, allochthonous sources of bone (Behrensmeyer, 1975a, 1982) and consequently are time- and space-averaged assemblages (Aslan and Behrensmeyer, 1996). Taphonomy of the channel-lag assemblage is characterized by variable, usually intense abrasion and hydraulic sorting (Brinkman, 1990; Ryan, 1992).

The channel-lag assemblage is very rare in the LHCF. Sparse fragmentary fossils appear in packages A and J in estuarine sandstone-filled channels and in package E in troughs in relatively thick, amalgamated sand bodies associated with the grand-scale highstand.

The channel-fill assemblage, in which bones cluster in fine-grained or mixed fill of splay or abandoned channels, can be difficult to recognize in mudrock-dominated fluvial deposits (Behrensmeyer, 1988). Where the channel-fill mode of preservation was the common or dominant process of accumulation, such as in the late Jurassic Morrison Formation (Dodson et al., 1980a, b), the St. Mary River Formation (Nadon, 1993), the Maastrichtian Hell Creek Formation, and the Miocene Siwalik Group (Badgley, 1986b; Behrensmeyer 1987, 1988; Willis and Behrensmeyer, 1994), bones representing a variety of taxa and body mass accumulate in size-sorted, variably-weathered, packed bonebeds. Large bones may occur in articulation but are frequently scratched and broken by scavenging, etched by fungus, and variably oriented by trampling, infauna, and/or rooting (Toots, 1965b). Lenticular bodies of mudrock are present in the LHCF, obvious where color or grain-size variations allow them to stand out but usually detectable only where a sand body is unexpectedly truncated laterally (Rahmani, 1988; Eberth, 1996; Straight and Eberth, 2002). These channel fills do contain bone, both as packed bonebeds in gleyed mudrock and as thinner mixed fills in levee or paleosol facies bearing pond-fauna microsites. However, in the LHCF, packed bonebeds and non-intraclastic microsites are not significantly more common than channel-lag assemblages.

Attritional accumulation in the LHCF resulted in a scatter of solitary bones and sparse bonebeds in fossiliferous horizons that may extend for several kilometers through several fine-grained floodplain facies, even to the point of crossing facies boundaries. The assemblage produced is not similar to either the channel-lag or channel-fill mode, but instead reflects sustained complimentary sediment and bone supply to large areas of the floodplain. This “floodplain fill” mode of preservation is most prevalently recorded in the basal and middle members and is taphonomically characterized by well-preserved, unweathered disarticulated large bones from a variety of species, polished or scoured by fine sediment, corroded or mottled by fungal action, and encrusted by carbonate minerals or clay. A similar distribution of remains appears in the Permian Teekloof Formation (Smith, 1993a, 1993b, 1995) and in the Eocene Willwood (Bown and Kraus, 1981b, 1987), although in the latter bones are usually broken and extensively weathered.

The floodplain-fill assemblage may represent an expansion of the channel-fill assemblage, in which the entire floodplain aggraded at about the same rate, producing fluvial architecture typically associated with channel-fill assemblages but on the scale of the entire river valley. Overbank flow in such a river valley could have consolidated attritionally accumulated bone into topographic traps, deriving all types of fossil configurations from the same floodplain bone supply. However, although both the channel-lag and channel-fill assemblages feature fossils modified in some way by flow transport, the floodplain-fill assemblage suggests that flow transport was reduced or absent. Where splays drained into marshy or flooded backswamps, such as in environments proposed for the LHCF or the Teekloof Member of the Karoo Supergroup (Smith, 1995), or where overbank flows lacked the power or coverage to transport sand or collect bone, as in the Willwood environment (Behrensmeyer et al., 1995), bone was neither mobilized nor consolidated, even where suitable topographic lows were available, but was preserved instead directly on the floodplain. Whereas the floodplain-fill mode possesses a unique scale of accumulation and its own sedimentological context and taphonomic signature, it is proposed here as a mode of bone preservation parallel to the channel-lag and channel-fill modes.

Three Controls on Bone Accumulation

Three controls dictate when and how bone accumulates in fluvial deposits: bone supply, accommodation, and depositional rate. Methods for determining the rate of attritional accumulation of bone are still under debate (see review in Lyman and Fox, 1989; Lyman, 1994; Martin, 1999), but several empirical studies (Behrensmeyer, 1982; Fiorillo, 1988; Aslan and Behrensmeyer, 1996) indicate that between 10^2 and 10^4 years are required to accumulate enough bone to create a paleontologically significant assemblage, toward the lower estimate for large animals (Behrensmeyer and Chapman, 1993) and moderated by environmental conditions (Graham, 1993). The survival of a single bone on the surface is between 10 and 100 years (Behrensmeyer, 1978; Tappen, 1994). Thus sediment must accumulate quickly enough to bury past input but slowly enough to incorporate new additions, and this lockstep has to continue long enough to form a collection of such “bone rain.”

Bone burial depends on a relatively low, optimal depositional rate (Martin, 1999). Deposits created at rates of meters per year (10^2 cm/a) capture single carcasses, mired animals (Hungerbühler, 1998), or animals

in burrows (Smith, 1993a), and thus are more akin to event deposits than to preserved attritional accumulations. Events such as splays that bury loose bone without concentration produce taphonomic snapshots of the floodplain, each of which records less than 100 years (Behrensmeyer, 1982) and contains too little material to be recognized. Relatively constant deposition over similar time periods, such as the formation of tidal rhythmites in the mixed-fill estuarine complexes on the Bearpaw / LHCF contact (Rahmani, 1988; Ainsworth, 1994; Straight and Eberth, 1998), do not incorporate bone because sufficient quantities to produce lags are unavailable on such time scales. Deposits formed at rates between meters per decade and meters per century (10^1 to 10^0 cm/a) represent the best potential for the burial of vertebrates in fluvial deposits, with the higher rates associated with large-bone bonebeds and the lower rates more suited to preserving microsites. Rates of meters per millennium or slower (10^{-1} cm/a) permit bone to weather subaerially or pedogenically, although concentrations of small fragments and teeth could still accumulate in traps.

These first-order approximations for depositional rate are only guidelines in that they leave out moderating effects such as settling and bioturbation (Martin, 1999), processes which reduce burial time. However, these estimations of rates are broadly plausible for bone preservation in the LHCF. The ~2 Ma represented by a ~200 m succession suggests a mean accumulation rate of 10^{-2} cm /a, but numerous rooting horizons and paleosols in the upper member imply that most of the two million years recorded by the succession is represented by hiatal surfaces formed during the grand-scale base-level fall and bypass of the upper member. Local depositional rates in the basal member were high enough on some areas of the floodplain to exceed the optimum range for bone preservation, whereas the optimum range was often met during deposition of the middle member (Straight and Eberth, 2002).

Depositional rate is especially important in that it plays a dual role in bone preservation. Bone can be preserved in fluvial regimes whenever the local depositional rate paces bone supply. This generally low optimum depositional rate is temporally and spatially localized and is responsible for the burial of individual bones. A longer-term mean depositional (aggradation) rate, governed by the interaction of sediment supply and accommodation, dictates regional fluvial regimes and resulting architecture (Behrensmeyer, 1988). The contrast between the mean aggradation rate (G) and the optimum burial rate for bone (O) controls which mode

or modes of bone preservation occur in a given fluvial setting. Ideally, the greatest quantity of bone will be preserved where G O for extended periods of time.

Under low mean aggradation rates, preservation space is available only in the main channel system (Figure 11A), and even there only the highest flow conditions can produce G O. The low aggradation rate creates a fluvial regime in which sinuous, meandering channels deeply incise into older sediments (Behrensmeyer, 1988; Miall, 1992), reinforcing the channel-lag mode of preservation. Crevassing of levees does occur but avulsions fail where the thalweg is lower than the floodplain; hence carcasses and bone debris already in the channel are not exported because even the highest-flow events cannot lift bone or bedload onto the floodplain. Under such conditions, overbank flows deposit only thin, localized splays of fine sediment, making the chances of floodplain burial for large bones unlikely, and as it is above local base-level, parts of the floodplain can erode and expose bone already buried. Lateral migration of the channel belt further consolidates bone by reworking older deposits, while surface drainage tends to draw surface bone into the main channel (see Aslan and Behrensmeyer, 1996). Extensive soil development and efficient drainage limit water availability on the floodplain, tightening the ties of plant and animal communities to the channel belt and thereby increasing the likelihood of skeletal remains being left in riparian environments. Extremely low accommodation leaves behind a multistory stack of truncated sandstone-filled channels (e.g., Shanley and McCabe, 1995), but a slightly higher base-level produces a cross-cut sand-dominated mix of amalgamated trough-crossbedded sheets interbedded with thinner fine-grained floodplain facies with advanced, possibly overlapping paleosols. Unusual event deposits, possibly containing numerous articulated skeletons, have a good chance of permanent preservation on the floodplain, but the dominant mode for preservation of attritionally accumulated bone will necessarily be the channel-lag mode, with other modes rare or absent.

Moderate aggradation rates can regularly match the optimal depositional rate, but not in the main channels, which usually fill too fast to incorporate bone. Shallow sinuous or anastomosing channels flow between sand bars and/or point bars, on which stranded carcasses can be rapidly buried as the channel belt aggrades (Figure 11B). Initial sheet-flow stages of splay or avulsion development (*sensu* Smith et al., 1989) may consolidate scattered bone into floodplain traps, whereas later stages with deep enough crevassing sweep bone from the main channel into the splay or avulsion complex. Distal ponds and proximal abandoned

channels serve as ephemeral watering holes, around which bone is churned into fine-grained floodplain sediments or imported and buried by overbank sedimentation. The floodplain may be seasonally saturated, contributing to soil development and to weathering and rapid mineralization of buried bone, particularly in highly calcareous sediments, which may preserve shells of invertebrates and eggs (Retallack, 1990). Deposits preserved under moderate aggradation include ribbon and shoestring sandstone bodies with lateral accretion surfaces, sand- and mud-filled abandoned channels, and fine-grained levees. Paleosols and rare lacustrine carbonates may collect and preserve microvertebrate debris, invertebrate traces, root casts, desiccation cracks, and footprints. In such deposits, bone may be relatively abundant and the channel-fill mode dominates its preservation (Behrensmeyer, 1988). Channel lags with transport-abraded bone can still form, but with less bone and relatively low incidence of reworking in the main channels.

Under high aggradation, the mean aggradation rate usually exceeds the optimum depositional rate for bone burial (G > O). The fluvial regime involves an anastomosing network or distributary system consisting of ephemeral channels between narrow levees (Figure 11C). Saturated or submerged interfluves between alluvial ridge partitions fill with peat in the absence of sediment supply, but routine avulsions deposit thick sheets of mud, along with floating carcasses and disarticulated bones, across these bogs and marshes. Abandoned channels are common but fill with mud too fast to serve as efficient bone traps. Instead, bone accumulates across the floodplain, where it is shaded, anchored by vegetation, and churned into sediments. Saturation of these sediments promotes anoxia (Retallack, 1990), slowing decomposition of organic material and inhibiting soil development. The resulting architecture is characterized by shoestring-sandstone bodies encased in laterally continuous sheets of mudrock. Coal, carbonaceous rocks, and gleyed mudrocks are common, paleosols and rooted horizons are weakly developed, and sparsely distributed fossils are supplemented by wood, leaves, cones, seeds, and coprolites. The floodplain fill mode dominates the preservation of attritional accumulations in this case, although material can still be found in channel fills and more rarely as lag accumulations.

Horizons as Terrestrial Condensed Sections

In the floodplain-fill mode, the optimum depositional rate associated with bone preservation can occur at any time but will be especially characteristic of times when base-level approaches or departs from a stillstand. Under these conditions, little new accommodation is created, but sediment supply is still available, resulting in a "trickle-fill" of the last available space as mechanisms for sediment bypass are engaged. A deposit of attritionally accumulated fossils is therefore most likely to form in the final infill of accommodation prior to highstand or following lowstand. Fossiliferous horizons in the basal member of LHCF lie just under internal surfaces, which correspond to highstand markers; horizons in the middle and upper members are concentrated in mudrocks above the basal scour, associated with a lowstand (Straight and Eberth, 2002). Similar distinctive, laterally extensive fossiliferous horizons formed under low depositional rates and relatively stable base-level are associated with condensed sections in marine deposits (Kidwell, 1986, 1988; Courville and Collin, 2002). The surface of base-level in fluvial regimes is locally convoluted and always adjusting toward an ideal profile (Quirk, 1996), which is essentially unattainable as a result of variations in local topography and daily changes in the air/water interface. In addition, vertebrate fossils are generally larger, fewer in number, and more often moved or destroyed by their environment than are their marine invertebrate counterparts. Therefore, the LHCF represents a rare chance to examine continental analogs of condensed sections.

The trickle-fill concept explains the patterns in LHCF fossil data in terms of the previously developed stratigraphic framework. Fossiliferous horizons formed when the three controls on bone accumulation—bone supply, accommodation, and depositional rate—were proportionately available, a condition characteristic of trickle-fill. Horizons in the basal member (packages A-C) developed during the early phase of deposition, when rapid increases in accommodation dominated the other controls. Fossiliferous horizons formed only when a relative stillstand or fall of package-scale counteracted the rapid increase of accommodation related to grand-scale base-level rise. The middle member, especially package D, represents deposits formed when the three controls on bone accumulation were almost continuously in balance. However, the greatest density of fossil sites occurs in package F, which contains a fifth of the material recorded in the survey: it contains almost three times the number of fossils of other packages, but is only a third of the thickness of typical packages.

This highly fossiliferous interval represents an interaction of controls in which accommodation, diminished following grand-scale highstand, was briefly increased during package-scale base-level rise, regaining the balance between controls that produce fossiliferous horizons. The unusually thick (~4m) fossiliferous horizon in package F may be the result of more than one cycle of base-level, such that package F could be an amalgamation of two or more thin rise-intervals, formed at trickle-fill depositional rates. The association of this rich horizon with the grand-scale base-level fall represents an important stratigraphic marker in that it underlies an otherwise undetectable low-order flooding surface associated with the last transgression of the Bearpaw Sea recorded 155 to 160 meters above the base of the formation. The association of vertebrate fossils and critical stratigraphic boundaries does not occur in all sections (Rogers and Kidwell, 2000) but it does occur in the LHCF.

Mechanisms and Consequences

The position of bone accumulations with respect to channel shape and depth may provide a means of comparing mean aggradation rate between formations and within a single chronostratigraphic interval. Such a comparison is based on the assumption that the optimum depositional rate (O) is essentially a fixed value for bones of large terrestrial animals. The key to this comparison is the vertical position of the densest accumulation of bone in the sediment fill of a trap (Figure 12). Traps are topographic depressions, each of which possesses its own localized base-level, the limit to which it will eventually fill with sediment. The filling process involves multiple influxes of sediment into the trap, followed by periods of compaction and partial renewal of accommodation. Each flow into the trap encounters less accommodation than the previous flow, so depositional rates decline as the space fills. Attritional accumulations of bone forming at the channel base indicated that (G O) occurred at the highest depositional rates (Figure 12A), whereas accumulations in the upper portion of channel fill indicate that the optimum rate of G O was matched as the accommodation filling was nearly complete (Figure 12B). In traps filled under similar aggradation rates and bone supply rates, attritional accumulations of bone should be found at the same relative elevation within the sediment fill. In essence, each trap therefore contains its own terrestrial condensed section. Because the controls on the formation of such fossiliferous horizons are regional in extent, contemporary traps should have matching

condensed sections. This may explain why most large bone accumulations from channel-fills in the Siwaliks are characterized as being from the middle or upper portions of the fill (Badgley, 1986a, b; Behrensmeyer, 1987, 1988). If bone accumulations from a variety of contemporary sediment-filled traps occupy distinctly different relative elevations, either the local depositional rate guiding their formation was highly variable or some of the accumulations represent episodic events.

Bone supply is a function of animal population and community structure, both autocyclic controls. By contrast, the two scales of base-level variation reflected in the architectural and fossil record of the LHCF stem from two allocyclic controls, tectonism and climate. Basin subsidence is the most probable source of accommodation and occurs on time-scales consistent with the grand-scale cycle. Package-scale base-level variation is a function of cycles of climate change associated with Milankovitch orbital periodicity. Climatic influence, most likely through periodic changes in rainfall, created packages by simultaneously increasing both local accommodation and regional erosion rates.

An important consequence of these allocyclic controls on the distribution of fluvial architecture and attritional fossil accumulation is biostratigraphic distortion (Figure 13). In strata accumulated under high mean aggradation rates, the sequence of biostratigraphic events will appear dilated due to the short time span recorded in the succession. Strata deposited under low mean aggradation rate will preserve more fossils, but biostratigraphic ranges for taxa will be condensed and homogenized by the process of reworking. Periods of bypass or non-deposition will leave behind hiatal surfaces against which biostratigraphic ranges will appear truncated. Thus, the highest and lowest occurrences of any given fossil taxa will most likely appear in terrestrial condensed sections, where fossils and time are most concentrated (Figure 13). The paucity of fossils between condensed intervals will further serve to shorten ranges to the nearest fossiliferous horizon. The result is the imposition of cyclic lithostratigraphic patterns at several scales onto biostratigraphic ranges, simulating punctuation in the course of evolution where none occurred. Similarly, in successions formed by alternating rapid aggradation and bypass, this condensation of first and last occurrences may be profound enough to simulate mass extinctions and recovery (Signor and Lipps, 1982) where none occurred.

SUMMARY

A survey of vertebrate fossils was conducted in conjunction with a high-resolution stratigraphic study of the 210-meter thick, latest Campanian lower Horseshoe Canyon Formation in southern Alberta, Canada. Most fossil sites occur as scattered isolated sites or as low-density, laterally extensive bonebeds. Less common configurations include microsites and low-area high-density bonebeds. Most specimens are large bones and teeth representing a dinosaurian fauna dominated by hadrosaurs, ceratopsians, and tyrannosaurs; a small fraction of fossils represent a co-existing aquatic fauna of fish, turtles, champsosaurs, and skates. Taphonomically, bone in the LHCF is well-preserved, with abrasion, fracture, and hydraulic sorting relatively rare and fine-sediment scouring, fungal mottling, and pedogenic corrosion common, consistent with attritional accumulation.

The taphonomy of the LHCF is distinct from previously published modes of attritional accumulation, which feature high-density channel-bound hydraulically accumulated concentrations of bone. In contrast, this mode of preservation, termed the "floodplain fill" mode, produces fossiliferous sites that cluster stratigraphically in laterally extensive, facies-independent horizons 1-4 m thick predominantly in fine-grained floodplain facies. These horizons are also closely associated with two types of lithostratigraphic surfaces associated with base-level stillstands.

The preservation of attritional accumulations of bone appears to result from an interplay of three factors—bone supply, sediment supply, and accommodation—controlled externally by subsidence and climate and internally by population and community structure. The mode of bone preservation and architecture appear to be dictated by aggradation rate. Bone can be buried whenever supply of bone and sediment pace each other on millennial time scales, but burial of large-scale accumulations occurs during periods of "trickle-fill" depositional rates, in which the mean aggradation rate equals a local depositional rate optimum for bone burial. These conditions regularly co-occur when base-level approaches or departs from a stillstand, explaining the correspondence between fossiliferous horizons in the LHCF and stratigraphic surfaces and making them analogous to fossiliferous condensed sections in marine rocks.

ACKNOWLEDGEMENTS

Thanks to Becky Kowalchuk, Donna Sloan, and the rest of the staff and students at the Royal Tyrrell Museum in Drumheller. Thanks to the families of Victor Garson, David Hardy, Tyler and Randy James, Clint Moar, Brian Neill, Arnold Pascoe, Lloyd Riggs, Robert Tolman, Harry Wade, and Clint Watson for access to exposures on family property in the Drumheller area; please request permission before visiting any site on private property. The assistance, criticisms, and patience of Reese Barrick, Elana Leithold, Dale Russell, Alan Coulson, Jennifer Griffiths, and Roberta Straight are appreciated. This project was partially funded by an RC Graduate Student Research Grant, by the Heaton Student Support Grant through the Royal Tyrrell Museum of Palaeontology, and by donations to the Sedimentary Geology Program of the Museum by numerous hydrocarbon companies in Western Canada.

LITERATURE CITED

Ainsworth, R.B., 1991, Sedimentology and high resolution sequence stratigraphy of the Bearpaw-Horseshoe Canyon Transition (Upper Cretaceous), Drumheller, Alberta, Canada: Unpublished Master's Thesis, McMaster University, Hamilton, Ontario. 213 p.

Ainsworth, R.B., 1994, Marginal marine sedimentology and high resolution sequence analysis; Bearpaw-Horseshoe Canyon transition, Drumheller, Alberta, Canada: Bulletin of Canadian Petroleum Geology, v. 42, p. 26-54.

Andrews, P., 1995, Experiments in taphonomy: Journal of Archaeological Science, v. 22, p. 147-153.

Andrews, P., and Cook, J., 1985, Natural modifications to bones in a temperate setting: Man, New Series, v. 20, p. 675-691.

Argast, S., Farlow, J.O., Gabet, R.M., and Brinkman, D.L., 1987, Transport-induced abrasion of fossil reptilian teeth: implications for the existence of Tertiary dinosaurs in the Hell Creek Formation, Montana: Geology, v. 15, p. 927-930.

Aslan, A., and Behrensmeyer, A.K., 1996, Taphonomy and Time Resolution of Bone Assemblages in a Contemporary Fluvial System: The East Fork River, Wyoming: Palaios, v. 11, p. 411-421.

Aulenback, K.R., and Braman, D.R., 1991, A chemical extraction technique for the recovery of silicified plant remains from ironstones: Review of Palaeobotany and Palynology, v. 70, p. 3-8.

Aulenback, K.R., and LePage, B.A., 1998, Taxodium wallisii sp. nov.; First Occurrence of Taxodium from the Upper Cretaceous: International Journal of Plant Science, v. 159, p. 367-390.

Badgley, C., 1986a, Counting individuals in mammalian fossil assemblages from fluvial environments: Palaios, v. 1, p. 328-338.

Badgley, C., 1986b, Taphonomy of mammalian fossil remains from Siwalik rocks of Pakistan: Paleobiology, v. 12, p. 119-142.

Banerjee, I., and Kidwell, S.M., 1991, Significance of molluscan shell beds in sequence stratigraphy: an example from the lower Cretaceous Manville Group of Canada: Sedimentology, v. 38, p. 913-934.

Bao, H., Koch, P.L., and Hepple, R.P., 1998, Hematite and calcite coatings on fossil vertebrates: Journal of Sedimentary Research, v. 68, p. 727-738.

Bartlett, J., Coulson, A., Woodward, H., and Straight, W., 2003, Comparing transport-induced abrasion of fresh and fossilized skeletal remains, Geological Society of America, Southeast Section Meeting Abstracts with Programs v. 35, p. 63.

Baszio, S., 1997a, Investigations on Canadian dinosaurs: palaeoecology of dinosaur assemblages throughout the late Cretaceous of south Alberta, Canada, Courier Forschungsinstitut Senckenberg, v. 196, p. 1-31.

Baszio, S., 1997b, Investigations on Canadian dinosaurs: systematic palaeontology of isolated dinosaur teeth from the latest Cretaceous of south Alberta, Canada: Courier Forschungsinstitut Senckenberg, v. 196, p. 33-77.

Behrensmeyer, A.K., 1975, Taphonomy and paleoecology in the hominid fossil record: Yearbook of Physical Anthropology, v. 19, p. 36-50.

Behrensmeyer, A.K., 1975b, The taphonomy and paleoecology of Plio-Pleistocene vertebrate assemblages of Lake Rudolf, Kenya: Bulletin of the Museum of Comparative Zoology, v. 146, p. 473-578.

Behrensmeyer, A.K., 1978, Taphonomic and ecologic information from bone weathering: Paleobiology, v. 4, p. 150-162.

Behrensmeyer, A.K., 1982, Time resolution in fluvial vertebrate assemblages: Paleobiology v. 8, p. 211-227.

Behrensmeyer, A.K., 1983, Patterns of natural bone distribution on recent land surfaces: implications for archaeological site formation: *in* Clutton-Brock, J., and Grigson, C., eds., Animals and Archaeology: (1) Hunters and their prey: BAR International Series No. 163., pp. 93-106.

Behrensmeyer, A.K., 1987, Miocene Fluvial Facies and Vertebrate Taphonomy in Northern Pakistan: *in* Ethridge, F.G., Flores, R.M., and Harvey, M.D., eds., Recent Developments in Fluvial Sedimentology: Society of Economic Paleontologists and Mineralogists, Special Publication No. 39, p. 169-176.

Behrensmeyer, A.K., 1988, Vertebrate preservation in fluvial channels: Palaeogeography, Palaeoclimatology, Palaeoecology, v. 63, p. 183-199.

Behrensmeyer, A.K., 1991, Terrestrial Vertebrate Accumulations: *in* Allison, P.A., and Briggs, D.E.G., eds., Taphonomy: Releasing the Data Locked in the Fossil Record: Topics in Geobiology Series V. 9, Plenum Press, New York, pp. 291-335.

Behrensmeyer, A.K., and Chapman, R.E., 1993, Models and simulations of time-averaging in terrestrial vertebrate accumulations: *in* Behrensmeyer, A.K., and Kidwell, S.M., eds., Taphonomic Approaches

to Time Resolution in Fossil Assemblages: The Paleontological Society Short Courses in Paleontology No. 6, pp. 102-124.

Behrensmeyer, A.K., Western, D., and Dechant-Boaz, D.E., 1979, New perspectives in vertebrate paleoecology from a recent bone assemblage: Paleobiology, v. 5, p. 12-21.

Behrensmeyer, A.K., Gordon, K.D., and Yanagi, G.T, 1986, Trampling as a cause of bone surface damage and pseudo-cutmarks: Nature, v. 319, p. 768-771.

Behrensmeyer, A.K., Willis, B.J., and Quade, J., 1995, Floodplains and paleosols of Pakistan Neogene and Wyoming Paleogene deposits: a comparative study: Palaeogeography Palaeoclimatology Palaeoecology, v. 115, p. 37-60.

Beland, P., and Russell, D.A, 1978, Paleoecology of Dinosaur Provincial Park (Cretaceous), Alberta, interpreted from the distribution of articulated remains: Canadian Journal of Earth Science, v. 15, p. 1012-1024.

Blob, R.W., 1997, Relative hydrodynamic dispersal potentials of soft-shelled turtle elements: implications for interpreting skeletal sorting in assemblages of non-mammalian terrestrial vertebrates: Palaios, v. 12, p. 151-164.

Blob, R.W., and Fiorillo, A.R., 1996, The significance of vertebrate microfossil size and shape distributions for faunal abundance reconstructions: a late Cretaceous example: Paleobiology, v. 22, p. 422-435.

Boaz, N.T., and Behrensmeyer, A.K., 1976, Hominid taphonomy: transport of human skeletal parts in an artificial fluviatile environment: American Journal of Physical Anthropology, v. 45, p. 53-60.

Bown, T.M., and Kraus, M.J., 1981b, Vertebrate fossil-bearing paleosol units (Willwood Formation, lower Eocene, northwest Wyoming, U.S.A.): implications for taphonomy, biostratigraphy, and assemblage analysis: Palaeogeography, Palaeoclimatology, Palaeoecology, v. 34, p. 31-56.

Bown, T.M., and Kraus, M.J., 1987, Integration of channel and floodplain suites, I. Developmental sequence and lateral relations of alluvial paleosols: Journal of Sedimentary Petrology, v. 57, p. 587-601.

Bown, T.M., and Kraus, M.J., 1993, Time-stratigraphic reconstruction of paleopedologic, sedimentologic, and biotic events (Willwood Formation, Lower Eocene, northwest Wyoming, U.S.A.): Palaios, v. 8, p. 68-80.

Brain, C.K., 1967, Bone weathering and the problem of bone pseudo-tools: South African Journal of Science, v. 3, p. 97-99.

Braman, D.R., and Eberth, D.A., 1988, Paleontology and Geology of the Edmonton Group (late Cretaceous to early Paleocene), Red Deer River Valley, Alberta, Canada: Society of Vertebrate Paleontology 48th Annual Meetings Field Trip C, Occasional Paper of the Tyrrell Museum of Palaeontology No. 8, p. 1-25.

Braman, D.R., Johnston, P.A., and Haglund, W.M., 1995, Upper Cretaceous Paleontology, Stratigraphy, and Depositional Environments at Dinosaur Provincial Park and Drumheller, Alberta: Canadian Paleontology Conference Field Trip Guidebook No. 4, p. 1-119.

Brett, C.E., 1995, Sequence Stratigraphy, Biostratigraphy, and Taphonomy in Shallow Marine Environments: Palaios, v. 10, p. 597-616.

Brett, C.E., 1998, Sequence Stratigraphy, Paleoecology, and Evolution: Biotic Clues and Responses to Sea-Level Fluctuations: Palaios, v. 13, p. 241-262.

Brinkman, D.B., 1990, Paleoecology of the Judith River Formation (Campanian) of Dinosaur Provincial Park, Alberta, Canada: evidence from vertebrate microfossil localities: Palaeogeography, Palaeoclimatology, Palaeoecology, v. 78, p. 37-54.

Brinkman, D.B., Ryan, M., and Eberth, D.A, 1998, The Paleogeographic and Stratigraphic Distribution of Ceratopsids (Ornithischia) in the Upper Judith River Group of Western Canada: Palaios, v. 13, p. 160-169.

Cassiliano, M., 1997, Taphonomy of mammalian fossil across the Blancan-Irvingtonian boundary: Palm Spring Formation, Anza-Borrego desert of southern California: Palaeogeography, Palaeoclimatology, Palaeoecology, v. 129, p. 81-108.

Catuneanu, O., and Sweet, A.R., 1999, Maastrichtian-Paleocene foreland-basin stratigraphies, western Canada: a reciprocal sequence architecture: Canadian Journal of Earth Sciences, v. 36, p. 685-703.

Chure, D.J., Fiorillo, A.R., and Jacobsen, A., 1998, Prey bone utilization by predatory dinosaurs in the Late Jurassic of North America, with comments on prey bone use by dinosaurs throughout the Mesozoic: Gaia, v. 15, p. 227-232.

Coard, R., 1999, One bone, two bone, wet bones, dry bones: transport potentials under experimental conditions: Journal of Archaeological Science, v. 26, p. 1369-1375.

Coard, R., and Dennell, R.W., 1995, Taphonomy of some articulated skeletal remains: Transport potential in an artificial environment: Journal of Archaeological Science, v. 22, p. 441-448.

Coe, M., 1978, The decomposition of elephant carcasses in the Tsavo (East) National Park, Kenya: Journal of Arid Environments, v. 1, p. 71-86.

Cook, E., 1995, Taphonomy of two non-marine Lower Cretaceous bone accumulations from southern England: Palaeogeography, Palaeoclimatology, Palaeoecology, v. 116, p. 263-270.

Coulson, A., Bartlett, J., Decherd, S., and Kissel, R., 2002, Effects of transport induced-abrasion on avian skeletal elements: Journal of Vertebrate Paleontology, v. 22, p. 46A.

Courville, P., and Collin, P.Y., 2002, Taphonomic sequences--A new tool for sequence stratigraphy, Geology, v. 30, p. 511-514.

Dodson, P., 1971, Sedimentology and taphonomy of the Oldman Formation (Campanian), Dinosaur Provincial Park, Alberta, Canada: Palaeogeography, Palaeoclimatology, Palaeoecology, v. 10, p. 21-74.

Dodson, P., 1973, The significance of small bones in paleoecological interpretation: University of Wyoming Contributions to Geology, v. 12, p. 15-19.

Dodson, P., Bakker, R.T, Behrensmeyer, A.K., and McIntosh, J.S., 1980a, Paleoecology of the dinosaur-bearing Morrison Formation: National Geographic Society Research Reports, v. 15, p. 145-156.

Dodson, P., Behrensmeyer, A.K., Bakker, R.T., and McIntosh, J.S, 1980b, Taphonomy and paleoecology of the dinosaur beds of the Jurassic Morrison Formation: Paleobiology, v. 6, p. 208-232.

Dominguez-Rodrigo, M., 1999, Flesh availability and bone modifications in carcasses consumed by lions: palaeoecological relevance in hominid foraging patterns; Palaeogeography, Palaeoclimatology, Palaeoecology, v. 149, p. 373-388.

Eberth, D.A., 1990, Stratigraphy and sedimentology of vertebrate microfossil sites in the uppermost Judith River Formation (Campanian), Dinosaur Provincial Park, Alberta, Canada: Palaeogeography, Palaeoclimatology, Palaeoecology, v. 78, p. 1-35.

Eberth, D.A., 1995, Bearpaw/Horseshoe Canyon Formation Transition (Maastrichtian) in the East Coulee/ Willow Creek Area: Field Trip Guidebook, Canadian Society of Petroleum Geologists One Day Field Trip, 43 p.

Eberth, D.A., 1996, Origin and significance of mud-filled incised valleys (Upper Cretaceous) in southern Alberta, Canada: Sedimentology, v. 43, p. 459-477.

Eberth, D.A., and Brinkman, D.B., 1997, Paleoecology of an estuarine, incised-valley fill in the Dinosaur Park Formation (Judith River Group, Upper Cretaceous) of southern Alberta, Canada: Palaios, v. 12, p. 43-58.

Eberth, D.A., Berman, D.S, Sumida, S.S., and Hopf, H., 2000, Lower Permian terrestrial paleoenvironments and vertebrate paleoecology of the Tambach Basin (Thuringia, Central Germany): The Upland Holy Grail: Palaios, v. 15, p. 293-313.

Eberth, D.A., Currie, P.J., Brinkman, D.B., Ryan, M.J., Braman, D.R., Gardner, J.D, Lam, V.D., Spivak, D.N., and Neuman, A.G., 2001, Alberta' s dinosaurs and other fossil vertebrates: Judith River and Edmonton Groups (Campanian-Maastrichtian): Museum of the Rockies Occasional Paper No. 3, p. 47-78.

Efremov, J.A., 1940, Taphonomy: New branch of paleontology: Pan-American Geologist, v. 74, p. 81-93.

Erickson, G.M., 1996, Incremental growth lines of von Ebner in dinosaurs and the assessment of tooth replacement rates using growth line counts: Bulletin of the National Academy of Sciences, v. 93, p. 14623-14627.

Erickson, G.M., and Olson, K.H., 1996, Bite marks attributable to Tyrannosaurus rex: preliminary description and implications: Journal of Vertebrate Paleontology, v. 16, p. 175-178.

Farlow, J.O., Brinkman, D.L., Abler, W.L., and Currie, P.J., 1991, Size, shape, and serration density of theropod dinosaur lateral teeth: Modern Geology, v. 16, p. 161-198.

Fiorillo, A.R., 1984, An introduction to the identification of trample marks: Abstracts of the First International Conference on Bone Modification, Carson City, Nevada, August 17-19, 1984, p. 11.

Fiorillo, A.R., 1987, Trample marks: Caution from the Cretaceous: Current Research in the Pleistocene, University of Maine, v. 4, p. 73-75.

Fiorillo, A.R., 1988, Aspects of bone modification applied to time-resolution in the fossil record--an example from the Miocene of Western Nebraska: Current Research in the Pleistocene, University of Maine, v. 5, p. 103-109.

Fiorillo, A.R., Padian, K., and Musikasinthorn, C., 2000, Taphonomy and depositional setting of the Placerias Quarry (Chinle Formation: Late Triassic, Arizona): Palaios, v. 15, p. 373-386.

Galloway, W.E., 1989, Genetic stratigraphic sequences in basin analysis I: architecture and genesis of flooding-surface bounded depositional units: Bulletin of American Association of Petroleum Geologists, v. 73, p. 125-142.

Gibson, D.W., 1977, Upper Cretaceous and Tertiary coal-bearing strata in the Drumheller-Ardley region, Red Deer River Valley, Alberta: Geological Survey of Canada Paper No. 76-35, p. 1-41.

Graham, R.W., 1993, Processes of time-averaging in the terrestrial vertebrate record: *in* Behrensmeyer, A.K., and Kidwell, S.M., eds., Taphonomic Approaches to Time Resolution in Fossil Assemblages: The Paleontological Society Short Courses in Paleontology No. 6, pp. 102-124.

Grayson, D.K., 1978, Minimum numbers and samples size in vertebrate faunal analysis: American Antiquity, v. 43, p. 53-65.

Hadly, E.A., 1999, Fidelity of terrestrial vertebrate fossils to a modern ecosystem: Palaeogeography, Palaeoclimatology, Palaeoecology, v. 149, p. 389-409.

Hamblin, A.P., 1998b, Edmonton Group / St. Mary River Formation: Summary of Literature and Concepts: Geological Survey of Canada Open File Report No. 3578, 36 p.

Haynes, G., 1988, Mass death and serial predation: comparative taphonomic studies of modern large mammal death sites: Journal of Archaeological Sciences, v. 15, p. 219-235.

Hill, A., 1979, Disarticulation and scattering of mammal skeletons: Paleobiology, v. 5, p. 261-274.

Hill, A., and Behrensmeyer, A.K., 1984, Disarticulation patterns of some modern East African mammals: Paleobiology, v. 10, p. 366-376.

Holland, S.M., 1995, The stratigraphic distribution of fossils: Paleobiology, v. 21, p. 92-109.

Holtz, T.R. Jr., 1995, The arctometatarsalian pes, an unusual structure of the metatarsus of Cretaceous Theropoda (Dinosauria: Saurischia): Journal of Vertebrate Paleontology, v. 14, p. 480-519.

Holz, M., and Barbarena, M.C., 1994, Taphonomy of the south Brazilian Triassic paleoherpetofauna: pattern of death, transport and burial: Palaeogeography, Palaeoclimatology, Palaeoecology, v. 107, p. 179-197.

Hungerbühler, A., 1998, Taphonomy of the prosauropod dinosaur Sellosaurus and its implications for carnivore faunas and feeding habits in the late Triassic: Palaeogeography, Palaeoclimatology, Palaeoecology, v. 143, p. 1-29

Jacobsen, A.R., 1998, Feeding behavior of carnivorous dinosaurs as determined by tooth marks on dinosaur bone: Historical Biology, v. 13, p. 17-26.

Kidwell, S.M., 1986, Models for fossil concentrations: paleobiologic implications: Paleobiology, v. 12, p. 6-24.

Kidwell, S.M., 1988, Reciprocal sedimentation and noncorrelative hiatuses in marine-paralic siliciclastics: Miocene outcrop evidence: Geology, v. 16, p. 609-612.

Kidwell, S.M., 1989, Stratigraphic condensation of marine transgressive records: origin of major shell deposits in the Miocene of Maryland: Journal of Geology, v. 97, p. 1-24.

Korth, W.W., 1979, Taphonomy of microvertebrate fossil assemblage: Annals of the Carnegie Museum of Natural History, v. 48, p. 235-285.

Koster, E.H., 1987, Vertebrate taphonomy applied to the analysis of ancient fluvial systems: *in* Ethridge, F.G., Flores, R.M., and Harvey, M.D., eds., Recent Developments in Fluvial Sedimentology: Society of Economic Paleontologists and Mineralogists, Special Publication No. 39, p. 159-168.

Koster, E.H., and Currie, P.J., 1987, Upper Cretaceous coastal plain sediments at Dinosaur Provincial Park, southeast Alberta: Geological Society of America Centennial Field Guide, Rocky Mountain Section, pp. 9-14.

Kowalewski, M., Flessa, K., and Hallman, D.P., 1995, Ternary taphograms: triangular diagrams applied to taphonomic analysis: Palaios, v. 10, p. 478-483.

Lawton, R., 1977, Taphonomy of the dinosaur quarry, Dinosaur National Monument: University of Wyoming Contributions to Geology, v. 15, p. 119-126.

Lehman, T.M., 1982, A Ceratopsian Bone Bed from the Aguja Formation (Upper Cretaceous) Big Bend National Park, Texas: Unpublished Master's Thesis, University of Texas, Austin , Texas, 210 p.

Lehman, T.M., 1987, Late Maastrichtian paleoenvironment and dinosaur biogeography in the Western Interior of North America: Palaeogeography, Palaeoclimatology, Palaeoecology, v. 60, p. 189-217.

Lehman, T.M., 1990, Paleosols and the Cretaceous/Tertiary transition in the Big Bend region of Texas: Geology, v. 18, p. 362-364.

Lorenz, J.C., 1981, Sedimentary and tectonic history of the Two Medicine Formation, Late Cretaceous (Campanian), northwestern Montana: Unpublished Doctoral Dissertation, Princeton University, New Jersey, 215 p.

Lyman, R.L., 1994, Vertebrate Taphonomy: Cambridge Manuals in Archaeology, Cambridge University Press, 524 p.

Lyman, R.L., and Fox, G.L., 1989, A critical evaluation of bone weathering as an indication of bone assemblage formation: Journal of Archaeological Science, v. 16, p. 293-317.

Martin, R.E., 1999, Taphonomy: A Process Approach: Cambridge Paleobiology Series No. 4, Cambridge University Press, 506 p.

Miall, A.D., 1992, Alluvial deposits: *in* Walker, R.G., and James, N.P., eds., Facies Models: Response to Sea Level Change: Geological Association of Canada, Newfoundland, pp. 119-142.

Miller, G.J., 1975, A study of cuts, grooves, and other marks on recent and fossil bones: II, weathering cracks, fractures, splinters, and other similar natural phenomena: *in* Swanson, E., ed., Lithic Technology: The Hague: Mouton, pp. 212-226.

Morgan, M.E., Badgley, C., Gunnell, G.F., Gingerich, P.D., Kappelman, J.W., and Maas, M.C., 1995, Comparative paleoecology of Paleogene and Neogene mammalian faunas: body-size structure; Palaeogeography, Palaeoclimatology, Palaeoecology, v. 115, p. 287-317.

Nadon, G.C., 1993, The association of anastomosed fluvial deposits and dinosaur tracks, eggs, and nests: Implications for the interpretation of floodplain environments and possible survival strategy for ornithopods: Palaios, v. 8, p. 31-44.

Olsen, S.L., and Shipman, P., 1988, Surface modification on bone: Trampling versus butchery: Journal of Archaeological Science, v. 15, p. 535-553.

Paik, I.S., 2000, Bone chip-filled burrows associated with bored dinosaur bone in floodplain paleosols of the Cretaceous Hasandong Formation, Korea: Palaeogeography, Palaeoclimatology, Palaeoecology, v. 157, p. 213-205.

Peng, J., Russell, A.P., and Brinkman, D.B., 2001, Vertebrate microsite assemblages (exclusive of mammals) from the Foremost and Oldman Formations of the Judith River Group (Campanian) of southern Alberta: An illustrated guide: Provincial Museum of Alberta, Natural History Occasional Paper No. 25, 54 p.

Posamentier, H.W., and Vail, P.R., 1988, Eustatic controls on clastic deposition, II. Sequence and systems tract models: *in* Wilgus, C.K., Hastings, B.S., Kendall, C.G.S., Posamentier, H.W., Ross, C.A., and Van Wagoner, J.C., eds., Sea-Level Changes: An Integrated Approach: Society of Economic Paleontologists and Mineralogists Special Publication No. 42, p. 125-154.

Quirk, D.G., 1996, ' Base profile' : a unifying concept in alluvial sequence stratigraphy: *in* Howell, J.A., and Aitken, J.F., eds., High Resolution Sequence Stratigraphy: Innovations and Applications: Geological Society (London) Special Publication No. 104, p. 37-50.

Rahmani, R.A., 1988, Estuarine tidal channel and nearshore sedimentation of a Late Cretaceous epicontinental sea, Drumheller, Alberta, Canada: in de Boer, P.L., van Gelder, A., and Nio, S.D., eds., Tidal-Influenced Sedimentary Environments and Facies: D. Reidel Publishing Company, Dordrecht, p. 433-471.

Rahmani, R., 1989, Cretaceous Tidal Estuarine and Deltaic Deposits, Drumheller, Alberta: Canadian Society of Petroleum Geologists' field guide, Second International Research Symposium on Clastic Tidal Deposits, Calgary, Alberta, 55 p.

Retallack, G.J., 1990, Soils of the Past: An Introduction to Paleopedology: Harper Collins Academic Press, London, 520 p.

Rogers, R.R., 1989, Taphonomy of three monospecific dinosaur bone beds in the Late Cretaceous Two Medicine Formation, northwestern Montana: Evidence for dinosaur mass mortality related to episodic drought: Unpublished Master's Thesis, University of Montana, 102 p.

Rogers, R.R., 1990, Taphonomy of three dinosaur bone beds in the Upper Cretaceous Two Medicine Formation of northwestern Montana: Evidence for drought-related mortality: Palaios, v. 5, p. 394-413.

Rogers, R.R., and Kidwell, S.M., 2000, Association and taphonomy of terrestrial vertebrate fossils with terrestrial discontinuity surfaces in Judith River Formation, Montana: Journal of Geology, v. 108, p. 131-154.

Russell, D.A., and Chamney, T.P., 1967, Notes on the biostratigraphy of dinosaurian and microfossil faunas in the Edmonton Formation (Cretaceous), Alberta: National Museum of Canada, Natural History Paper No. 35, 22 p.

Ryan, M.J., 1992, The taphonomy of a Centrosaurus (Reptilia: Ornithischia) bone bed (Campanian), Dinosaur Provincial Park, Alberta, Canada: Unpublished Master's Thesis, University of Calgary, Alberta, 526 p.

Ryan, M.J., Russell, A.P., Eberth, D.A., and Currie, P.J., 2001, The taphonomy of a Centrosaurus (Ornithischia: Ceratopsidae) bone bed from the Dinosaur Park Formation (Upper Campanian), Alberta, Canada, with comments on cranial ontogeny: Palaios, v. 16, p. 482-506.

Sankey, J.T., Brinkman, D.B., Guenther, M., and Currie, P.J., 2002, Small theropod and bird teeth from the late Cretaceous (late Campanian) Judith River Group, Alberta: Journal of Paleontology, v. 76, p. 751-763.

Shanley, K.W., and McCabe, P.J., 1995, Sequence stratigraphy of Turonian-Santonian strata, Kaiparowits Plateau, southern Utah, USA: Implications for regional correlation and foreland basin evolution: *in* van Wagoner, J.C., and Bertram, G.T., eds., Remote Sensing: Outcrop and Subsurface Examples from the Cretaceous of North America: American Association of Petroleum Geologists Memoir 64, pp. 103-136.

Sheehan, P.M., Fastovsky, D.E., Hoffman, R.G., Berghaus, C.B., and Gabriel, D.L., 1991, Sudden extinction of the dinosaurs: Latest Cretaceous, Upper Great Plains, U.S.A: Science, v. 254, p. 835-839.

Sheehan, P.M., Fastovsky, D.E., Barreto, C., and Hoffmann, R.G., 2000, Dinosaur abundance was not declining in a "3 m gap" at the top of the Hell Creek Formation, Montana and North Dakota: Geology, v. 28, p. 523-526.

Shotwell, J.A., 1955, An approach to the paleoecology of mammals: Ecology, v. 36, p. 327-337.

Siggerud, E.I.M., and Steel, R.J., 1999, Architecture and trace-fossil characteristics of a 10,000-20,000 year fluvial-to-marine sequence, SE Ebro Basin, Spain: Journal of Sedimentary Research, v. 69, p. 365-383.

Signor, P.W., and Lipps, J.H., 1982, Sampling bias, gradual extinction patterns, and catastrophes in the fossil record: in Silver, L.T., and Schultz, P.H., eds., Geological Implications of Impacts of Large Asteroids and Comets on the Earth: Geological Society of America Special Paper No. 190, p. 291-296.

Smith, N.D., Cross, T.A., Dufficy, J.P., and Clough, S.R., 1989, Anatomy of an Avulsion: Sedimentology, v. 36, p. 1-23.

Smith, R.M.H., 1993, Vertebrate taphonomy of late Permian floodplain deposits in the southwestern Karoo Basin of South Africa: Palaios, v. 8, p. 45-67.

Smith, R.M.H., 1993, Sedimentology and ichnology of floodplain paleosurfaces in the Beaufort Group (Late Permian), Karoo Sequence, South Africa: Palaios, v. 8, p. 339-357.

Smith, R.M.H., 1995, Changing fluvial environments across the Permian-Triassic boundary in the Karoo Basin, South Africa and possible causes of tetrapod extinctions: Palaeogeography, Palaeoclimatology, Palaeoecology, v. 117, p. 81-104.

Srivastava, S.K., 1968, Angiospermic microflora of the Edmonton Formation, Alberta: Unpublished Doctoral Dissertation, University of Alberta, 343 p.

Straight, W.H., 1996, Stratigraphy and paleontology of the Cretaceous-Tertiary boundary, Big Bend National Park, Texas: Unpublished Master's Thesis, Texas Tech, Lubbock, Texas, 103 p.

Straight, W.H., and Eberth, D.A., 1998, Sequences, stratigraphy, and depositional environments of the Horseshoe Canyon Formation in the Drumheller region: Geo-Triad Convention Post-meeting Field Trip 6, guidebook, 56 p.

Straight, W.H., and Eberth, D.A., 2002, Testing the utility of vertebrate remains in recognizing patterns in fluvial deposits: An example from the lower Horseshoe Canyon Formation, Alberta; Palaios, v. 17, p. 472-490.

Straight, W.H., Barrick, R.E., Showers, W.J., and Genna, B., 2001, Late Cretaceous continental seasonality derived from oxygen isotopes from Albertosaurus tooth enamel: 61st Annual Meeting, Abstracts of Papers, Journal of Vertebrate Paleontology, v. 21, p. 105.

Straight, W.H., Barrick, R.E, and Eberth, D.A., 2003, Reflections of surface water, seasonality and climate in stable oxygen isotopes from tyrannosaurid tooth enamel: Palaeogeography, Palaeoclimatology, Palaeoecology, in press.

Tanke, D.H., and Currie, P.J., 1998, Head-biting behavior in theropod dinosaurs: paleopathological evidence: Gaia, 15, p. 167-184.

Tappen, M.J., 1994, Bone weathering in the tropical rain forest: Journal of Archaeological Science, v. 21, p. 663-673.

Tappen, N.C., and Peske, G.R., 1970, Weathering cracks and split-line patterns in archaeological bone: American Antiquity, v. 35, p. 383-386.

Therrien, F., and Fastovsky, D.E., 2000, Paleoenvironment of early Theropoda, Chinle Formation (late Triassic), Petrified Forest National Park, Arizona: Palaios, v. 15, p. 194-211.

Toots, H., 1965a., Sequence of disarticulation in mammalian skeletons: Contributions to Geology, University of Wyoming, v. 4, p. 37-39.

Toots, H., 1965b, Random orientation of fossils and its significance: Contributions to Geology, University of Wyoming, v. 4, p. 59-62.

Van Wagoner, J.C., Posamentier, H.W., Mitchum, R.M. Jr., Vail, P.R., Sarg, J.F., Loutit, T.S., and Hardenbol, J., 1988, An Overview of the Fundamentals of Sequence Stratigraphy and Key Definitions: *in* Sea

Level Changes: An Integrated Approach: Society of Economic Paleontologists and Mineralogists Special Publication, No. 42, p. 39-46.

Voorhies, M., 1969, Taphonomy and population dynamics of an early Pliocene vertebrate fauna, Knox County, Nebraska: University of Wyoming Contributions to Geology, Special Paper No. 1, 69 p.

Weigelt, J., 1989, Recent vertebrate carcasses and their paleobiological implications: University of Chicago Press, Chicago, 188 p., English translation of Weigelt, J. 1927. Rezente Wirbeltierleichen und ihre palaobiologische Bedeutung, Verlag von Max Weg, Leipzig.

White, P.D., Fastovsky, D.E., and Sheehan, P.M., 1998, Taphonomy and Suggested Structure of the Dinosaurian Assemblage of the Hell Creek Formation (Maastrichtian), Eastern Montana and Western North Dakota: Palaios, v. 13, p. 41-51.

Willis, B.J., and Behrensmeyer, A.K., 1994, Architecture of Miocene overbank deposits in Northern Pakistan: Journal of Sedimentary Research, v. 64, p. 60-67.

Wood, J.M., Thomas, R.G., and Visser, J., 1988, Fluvial processes and vertebrate taphonomy: the upper Cretaceous Judith River Formation, south-central Dinosaur Provincial Park, Alberta, Canada: Palaeogeography, Palaeoclimatology, Palaeoecology, v. 66, p. 127-143.

TABLE CAPTION

TABLE 1—Breakdown of identified fossil elements by taxonomic group. Element abbreviations: (ct) count, (skl) skull, (tth) shed teeth, (vrt) vertebra, (grd) shoulder and pelvic girdle, (lmb) front and hind limb long bones, (pod) podial elements of manus and pes, (ung) unguals, (chv) chevrons, (arm) dermal armor such as scutes or carapace elements, (tnd) ossified tendons.

TABLE 2—Distribution of fossil sites among facies associations common to the LHCF.

TABLE 3—Modifications to bone in the Lower Horseshoe Canyon Formation. Abbreviations used in Table 4.

TABLE 4—Occurrence of taphonomic modifications. See Table 3 for abbreviations and interpretation. Values above diagonal represent percent of 529 sites in which two taphonomic modification types co-occur. Values below diagonal refer to number out of three statistical tests indicating a relationship in stratigraphic distribution of remains bearing two taphonomic modification types.

TABLE 5—Combined listing for Voorhies Groups I and I-II (most easily transported elements) for different taxa (compiled from Voorhies, 1969; Dodson, 1973; Behrensmeyer 1975b; Korth, 1979; Lehman, 1982; Blob, 1997). The transportability of turtle skulls, posterior costals, and nuchal elements depends on element orientation (Blob, 1997). Group II includes some vertebrae: thoracic vertebrae in horses (Behrensmeyer, 1975b) and dorsal vertebrae for ceratopsians (Lehman, 1982).

TABLE 6—Transport groupings for each faunal group in the LHCF. Visceral and appendage elements are fluvial-flow transport groups similar to Voorhies Groups I and III, after Lehman (1982). Radial and thoracic elements are groupings of bones corresponding to the disarticulation sequence of floating carcasses (after Weigelt, 1927; Hill, 1979) and count some of the same elements that appear in the flow-transport groups. Teeth counts exclude those still in place in cranial bones.

Table 1

	ct	%	skl	tth	vrt	rib	grd	lmb	pod	ung	chv	arm	tnd
hadrosaurids	320	43	11	40	36	79	20	82	3	9	3		25
tyrannosaurids	76	10	2	46	6	6	2	9		4			
ceratopsians	53	7	17	12	1	14	3	5					
fish	23	3	2		2							19	
troodontids	22	3		19	1			1		1			
turtles	16	2				1		2				12	
champsosaurs	13	2	1		8			4					
skates	13	2		13									
ankylosaurians	10	1		3				4				1	
ornithomimids	10	1				1		3	1	5			
unknown			5		11	37	6	32	1	3		1	

Table 2

of 521 sites…	solitary	sparse bb	packed bb	microsite	*% by assoc.*
association					
1) channel	14	1	8	1	*5%*
2) splay	63	35	9	9	*22%*
3) backswamp	104	116	2	17	*46%*
4) floodplain	57	47	20	18	*27%*
% by site type	*46%*	*38%*	*8%*	*8%*	

Table 3

	Modification	% Sites	Abbrev.	Interpretation
mineralization				
	siderite encrustation	35	enc	bone preserved rapidly in saturated soil
	clay encrustation	5	enc	bone preserved in reducing backswamp
abrasion				
	brushmarks	45	bru	scoured by burial in mud/saturated soil
	grooves	19	grv	trampling
	polish	39	pol	scoured by burial in mud/saturated soil
	sinusoidal mottles	26	mot	“root etching” by plants/fungus
	pits and punctures	8	pit	bite marks/insect damage
	borings	1	bor	insect damage
destruction				
	rounding	18	rnd	transport or compression wear in mud
	removal	9	rem	exposure before burial
	corrosion	39	cor	chemical/bacterial weathering
	fractures	7	frc	trampling? /modern erosion
	weathering (> stage 1)	10	wth	exposure

Table 4

	grv	pit	wth	frc	rnd	rem	bru	pol	mot	bor	cor	enc
grv		3	1	2	3	2	12	8	4	<1	8	7
pit	*1*		1	1	2	1	5	4	1	0	4	3
wth				1	1	1	3	3	2	0	4	4
frc		2			2	1	3	2	1	0	2	1
rnd						2	11	8	5	0	10	9
rem		1			*1*		3	2	1	0	6	4
bru				*2*				20	16	<1	17	20
pol	*1*				*2*		*1*		15	<1	11	15
mot	*1*				*2*		*1*	*3*		<1	10	11
bor											<1	0
cor	*2*				*1*							21
enc	*2*					*1*					*1*	
# sites	99	43	52	35	94	47	238	204	138	4	205	212
% sites	19	8	10	7	18	9	45	39	26	<1	39	40

Table 5

Mouse	*Sheep*	*Pig*	*Horse*	*Hippo*	*Turtle*	*Ceratopsian*
vertebra	vertebra		vertebra*		atlas	vertebra*
ribs	ribs				free rib	
	sacrum					
	sternum				sternum	
					shell*	
scapula	scapula					
pelvis						ischium
	humerus					
radius						
ulna	ulna					
	patella	patella	patella			
	sesamoids	sesamoids	sesamoids	sesamoids		
			calcaneum		calcaneum	
podials	metacarpals	podials	podials			metapodials
phalanges	phalanges	phalanges	phalanges	phalanges		phalanges
maxilla					skull*	

Table 6

	visceral	*appendage*		*thoracic*	*radial*		*teeth*
faunal group by assemblage							
hadrosaurids	115	113		138	108		40
tyrannosaurids	12	13		14	15		56
ceratopsians	15	25		19	21		12
fish	2	2		2	2		0
troodontids	1	1		1	2		19
turtles	1	2		1	2		0
champsosaurs	8	5		8	5		0
skates	0	0		0	0		13
ankylosaurians	0	4		0	5		3
ornithomimids	1	3		0	9		0

FIGURE CAPTIONS

FIGURE 1—Map of the field area and survey sites along the Red Deer River, Alberta, Canada.

FIGURE 2—Composite stratigraphic framework and lithologic section for the lower Horseshoe Canyon Formation. The section is scaled in meters above the Bearpaw / LHCF contact. The coal seam numbering follows the nomenclature of Gibson (1977). The section is divided into three members (solid lines): a fossil-poor, coal-rich basal member; a fossil-rich, coal-poor member; and a fossil-poor, coal-poor upper member. Member boundaries coincide with package basal scours (also heavy broken lines). Packages of the basal and middle members (A-C and D-F, respectively) each contain two intervals, a lower rise-interval and an upper fall-interval, separated by an internal surface (dotted lines). The upper member packages (G-J) contain only rise-intervals. The stratigraphic positions of fossiliferous horizons are shown as open triangles, with each symbol representing 10 fossil-bearing sites.

FIGURE 3—Stratigraphic distribution of LHCF sites and fossil configurations. (A) Number of sites by interval. (B) Number of sites per meter of interval thickness. (C, D, E) Proportion of solitary, microsite, and bonebed configurations, respectively, among sites by interval. Bar chart format follows the framework in Figure 2. Proportion bars for package I and the fall-interval of package F were omitted due to small sample size.

FIGURE 4—Stratigraphic distribution of specimens. (A) Number of specimens per interval. (B) Number of specimens per site. (C, D, E) Proportion of solitary, microsite, and bonebed configurations, respectively, among specimens by interval. Bar chart format follows the framework in Figure 2. Proportion bars for package I and the fall-interval of package F were omitted due to small sample size.

FIGURE 5—Stratigraphic distribution of dinosaur teeth. In the bar charts (A-D), the absence of a bar indicates that no teeth (or no fossils) were found in the interval. (A) Proportion of teeth among the specimens

found in each interval. (B-D) Proportion of hadrosaurid, tyrannosaurid, and dromaeosaurid teeth, respectively, among the teeth from each interval. Bar chart format follows the framework in Figure 2. (E) Pie chart reflecting the representation of various skeletal elements and body components among the survey assemblage. Abbreviations for faunal groups: hadrosaurids (hdr), tyrannosaurids (tyr), ceratopsians (cer), ankylosaurians (ank), troodontids (tro), dromaeosaurids (dro), ornithomimids (orn), crocodilians (crc), champsosaurs (chp), fish (fsh), skates (skt), and turtles (trt). (F) Taphogram showing the distribution of teeth by faunal group among the three types of fossil configurations. Abbreviations are as listed for Figure 3.

FIGURE 6—Distribution of LHCF specimens by faunal groups. (A) Stratigraphic distribution of faunal groups. Abbreviations for faunal groups are as in Figure 5, and the chart format follows the stratigraphic framework in Figure 2. Faunal groups are ranked in order of highest to lowest abundance in each package. Ties are given matching ranks, and blanks indicate that no specimens from that group were found in that package. (B) Pie chart showing the proportion of the twelve faunal groups in the whole assemblage. (C) Taphogram showing the representation for each faunal group among the three types of fossil configurations.

FIGURE 7—Bone size and distribution of hadrosaurid remains as indicators of bone transport. (A) Greatest long-axis measurement for specimens by interval. (B) Proportion of hadrosaurid remains among all specimens. (C) Proportion of bones to teeth among hadrosaurid remains. (D) Flow-transport ratio for hadrosaurids based on comparison of visceral (vertebrae and ribs) to appendage (limbs, hip and shoulder girdles, sacrum, and skull) elements, following scheme of Lehman (1982). (E) Flotation ratio for hadrosaurids based on comparison of thoracic (vertebrae, ribs, hip and shoulder girdles) to radial (skull, feet, limbs, tail) elements.

FIGURE 8—Stratigraphic distribution of sites by facies association. Proportion of sites in each interval found in (A) sand-filled channels or point-bar facies, (B) proximal splay facies, (C) saturated backswamp facies, and (D) distal floodplain facies. Packages G and I and the rise-interval of package D include sites associated with an upper estuary facies not represented on the bar charts. Abbreviations for faunal groups are as in Figure 5,

and the chart format follows the framework in Figure 2. (E) Taphogram showing the distribution of faunal groups by facies association. Sites from the backswamp and splay facies associations were combined into a single component to reflect a proximal floodplain environment. Abbreviations are as listed for Figure 3.

FIGURE 9—Stratigraphic distribution of selected taphonomic modifications. Bars reflect proportion of sites in which fossils bear (A) secondary mineral growth, (B) polish, (C) brushmarks, (D) grooves, or (E) fungal mottling. Bar chart format follows the framework in Figure 2. Proportion bars for package I and the fall-interval of package F were omitted due to small sample size.

FIGURE 10—Typical bone fragment from the lower Horseshoe Canyon Formation. This specimen from the rise-interval of package D probably comes from the mid-shaft of a hadrosaurid rib, long bone, or ischium. (A) Modern fracture surface, showing calcite infill of cancellous interior. (B) Polished, pitted cortical bone with calcite filled linear fissures.

FIGURE 11—Idealized taphonomic and architectural responses to different modes of aggradation and accommodation. Symbols and shading scheme as in Figure 2. (A) Channel-lag assemblages in troughs within amalgamated channel sandstone sheets are produced by the channel-directed movement of bone under a low mean aggradation rate. Bone accumulates in channels through extensive reworking of older deposits, but is generally destroyed if buried in other facies. (B) Under moderate mean aggradation rate, channel-fill assemblages are preserved in fine-grained or mixed-sediment fill of floodplain traps and on the upper ends of aggrading, laterally migrating point bars. Bone export and import to the channel is balanced by reworking and avulsion. (C) A high mean aggradation rate produces thick sheets of floodplain mudrocks filled with highly dispersed, rapidly buried bones. Avulsions of perched channels export any bone in ephemeral channels to the floodplain, limiting preservation of bone in shoestring sandstone bodies.

FIGURE 12—Estimation of relative aggradational rate from the position of bone accumulations in trap fills. (A) A channel-lag assemblage concentrated at the top of the basal third of the channel fill. (B) A channel-fill

assemblage accumulated just beneath the top of the fill. In each fill, the elevation of the greatest concentration of bone represents the point at which the trap fill rate (G) equaled the optimum depositional rate for bone burial (O). Thus the interval between the assemblage and the top of the fill records the same change in depositional rate for both fills. If (A) and (B) represent the mean architecture of preservation from two different successions, they suggest that the initial depositional rate for (B) was much greater than that for (A). If (A) and (B) represent specific architecture from the same succession, at least one of them is probably an event deposit.

FIGURE 13—Distortion of biostratigraphic ranges caused by cyclic patterns in mean aggradation rate. A succession of hypothetical taxa evolve and become extinct through the passage of increments of geologic time. For these species the rate of evolutionary event occurrence (origins and extinctions) is constant. When remains of these species are converted to a fossil record in a succession of rock deposited under a cyclically variable aggradation rate, the biostratigraphic ranges representing the fossil species are distorted. Events (first and last appearances, FA and LA respectively) become concentrated in intervals deposited under low or zero net aggradation, and ranges are expanded in rapidly accreted strata.

Figure 1

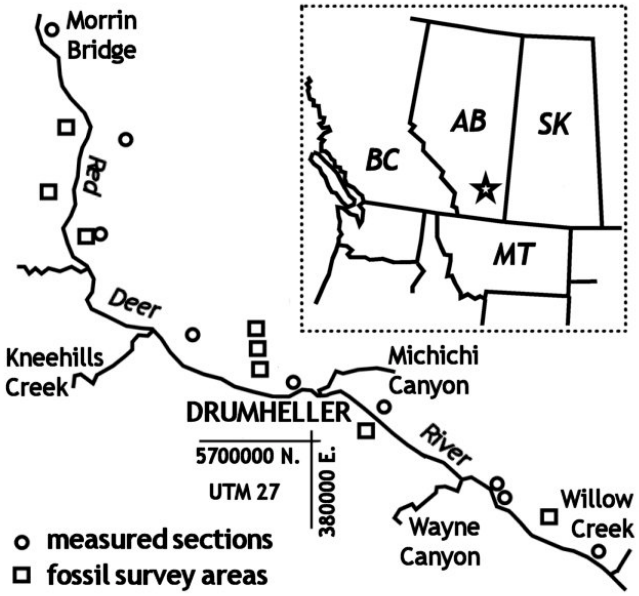
Morrin
Bridge
Red
Deer
Kneehills
Creek
DRUMHELLER
5700000 N.
UTM 27
380000 E.
Michichi
Canyon
River
Wayne
Canyon
Willow
Creek
measured sections
fossil survey areas
AB
SK
BC
MT

Figure 2

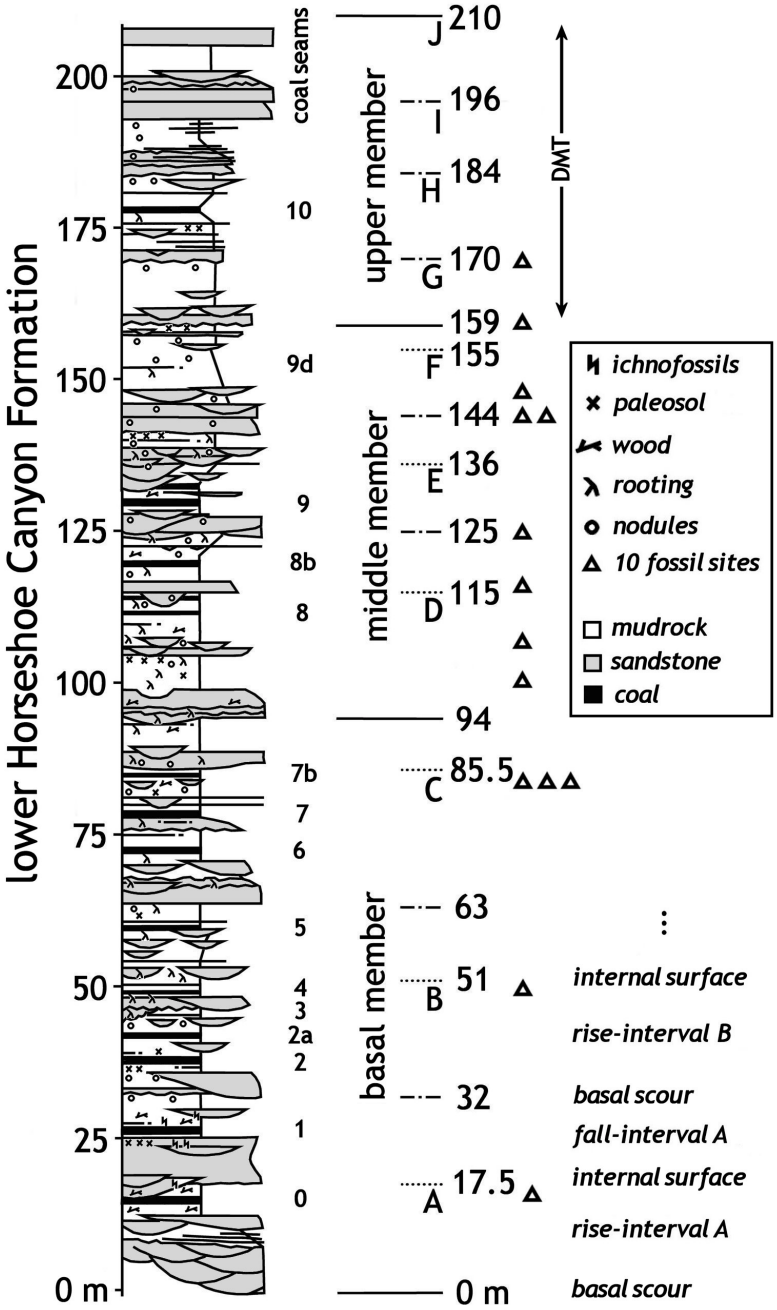
lower Horseshoe Canyon Formation
200
175
150
125
100
75
50
25
0 m
coal seams
10
9d
9
8b
8
7b
7
6
5
4
3
2a
2
1
0
upper member
middle member
basal member
J
I
H
G
F
E
D
C
B
A
210
196
184
170
159
155
144
136
125
115
94
85.5
63
51
32
17.5
0 m
DMT
ichnofossils
paleosol
wood
rooting
nodules
10 fossil sites
mudrock
sandstone
coal
internal surface
rise-interval B
basal scour
fall-interval A
internal surface
rise-interval A
basal scour

Figure 3

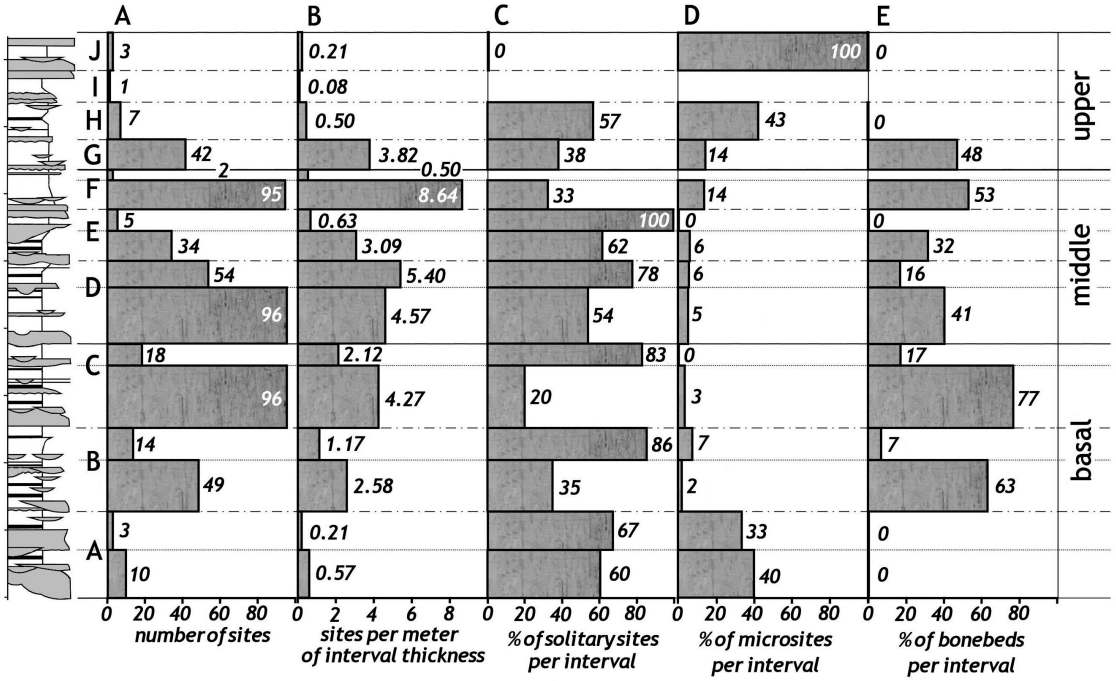
A
B
C
D
E
J
I
H
G
F
E
D
C
B
A
3
1
7
42
2
95
5
34
54
96
18
96
14
49
3
10
0.21
0.08
0.50
3.82
0.50
8.64
0.63
3.09
5.40
4.57
2.12
4.27
1.17
2.58
0.21
0.57
0
57
38
33
100
62
78
54
83
20
86
35
67
60
100
43
14
14
0
6
6
5
0
3
7
2
33
40
0
0
48
53
0
32
16
41
17
77
7
63
0
0
upper
middle
basal
0 20 40 60 80
number of sites
0 2 4 6 8
sites per meter of interval thickness
0 20 40 60 80
% of solitary sites per interval
0 20 40 60 80
% of microsites per interval
0 20 40 60 80
% of bonebeds per interval

Figure 4

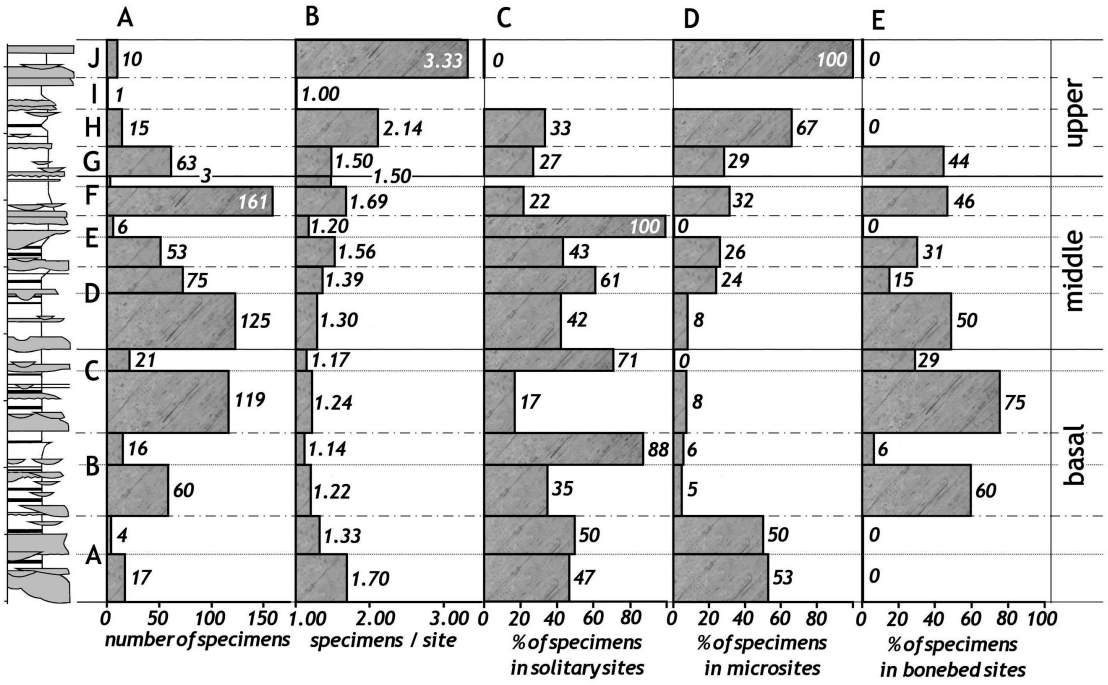
A
B
C
D
E
J
I
H
G
F
E
D
C
B
A
10
1
15
63
3
161
6
53
75
125
21
119
16
60
4
17
3.33
1.00
2.14
1.50
1.50
1.69
1.20
1.56
1.39
1.30
1.17
1.24
1.14
1.22
1.33
1.70
0
33
27
22
100
43
61
42
71
17
88
35
50
47
100
67
29
32
0
26
24
8
0
8
6
5
50
53
0
0
44
46
0
31
15
50
29
75
6
60
0
0
upper
middle
basal
0 50 100 150
number of specimens
1.00 2.00 3.00
specimens / site
0 20 40 60 80
% of specimens in solitary sites
0 20 40 60 80
% of specimens in microsites
0 20 40 60 80 100
% of specimens in bonebed sites

Figure 5

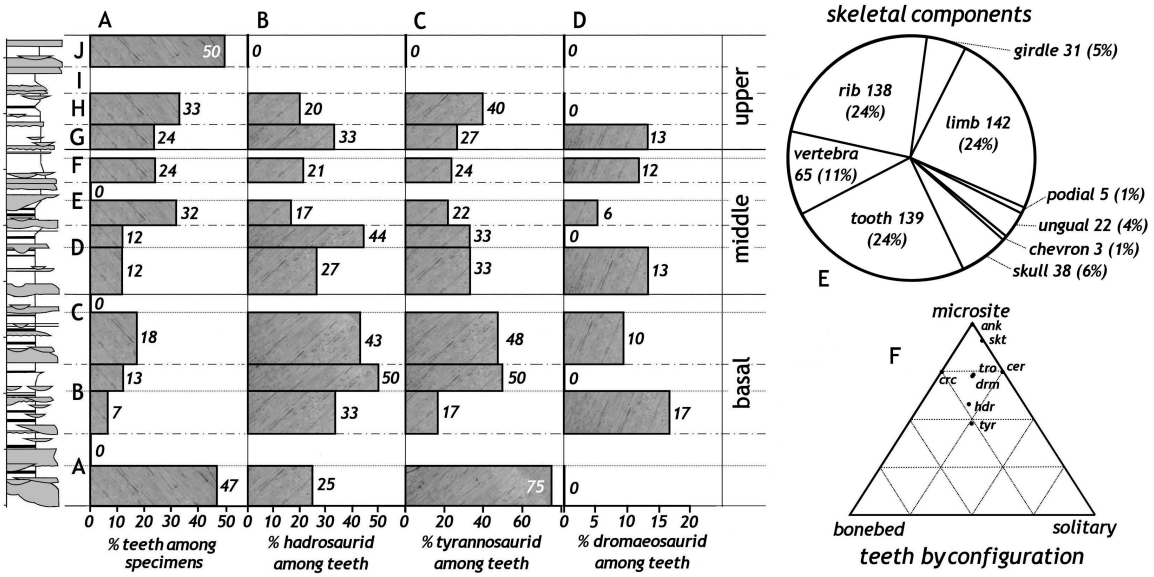
A
B
C
D
J
I
H
G
F
E
D
C
B
A
upper
middle
basal
50
0
0
0
33
20
40
0
24
33
27
13
24
21
24
12
0
32
17
22
6
12
44
33
0
12
27
33
13
0
18
43
48
10
13
50
50
0
7
33
17
17
0
47
25
75
0
0 10 20 30 40 50
% teeth among specimens
0 10 20 30 40 50
% hadrosaurid among teeth
0 20 40 60
% tyrannosaurid among teeth
0 5 10 15 20
% dromaeosaurid among teeth
skeletal components
girdle 31 (5%)
rib 138 (24%)
limb 142 (24%)
vertebra 65 (11%)
podial 5 (1%)
ungual 22 (4%)
tooth 139 (24%)
chevron 3 (1%)
skull 38 (6%)
E
microsite
ank
skt
F
cer
tro
crc
drm
hdr
tyr
bonebed
solitary
teeth by configuration

Figure 6

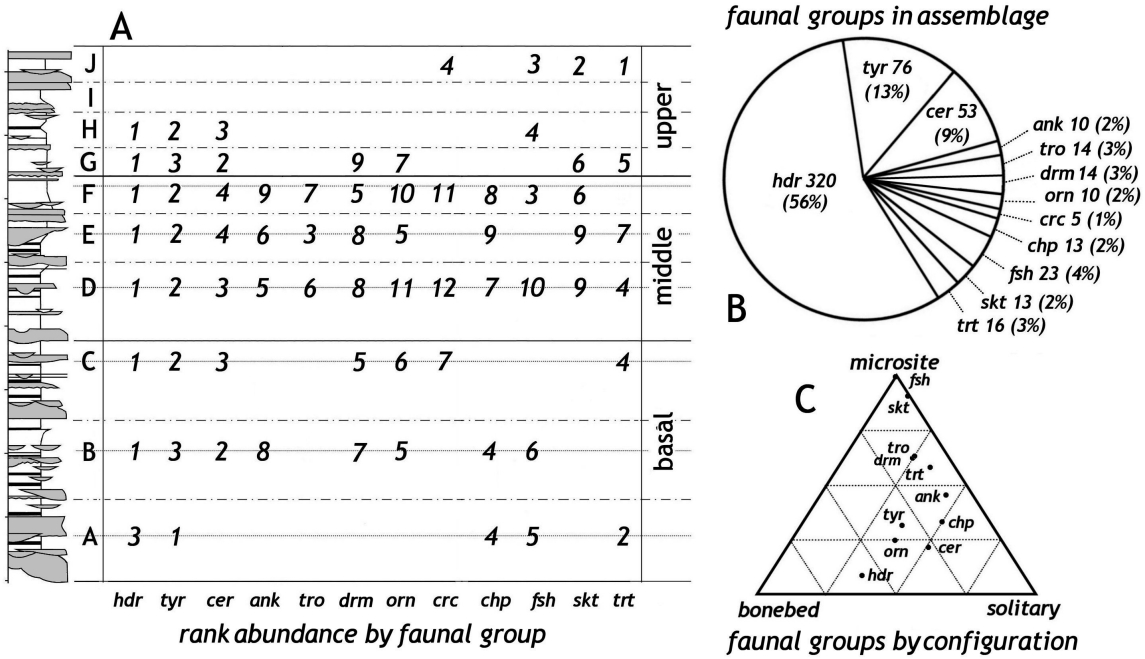
A
J 4 3 2 1
I
H 1 2 3 4
G 1 3 2 9 7 6 5
F 1 2 4 9 7 5 10 11 8 3 6
E 1 2 4 6 3 8 5 9 9 7
D 1 2 3 5 6 8 11 12 7 10 9 4
C 1 2 3 5 6 7 4
B 1 3 2 8 7 5 4 6
A 3 1 4 5 2
upper
middle
basal
hdr tyr cer ank tro drm orn crc chp fsh skt trt
rank abundance by faunal group
faunal groups in assemblage
tyr 76 (13%)
cer 53 (9%)
ank 10 (2%)
tro 14 (3%)
drm 14 (3%)
orn 10 (2%)
crc 5 (1%)
chp 13 (2%)
fsh 23 (4%)
skt 13 (2%)
trt 16 (3%)
hdr 320 (56%)
B
C
microsite
fsh
skt
tro
drm
trt
ank
tyr
chp
cer
orn
hdr
bonebed
solitary
faunal groups by configuration

Figure 7

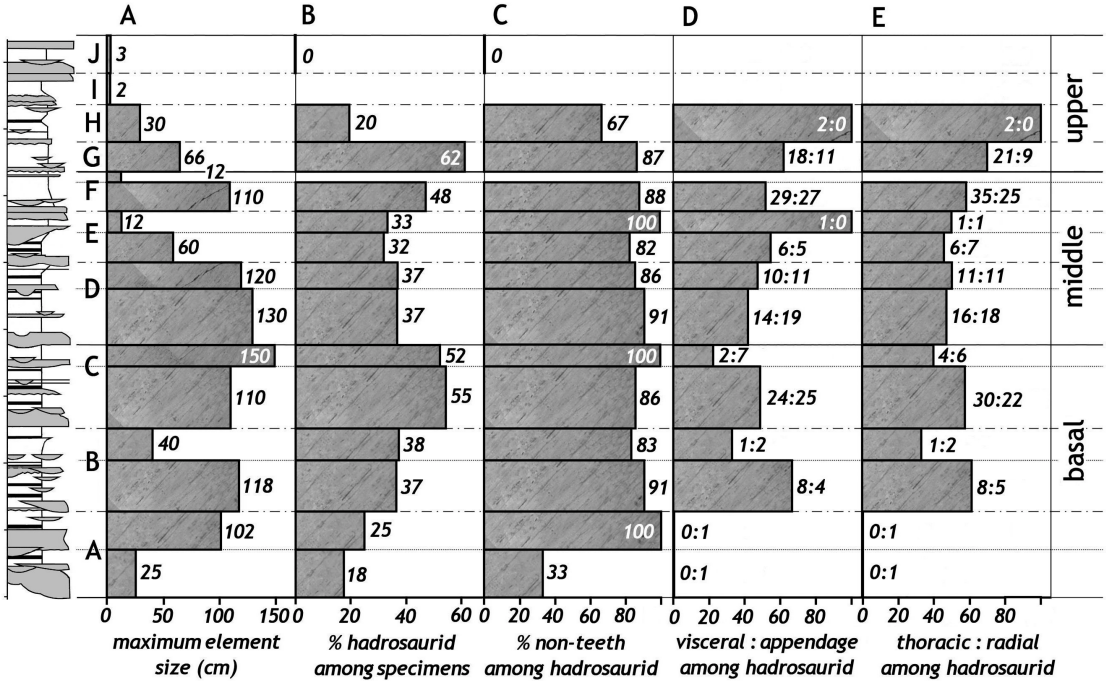
A
B
C
D
E
J
I
H
G
F
E
D
C
B
A
upper
middle
basal
3
2
30
66
12
110
12
60
120
130
150
110
40
118
102
25
0
20
62
48
33
32
37
37
52
55
38
37
25
18
0
67
87
88
100
82
86
91
100
86
83
91
100
33
2:0
18:11
29:27
1:0
6:5
10:11
14:19
2:7
24:25
1:2
8:4
0:1
0:1
2:0
21:9
35:25
1:1
6:7
11:11
16:18
4:6
30:22
1:2
8:5
0:1
0:1
0 50 100 150
maximum element size (cm)
0 20 40 60
% hadrosaurid among specimens
0 20 40 60 80
% non-teeth among hadrosaurid
0 20 40 60 80
visceral : appendage among hadrosaurid
0 20 40 60 80
thoracic : radial among hadrosaurid

Figure 8

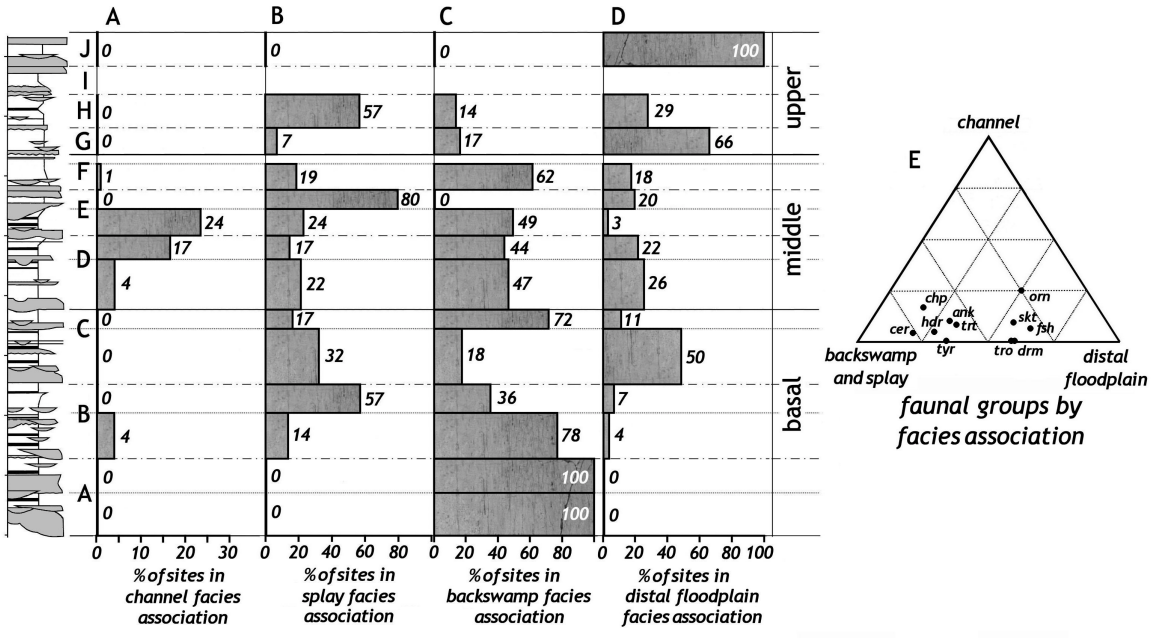
A
B
C
D
J
I
H
G
F
E
D
C
B
A
upper
middle
basal
0
100
57
14
29
7
17
66
1
19
62
18
80
20
24
3
49
17
22
44
4
22
47
26
72
11
32
18
50
57
36
7
14
78
4
100
100
0 10 20 30
0 20 40 60 80
0 20 40 60 80
0 20 40 60 80 100
%of sites in channel facies association
%of sites in splay facies association
%of sites in backswamp facies association
%of sites in distal floodplain facies association
channel
E
chp
orn
ank
hdr
trt
skt
fsh
cer
tyr
tro
drm
backswamp and splay
distal floodplain
faunal groups by facies association

Figure 9

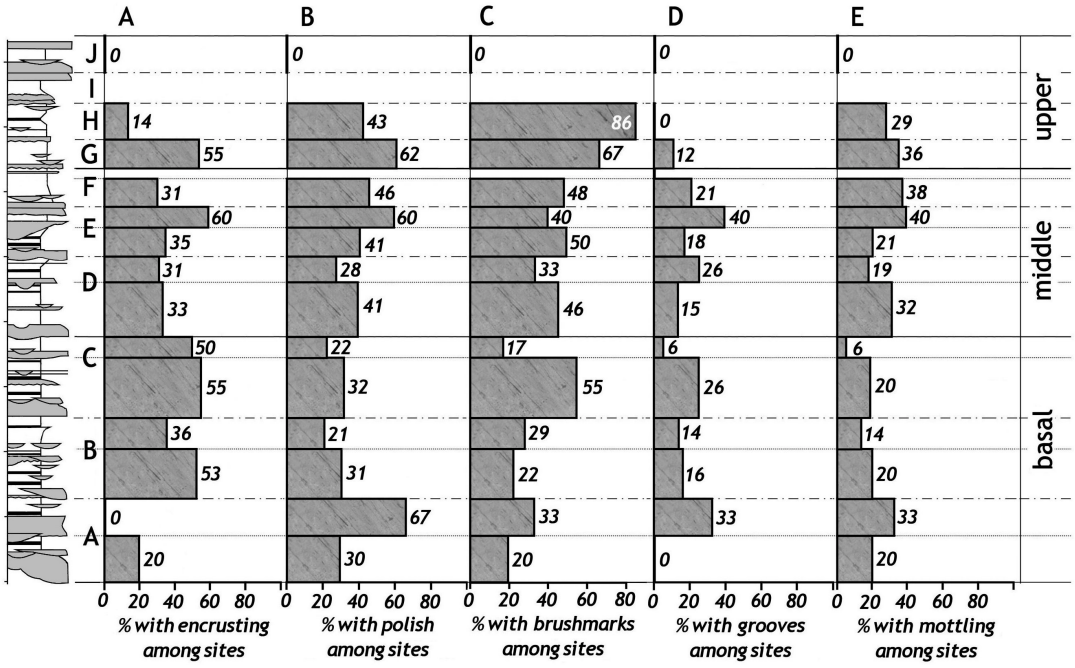
A
B
C
D
E
J
I
H
G
F
E
D
C
B
A
upper
middle
basal
0 20 40 60 80
% with encrusting among sites
% with polish among sites
% with brushmarks among sites
% with grooves among sites
% with mottling among sites

Figure 10

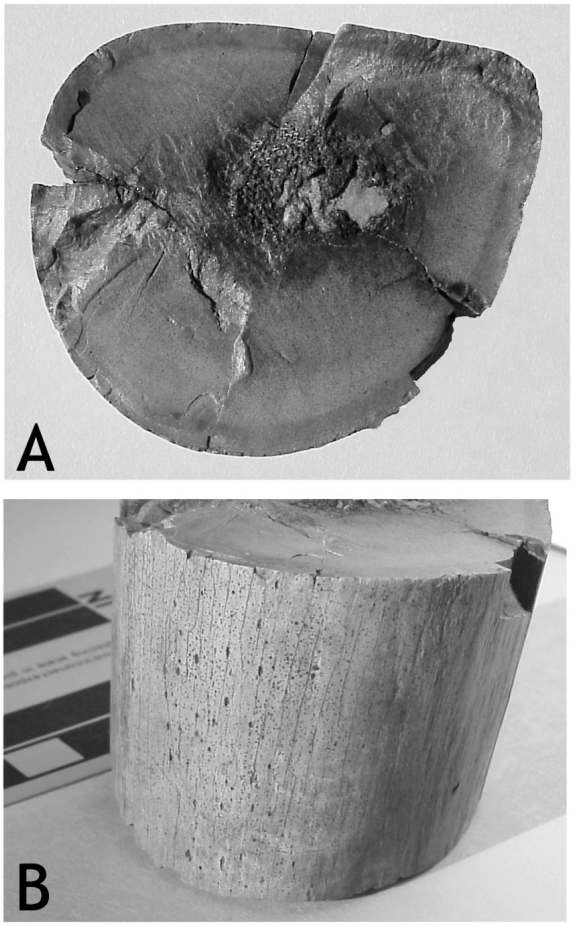

Figure 11

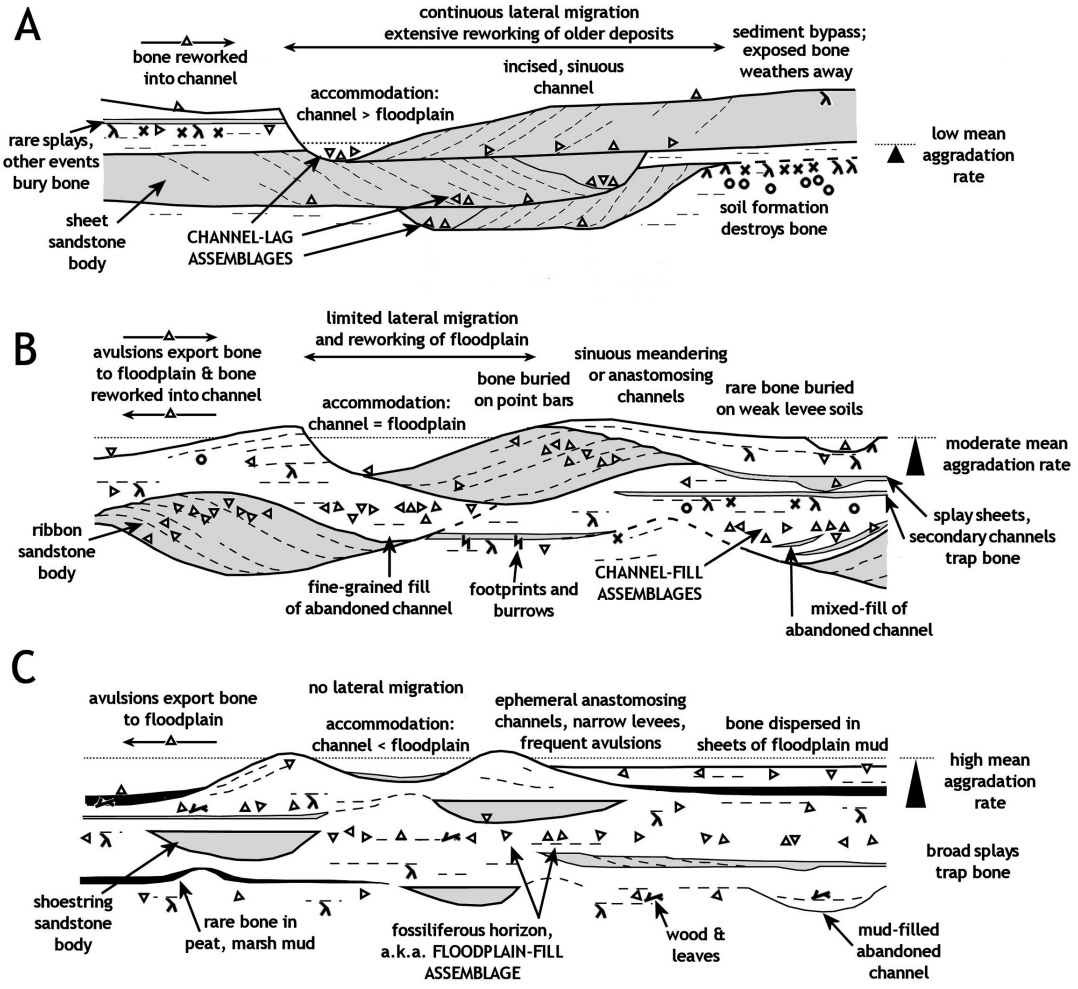
A
continuous lateral migration
extensive reworking of older deposits
sediment bypass;
exposed bone
weathers away
bone reworked
into channel
incised, sinuous
channel
accommodation:
channel > floodplain
rare splays,
other events
bury bone
low mean
aggradation
rate
sheet
sandstone
body
CHANNEL-LAG
ASSEMBLAGES
soil formation
destroys bone
B
limited lateral migration
and reworking of floodplain
avulsions export bone
to floodplain & bone
reworked into channel
sinuous meandering
or anastomosing
channels
bone buried
on point bars
rare bone buried
on weak levee soils
accommodation:
channel = floodplain
moderate mean
aggradation rate
splay sheets,
secondary channels
trap bone
ribbon
sandstone
body
fine-grained fill
of abandoned channel
footprints and
burrows
CHANNEL-FILL
ASSEMBLAGES
mixed-fill of
abandoned channel
C
no lateral migration
avulsions export bone
to floodplain
accommodation:
channel < floodplain
ephemeral anastomosing
channels, narrow levees,
frequent avulsions
bone dispersed in
sheets of floodplain mud
high mean
aggradation
rate
broad splays
trap bone
shoestring
sandstone
body
rare bone in
peat, marsh mud
fossiliferous horizon,
a.k.a. FLOODPLAIN-FILL
ASSEMBLAGE
wood &
leaves
mud-filled
abandoned
channel

Figure 12

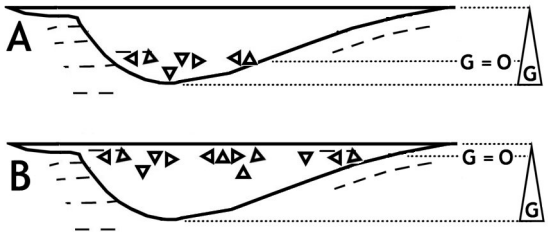

Figure 13

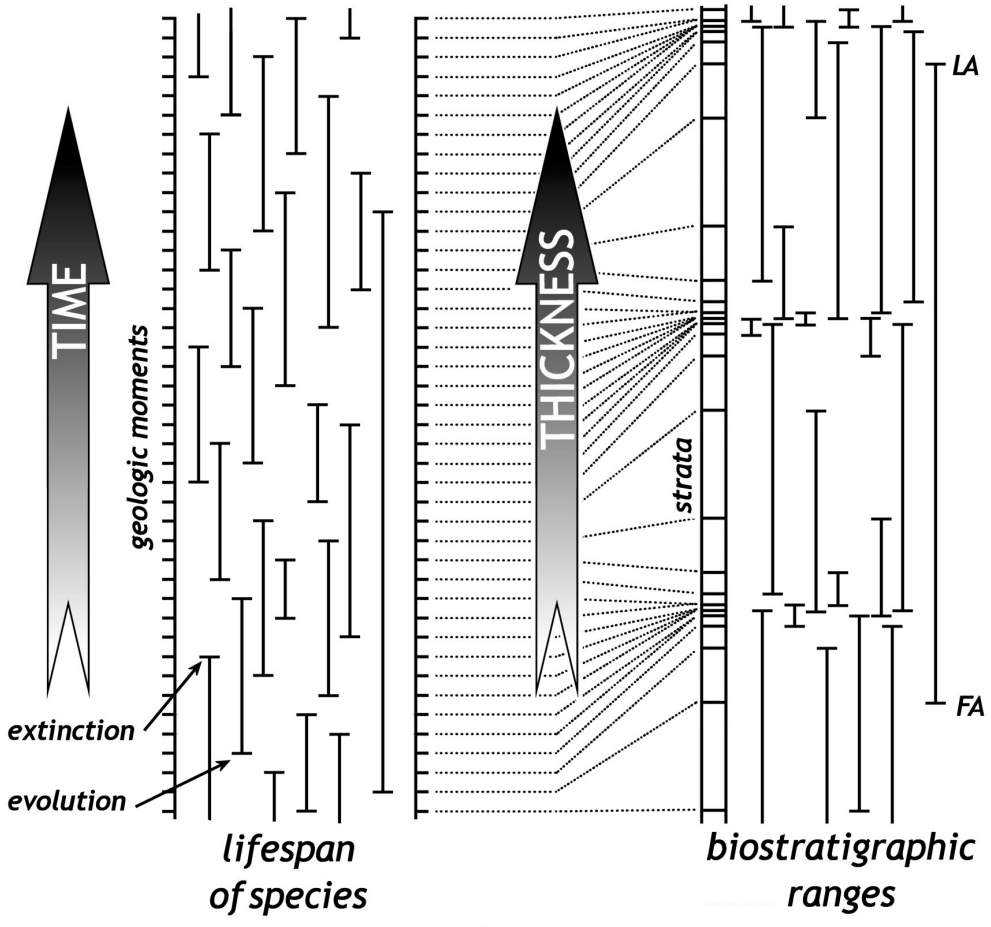
TIME
geologic moments
extinction
evolution
lifespan
of species
THICKNESS
strata
LA
FA
biostratigraphic
ranges

CHAPTER FOUR

Stable Oxygen Isotopes from Tyrannosaurid Tooth Enamel: Interlaboratory Comparison of Results and Cautionary Notes Concerning Reference Standards

WILLIAM H STRAIGHT
Marine, Earth, and Atmospheric Science Department,
North Carolina State University, Raleigh, NC 27695;
Duke Environmental Stable Isotope Laboratory (DEVIL)
Duke University Department of Biology & Nicholas School of the Environment and Earth Sciences, National Phytotron, Durham, NC 27708-0340

REESE E BARRICK
Marine, Earth, and Atmospheric Science Department,
North Carolina State University, Raleigh, NC 27695

JONATHAN D KARR
Technical Director, Duke Environmental Stable Isotope Laboratory (DEVIL)
Duke University Department of Biology & Nicholas School of the Environment and Earth Sciences, National Phytotron, Durham, NC 27708-0340

JULIA E COX
University of Arkansas Stable Isotope Laboratory,
Department of Biological Sciences, Fayetteville, AR 72701
Current address: Department of Geology, University of Georgia
Athens, GA 30602

DAVID A EBERTH
Royal Tyrrell Museum of Palaeontology
Box 7500, Drumheller, AB T0J 0Y0, Canada

for submission to *Rapid Communications in Mass Spectrometry*

The analysis of phosphate $\delta^{18}O$ in a sequence of enamel samples from a Campanian tyrannosaurid tooth were repeated at three different facilities using thermochemical decomposition in a Finnigan MAT TC/EA attached to a Finnigan MAT Delta Plus XL mass spectrometer. Each lab ran the sequence as silver phosphate derived from enamel, and one lab also ran the sequence as unprocessed enamel. Results revealed significant interference between the NIST reference material 8557, barium sulfate (NBS-127), and both types of phosphate samples. Once the deviation caused by the interference was repaired in the silver phosphate data, all three laboratories produce similar, significantly correlated two-peaked $\delta^{18}O$ patterns with a 2‰ range, consistent with previous results from contemporaneous teeth. Interference by sulfate standards does not account for the majority of the variability and deviation of unprocessed enamel $\delta^{18}O$, but sulfate does interfere to a lesser degree with $\delta^{18}O$ measurement in other substances. Whereas both unprocessed enamel and the NIST RM 8557 barium sulfate should be applied to biological phosphate ("biophosphate") stable isotope research with caution, seasonal variations in enamel phosphate $\delta^{18}O$ are a reproducible phenomenon in theropod dinosaur teeth.

INTRODUCTION

Of several biophosphate phases, tooth enamel is regarded as the most isotopically stable on geologic timescales due to its high original density and crystallinity and its extremely low organic content (1-4). During each day of tooth growth in an animal, an enamel band ~20 μm thick extends the length of the tooth (1,5-7) and preserves a record of the animal's body water $\delta^{18}O$ (8-13). The $\delta^{18}O$ signal of the body water reservoir is derived primarily from drinking water (14-19), but is modified by the $\delta^{18}O$ of food and food water, which frequently reflects evapotranspiration in vegetable matter (20-21). Body water $\delta^{18}O$ is also controlled by external temperature in heterotherms (22-26). Enamel of homeotherm predators record preserve the highest fidelity record of meteoric water $\delta^{18}O$ because (1) their body water $\delta^{18}O$ is not controlled by external temperature and (2) their body water reservoir derives a surface water $\delta^{18}O$ signal both through drinking and through water consumed by prey (19, 27).

Records of surface water $\delta^{18}O$ have been extracted from enamel of mammals (e.g., 19, 28-36) and dinosaurs (26, 27, 36-39) using a variety of sampling strategies (40). The most comprehensive extraction of surface water $\delta^{18}O$ from enamel involves the collection of a sequence of samples from tooth root to crown (40), producing dozens of samples where older techniques yielded three to five. This radical increase in sample count parallels recent improvements in the speed of sample processing procedures (41-43) and new developments in analytical equipment, important among them the continuous-flow gas-chromatography mass-spectrometer (44). This new technology has evolved so quickly that every laboratory has its own technique, lab standards, and analytical protocol. Although several laboratories have demonstrated seasonal signals in enamel $\delta^{18}O$ (e.g., 19, 31, 34, 36, 37), no consensus is yet available as to whether such measurements from a single tooth are consistent between laboratories. The present study presents the results of serial analysis of enamel $\delta^{18}O$ from one tyrannosaurid dinosaur tooth repeated at three different laboratories. In addition, unprocessed enamel from the tooth was analyzed at one facility to compare results with an established silver-phosphate processing technique (43, 45).

METHODS

A 46-millimeter-long shed tooth from the late Campanian tyrannosaurid theropod dinosaur *Albertosaurus* was collected during a survey of taphonomy in the lower Horseshoe Canyon Formation of south-central Alberta, Canada (46, 47). On this tooth, twenty-six ~1.0-mm-wide grooves were cut into the enamel, paralleling daily growth bands (5, 27). Each groove spans approximately ten daily growth bands, thus homogenizing about ten days of the enamel isotope record in each 1.5 to 3 mg sample of enamel powder. On this tooth, narrow bands of enamel were left between grooves to avoid time-averaging of the isotopic signal between adjacent grooves (48). The suite of enamel samples from this tooth covers a period of approximately ten months of the dinosaur's life, based on the tooth length and published estimates of tyrannosaurid tooth growth rate (5).

Part of the enamel powder from each groove was processed according to the method described in the data repository for Dettman *et al*., (43), yielding 2.0 to 2.4 mg of silver phosphate from each 1.0 mg of sample powder. Three sets of silver phosphate samples packed in capsules were prepared for isotopic analysis, each

set containing at least one sample from each groove. Each set contained three to four sample replicates and capsules loaded with laboratory silver phosphate standards, either from NBS 120c Florida Phosphate Rock or from a sodium phosphate solution, made during enamel processing with the same technique. Three university stable isotope laboratories each analyzed a set of processed enamel samples: the Duke Environmental Stable Isotope Laboratory (DEVIL) in Durham, NC; the stable isotope facility in the Marine, Earth, and Atmospheric Sciences Department at North Carolina State University (NCSU) in Raleigh, NC; and the University of Arkansas State Isotope Laboratory (UASIL) in Fayetteville, AR. The DEVIL facility also analyzed a set of unprocessed enamel powder samples from this dinosaur tooth.

At each lab, silver phosphate samples were thermochemically decomposed under an oxygen-free, helium atmosphere at ~1450 º C in an automated Finnigan MAT (Bremen, Germany) TC/EA (thermochemical elemental analyzer) connected to a Finnigan MAT Delta Plus XL continuous-flow mass spectrometer, generally following previously published techniques (44, 49, 50). At each lab, sample sequences were processed in single runs on the same day, but within each run, samples were ordered differently: at the NCSU lab, the samples were run in the order presented (Figure 1) from tooth tip toward root (0 mm to 44.5 mm); at the DEVIL facility, the samples were analyzed from the root toward the tip; and at the UASIL lab, the samples were randomized. The two sets analyzed at the DEVIL facility, silver phosphate and unprocessed enamel, were processed in the same order, except that the replicates in the unprocessed enamel set were grouped at the end of the run.

At each facility, standards included the same two reference materials, sucrose ANU (NIST RM 8542, $\delta^{18}O$ = + 36.4‰vs. V-SMOW; 51, 52) and barium sulfate, also called NBS 127 (NIST RM 8557,$\delta^{18}O$ = + 9.4‰vs. V-SMOW). Each facility also used its own mix of laboratory standards, including HEKAtech (Wegberg, Germany) benzoic acid, IAEA C3 cellulose, IAEA N3, sucrose, and citric acid. At the UASIL and NCSU facilities, standards were interspersed throughout the sample run, whereas at the DEVIL lab, standards were run in blocks of three replicates before and after each sequence of analyses. A correction for analytical offset was calculated for each set of results, using a two-point correction based on the comparison of published and measured values for the NIST reference materials.

SILVER PHOSPHATE RESULTS AND INTERPRETATION

Results from silver phosphate analysis from each of the three laboratories (Figure 1) include averaged pairs of values for replicated samples. In results from the DEVIL facility, six replicates feature an average separation of 0.22‰, and in three replicates from the NCSU lab, three replications have an average separation of 0.44‰ Although UASIL did not analyze replicates for samples from this tyrannosaur tooth, ten sample duplicates from other tyrannosaur teeth from the same formation had an average difference of 0.35‰ Results from the three labs feature a similar pattern of $\delta^{18}O$ variation within the tyrannosaurid tooth: (a) a minimum $\delta^{18}O$ of ~+ 11.7‰at the tooth tip; (b) a enrichment from the tip to 21 mm, reaching a maximum $\delta^{18}O$ of ~+ 13.6‰; (c) a depletion from 21 mm toward a minimum around 38 mm; and (d) two positive excursions at 28 and 43 mm. The three patterns are not identical, however. The isotopic range of each pattern is 1.69‰ (NCSU), 2.07‰(DEVIL), and 2.19‰(UASIL). The NCSU data indicates smooth enrichment and depletion trends, whereas the UASIL data features a series of minor peaks. Most notably, both the UASIL and NCSU patterns show an enrichment trend in the last (rootward) 15 mm, but the DEVIL data continues the progressive depletion from the maximum at 21 mm. Although the position of $\delta^{18}O$ excursions is the same for all three patterns, the deviation between the DEVIL results and the results from other facilities increases in the last 12 samples toward the tooth root, making the DEVIL value at the root is 1.2‰more negative than the other measurements from the same sample.

The sample with the greatest offset in the DEVIL pattern was the first enamel sample analyzed during the analytical run, following three capsules each of barium sulfate and citric standards. In successive samples, the difference between the DEVIL pattern and those from the other labs diminishes. Thus, the offset between the DEVIL data and other lab results is interpreted as interference from the group of standard samples analyzed just prior to the first tooth samples.

To test the hypothesis that the standards and the enamel silver phosphate were interacting in the TC/EA, an homogenized sample from reagent-grade Alfa-Aesar (Ward Hill, MA) silver phosphate was compared in several runs against the standards used in the tooth study. When run following capsules of organic standards the silver phosphate produced a $\delta^{18}O$ value of + 7.9‰± 0.19‰ However, each time the phosphate samples followed samples of the barium sulfate standard in an analytical run, the first phosphate

values were depleted by 1.0‰or more and the phosphate deviation increased to as much as ± 0.79‰. A single capsule of barium sulfate standard produced erratic deviation of $\delta^{18}O$ up to 2‰in one or two following silver phosphate samples. An analytical run in which samples of the barium sulfate standard NIST RM 8557 preceded 18 samples of silver phosphate shows a significant interaction between the two substances in the TC/EA (Figure 2). The majority of the 2.6‰initial offset is recovered after six phosphate samples have run, but the offset persists for ~15 samples. The barium sulfate standard does not interfere as strongly with organic standards or samples, although for a variety of materials, a positive excursion averaging 2‰afflicts 1-2 samples run about 12 positions and over two hours after a group of barium sulfate samples. In the phosphate test sequence, this "cough" seems to indicate the end of the sulfate interference.

Results of the enamel analysis from the other two laboratories were inspected for sulfate interference. The NCSU run included two capsules of barium sulfate interspersed through the sequence. Two phosphate samples, one sample following each standard capsule, produced $\delta^{18}O$ values slightly depleted (~0.5‰) relative to the $\delta^{18}O$ of preceding and subsequent phosphate samples. However, the NCSU data for sulfate standards is insufficient to compute a meaningful correction. Instead, the two phosphate samples influenced by the sulfate standard were omitted. During the analysis of *Albertosaurus* tooth enamel at the UASIL lab, barium sulfate standards were analyzed after the silver phosphate samples and therefore did not interact with them. However, subsequent data collected at UASIL shows minor depletion in $\delta^{18}O$ for one or two phosphate standard samples immediately following a barium sulfate analysis.

The results for the phosphate test sequence were used to correct for the interference caused by RM 8557 in the *Albertosaurus* enamel data from the DEVIL facility. To achieve this restoration, the difference between the measured and standard $\delta^{18}O$ value was computed for each analysis in the phosphate test sequence. To fill gaps in the test sequence, which included a silver capsule blank after every sixth phosphate sample, a restoration value was interpolated by averaging the correction values for the preceding and following samples. Otherwise, no other interpolation or curve-fitting was applied to the test results. The restoration curve thus comprises 20 values, ranging from 2.4‰in the first analytical position to less than 0.1‰in each of the last four positions.

When the restoration curve is applied to the first 20 samples of the DEVIL theropod enamel data, the deviation between that data and the results from the other facilities is eliminated (Figure 3). Prior to removal of the sulfate interference from the DEVIL results, NCSU and UASIL data correlate ($r = 0.88$, $a = 0.01$) whereas DEVIL results do not correlate at the same level of confidence. With the restoration applied, DEVIL results correlate with both the NCSU ($r = 0.77$) and UASIL ($r = 0.80$) patterns. Following the repair of the DEVIL data, the results from all three labs are consistent with one another and with the shape of the isotopic patterns in $\delta^{18}O$ from other contemporaneous tyrannosaurid teeth (27).

UNPROCESSED ENAMEL RESULTS AND INTERPRETATION

The set of unprocessed enamel samples was run at the DEVIL facility using the same techniques and standards as the processed enamel set. The $\delta^{18}O$ pattern from unprocessed enamel features the same general trend and maximum as the patterns of processed enamel, but also shows greater scatter, with six replicate pairs separated by an average of 0.85‰and a total isotopic range of 4.6‰ As with the results from the processed sample set, the last (rootward) 15 $\delta^{18}O$ analyses of unprocessed enamel were depleted by interference from a group of barium sulfate standards at the beginning of the analytical run. The interference curve that restored the silver phosphate results does not repair the offset in the unprocessed enamel results (Figure 4).

In unprocessed enamel, this offset may represent a greater interaction between the sulfate standard and silver phosphate. If each value in the restoration curve is magnified 4.5 times and applied, the reset unprocessed enamel data generally match the arching trend described by all processed enamel results. However, individual values in the unprocessed sequence vary by ± 1.0‰around that trend, and the $\delta^{18}O$ of five additional replicate samples run at the end of the sequence differ by as much as 2.66‰from samples from the same position. Therefore, although the last fifteen unprocessed enamel samples run are consistent with the silver phosphate results, unprocessed enamel is generally an unreliable source for paleoecologically meaningful $\delta^{18}O$ analysis.

DISCUSSION AND CONCLUSIONS

The NIST standard RM 8557 has been critically important for the analysis of biophosphate stable oxygen isotopes because the $\delta^{18}O$ of the sulfate falls in the same range as typical fossil enamel $\delta^{18}O$. However, like most standards this material was introduced prior to the development of thermochemical elemental analysis, continuous flow stable isotope mass-spectrometry, and research interest in biophosphate stable oxygen. The interaction of barium sulfate with phosphate samples may be due to ions, possibly sulfur, liberated by the high-temperature decomposition scavenging the oxygen from the phosphate, but little is known about the interactions of sample residues in TC/EA technology. The standard measures for avoiding sulfur interference (use of silver capsules, silver wool packing in reactors) apparently cannot prevent these undesirable effects. Results show that analysis of one capsule of this sulfate standard in a TC/EA sequence can disrupt the following 2-3 sample values, and three or more capsules of sulfate standard in a row can distort the results in fifteen or more samples. This disruption may extend to materials other than silver phosphate. Until the cause of the interference can be identified and removed, the NIST RM 8557 should be used with caution and is presently unsuitable for use with silver phosphate samples. However, it can still be used for initial calibration of sulfur-free internal standards as long as the barium sulfate is run last within each analytical run.

Processing of enamel to silver phosphate before analysis is critically important. Results derived from unprocessed enamel include a higher variability than processed enamel. This variability is not a proportional response to the carbonate present in enamel, which averages 3% by mass in teeth (3), but may instead arise when calcium ions liberated by decomposition scavenge the oxygen released from phosphate bonds. Calcium is commonly used in the steel industry as a scavenger of oxygen, sulfur, and phosphorus (53), all of which are present in the reactor when unprocessed enamel is run with the barium sulfate standard. This scavenging may partly explain the higher variability of other types of unprocessed enamel analysis, such as the laser ablation technique (4). Isotopic analysis of theropod tooth enamel by the spot ablation technique (54) produced patterns with isotopic mean, range, and general trends consistent with *Albertosaurus* teeth presented here and elsewhere (27). However, the 0.5‰variability in the spot ablation data aided a conclusion that no seasonal signals were present (55). As shown herein using data acquired through thermochemical decomposition techniques,

patterns in the $\delta^{18}O$ of enamel phosphate are a real, reproducible phenomenon and not a function of machine variability.

SUMMARY

Four measurements of phosphate $\delta^{18}O$ were taken from each sample in a tip-to-root sequence of growth-parallel grooves in the enamel of a 46-mm-long Campanian tyrannosaurid tooth. Three measurements were taken from enamel converted to silver phosphate, one at each of three stable isotope facilities, all using thermochemical decomposition in a Finnigan MAT TC/EA attached to a Finnigan MAT Delta Plus XL continuous-flow mass spectrometer. The fourth measurement was taken from unprocessed enamel powder on the same equipment. Two of the three sequences of data from silver phosphate match with no more than analytical correction. The analysis of the third sequence was hampered by interference between the NIST reference material 8557, barium sulfate (NBS-127), and the silver phosphate. Once the sulfate distortion is removed, all three sequences feature a significantly correlated two-peaked pattern with a 2‰range, consistent with previous results from contemporaneous teeth. Sulfate interference also impacts the results from the unprocessed enamel analysis, but the majority of the ~2‰scatter and 3.5‰offset in the first 10 to 20 unprocessed enamel analyses is not amended by the sulfate correction demonstrated. Thus unprocessed enamel and NIST RM 8557 are not recommended for biophosphate stable isotope research, but seasonal variations in enamel phosphate $\delta^{18}O$ can be repeatedly detected in theropod teeth.

ACKNOWLEDGEMENTS

Thanks to Jonathan Perry and Patty Ralrick for help during the fossil recovery, to Bernard Genna and Dr. W.J. Showers for isotopic analysis at the NCSU facility, and to Dr. Robert Jackson for the opportunity to work through the Duke facility. This work was supported in part through an RC Graduate Student Support Grant and by the Heaton Student Support Grant through the Royal Tyrrell Museum of Palaeontology in Drumheller, Alberta.

REFERENCES

1. Hillson S. Teeth. Cambridge University Press. 1986; 376 p.

2. Lucas J, Prévôt LE. In: Allison PA, Briggs DEG, (eds.), Taphonomy: Releasing the Data Locked in the Fossil Record. Plenum Press, New York, 1999; pp. 389-409.

3. Rink WJ, Schwarcz HP. *J. Arch. Sci*. 1995; **22**:251-255.

4. Cerling TE, Sharp ZD. *Palaeogeogr. Palaeoclim. Palaeoecol*. **126**:173-186.

5. Erickson GM. *Bul. Nat. Acad. Sci*. 1996: **93**:14623-14627.

6. Sander M. *Muncher Geowissenshaftliche Abhandlungen*. 1999; **A-38**: 102 p.

7. Dean MC. In: Teaford MF, Smith MM, and Ferguson MWJ (eds.), Development, Function, and Evolution of Teeth. Cambridge University Press, Cambridge. 2000; pp. 119-130.

8. Longinelli A. *Geoch. Cosmo. Acta*. 1984; **48**:385-390.

9. Barrick RE, Fischer AG, Kolodny Y, Luz B, Bohaska D. *Palaios*. 1992; **7**:521-531.

10. Barrick RE, Fischer AG, Bohaska D. *Paleocean.* 1993; **8**:845-858.

11. Barrick RE, Fischer AG, Showers WJ. *Palaios*. 1999; **14**:186-191.

12. Bryant JD, Luz B, Froelich PN. *Palaeogeogr. Palaeoclim. Palaeoecol*. 1994; **107**:303-316.

13. Barrick RE. *Paleo. Soc. Pap*. 1998; **4**:101-137.

14. Luz B, Kolodny Y, Horowitz M. *Geoch. Cosmo. Acta.* 1984; **48**:1689-1693.

15. Luz B, Kolodny Y. *EPSL*. 1985; **75**:29-36.

16. Luz B, Kolodny Y. *Appl. Geoch*. 1989; 4:317-323.

17. D' Angela D, Longinelli A*Chem. Geol*. 1990; **86**:75-82.

18. Bryant JD, Froelich PN. *Geoch. Cosmo. Acta*. 1995; **59**:4523-4537.

19. Kohn MJ. *Geoch. Cosmo. Acta*. 1996; **60**:4811-4829.

20. Cormie AB, Luz B, Schwarcz HP. *Geoch. Cosmo. Acta*. 1994; **58**:3439-3449.

21. Kohn MJ, Schoeninger MJ, Valley JW. *Geoch. Cosmo. Acta*. 1996; **60**:3889-3896.

22. Barrick RE, Showers WJ. *Science*. 1994; **265**:222-224.

23. Barrick RE, Showers WJ. *Paleobiology*. 1995; **21**:552-560.

24. Barrick RE, Showers WJ, Fischer AG. *Palaios*. 1996; **11:**295-305.

25. Fricke HC, Clyde WC, O'Neil JR, Gingerich PD. *EPSL*. 1998; **160**:193-208.

26. Fricke HC, Rogers RR. Geology. 2000; **28**:799-802.

27. Straight WH, Barrick RE, Eberth DA. *Palaeogeogr. Palaeoclim. Palaeoecol*. In review.

28. Reinhard E, de Torres T, O'Neil JR. *Palaeogeogr. Palaeoclim. Palaeoecol.* 1996; **126**:45-59.

29. Bryant JD, Froelich PN, Showers WJ, Genna BJ. *Palaios*. 1996; **11**:397-408.

30. Fricke HC, O'Neil JR. *Palaeogeogr. Palaeoclim. Palaeoecol*. 1996; **126**:91-99.

31. Stuart-Williams HL, Schwarcz HP. *Geoch. Cosmo. Acta*. 1997; **61**:2539-2550.

32. Koch PL, Fisher DC, Dettman DL. *Geology*. 1989; **17**:515-519.

33. Koch PL, Hoppe KA, Webb SD. *Chem. Geol.* 1998; **152**:119-138.

34. Kohn MJ, Schoeninger MJ, Valley JW. *Chem. Geol.* 1998; **152**:97-112.

35. Sharp ZD, Cerling TE. *Geology*. 1998; **26**:219-222.

36. Feranec RS, MacFadden BJ. *Palaeogeogr. Palaeoclim. Palaeoecol*. 2000; **162**:155-169.

37. Straight WH, Barrick RE, Showers WJ, Genna B. *J. Vert. Paleo., Abs. Pap*. 2001; **21**:105.

38. Patchus R, Straight WH, Barrick RE, Showers WJ, Genna B. *J. Vert. Paleo., Abs. Pap*. 2001; **21**:87-88.

39. Thomas KJS, Carlson SJ. *Palaeogeogr. Palaeoclim. Palaeoecol*. In review.

40. Straight WH, Barrick RE. *GSA, Abs. Prog.*. 2002; **34**:534A.

41. O'Neil JR, Roe LJ, Reinhard E, Blake RE. *Isr. J. Earth Sci.* 1994; **43**:203-212.

42. Stephan E. *J. Arch. Sci*. 2000; **27**:523-535.

43. Dettman DL, Kohn MJ, Quade J, Ryerson FJ, Ojha TP, Hamidullah S. *Geology*. 2001; **29**:31-34.

44. Koziet J. *J. Mass. Spec.* 1997; **32**:103-108.

45. Fox DL, Fisher DC. *Palaios*. 2001; **16**:279-293.

45. Kohn, MJ. *pers. comm*. 2000.

46. Straight WH, Eberth DA. *Palaios.* 2002; **17**:472-490.

47. Straight WH, Eberth DA, Perry JMG, Ralrick PE. *Palaios*. In review.

48. Hoppe KA, Amundsen R. *J. Vert. Paleo., Abs. Pap.* 2001; **21**:63.

49. Kornexl BE, Gehre M, Hoffling R, Werner RA. *Rapid Commun. Mass Spectrom*. 1999; **13**:1685-1693.

50. Showers WJ, Barrick RE, Genna B. *Anal. Chem*. 2002; **74**:142A-150A.

51. Farquhar GD, Henry BK, Styles JM. *Rapid Commun. Mass Spectrom*. 1997; **11**:1554-1560.

52. Kornexl BE, Werner RA, Gehre M. *Rapid Commun. Mass Spectrom*. 1999; **13**:1248-1251.

53. Coplen TB et al. *USGS Water-Res. Invest. Rep.* 01-4222. 2002; 100 p.

54. Jensen ML. MS thesis, Univ. NM. 2000; 107 p.

55. Jensen ML, Sharp ZD, Lucas SG. *NM Mus. Nat. Hist. Sci. Bul.* 2000; **17**:91.

FIGURE CAPTIONS

FIGURE 1—Interlaboratory comparison of phosphate $\delta^{18}O$, measured from theropod tooth enamel converted to silver phosphate. Filled symbols represent the average of two measurements. The shaded area highlights the range of isotopic variability at each sampling position on the tooth.

FIGURE 2—Isotopic interference between the NIST RM 8557 barium sulfate standard and a silver phosphate lab standard. Analytical position refers to the order in which the test samples were analyzed.

FIGURE 3—Interlaboratory comparison of phosphate $\delta^{18}O$, following repair of sulfate interference in the DEVIL facility results. The shaded area highlights the adjusted range of isotopic variability at each sampling position. Small stars represent the original DEVIL measurements.

FIGURE 4—Comparison of processed and unprocessed enamel phosphate $\delta^{18}O$ after repair of sulfate interference. Both sets of data were produced at the DEVIL facility using the same technique and in order from root to tip. Filled symbols represent the average of two measurements, and arrows indicate replicates run at the end of the unprocessed enamel sequence. The shaded area highlights the adjusted range of isotopic variability and is the same as in Figure 2.

Figure 1

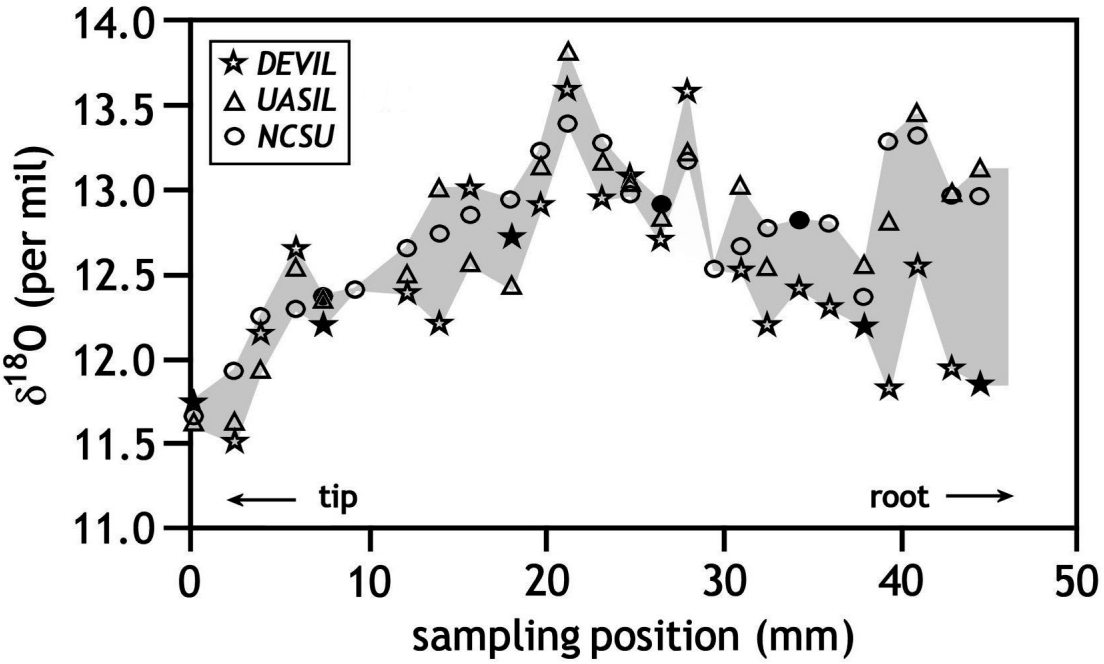
14.0
13.5
13.0
12.5
12.0
11.5
11.0
δ18O (per mil)
DEVIL
UASIL
NCSU
tip
root
0
10
20
30
40
50
sampling position (mm)

Figure 2

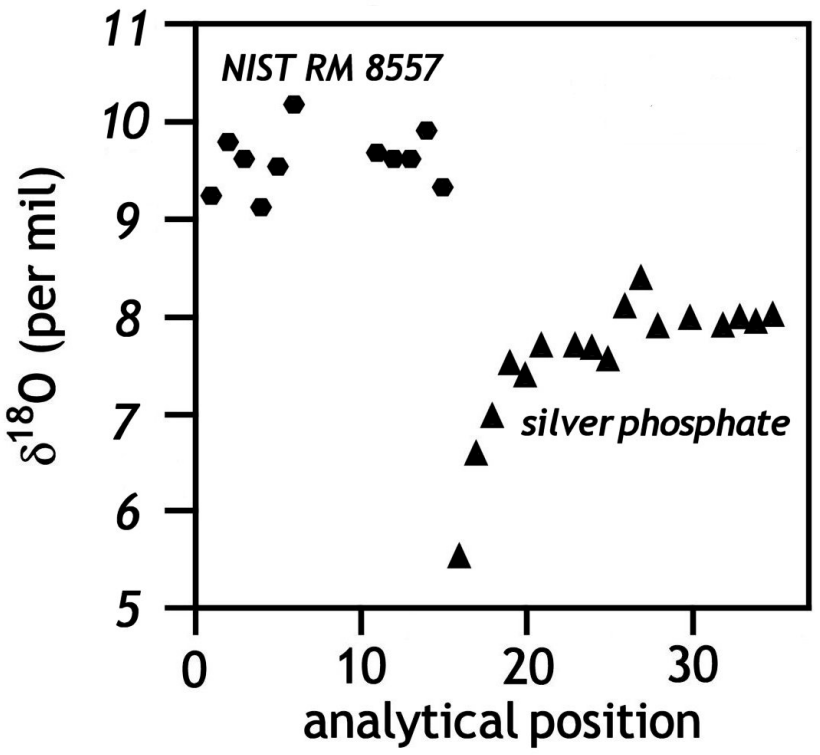
NIST RM 8557
silver phosphate
δ18O (per mil)
11
10
9
8
7
6
5
0
10
20
30
analytical position

Figure 3

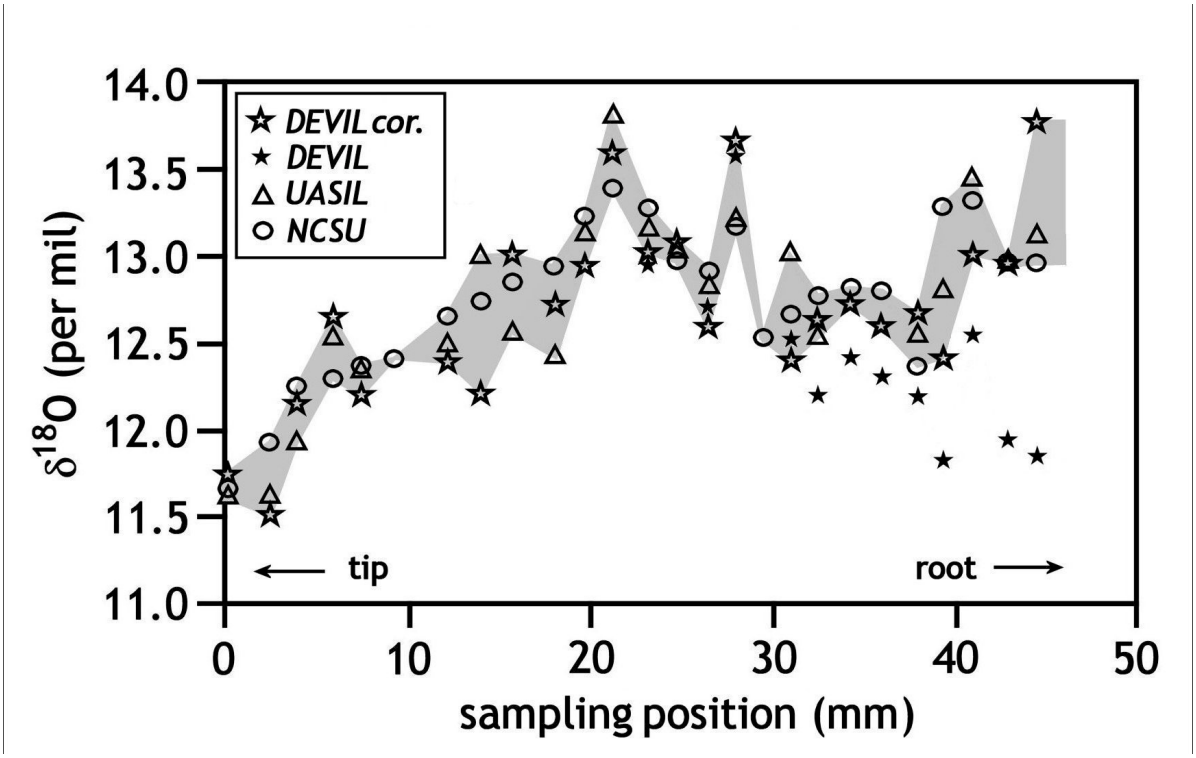
DEVIL cor.
DEVIL
UASIL
NCSU
tip
root
δ18O (per mil)
sampling position (mm)
14.0
13.5
13.0
12.5
12.0
11.5
11.0
0
10
20
30
40
50

Figure 4

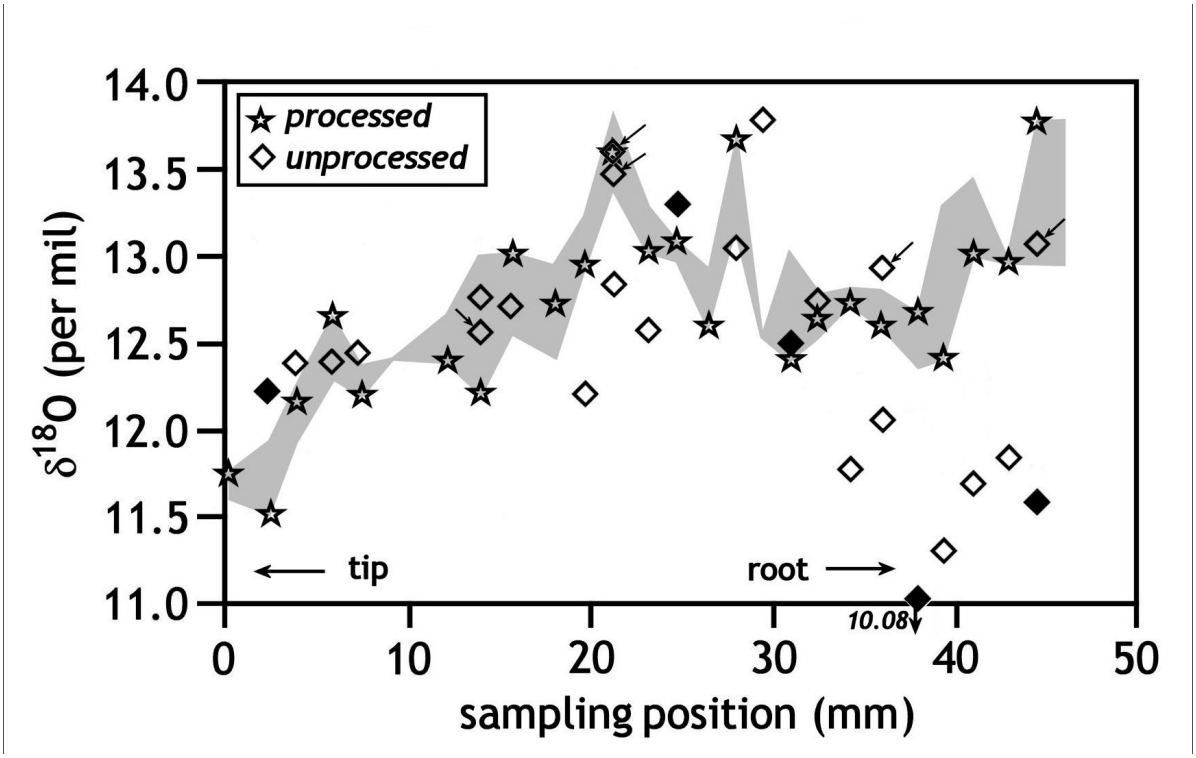
processed
unprocessed
tip
root
10.08
δ18O (per mil)
sampling position (mm)
14.0
13.5
13.0
12.5
12.0
11.5
11.0
0
10
20
30
40
50